НАУЧНОМ ВЕЋУ
ИНСТИТУТА ЗА ФИЗИКУ БЕОГРАД
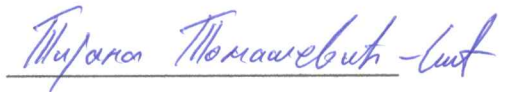УНИВЕРЗИТЕТ У БЕОГРАДУ

Предмет: Молба за покретање поступка за реизбор у звање научни сарадник

Молим Научно веће Института за физику, Универзитета у Београду, да у складу са Правилником о поступку, начину вредновања и квантитативном исказивању научно-истраживачких резултата истраживача, Министарства науке, технолошког развоја и иновација Републике Србије, покрене поступак за мој реизбор у звање научни сарадник.

У прилогу достављам:

1. Мишљење руководиоца пројекта са предлогом комисије која ће писати извештај;
2. Стручну биографију;
3. Преглед научне активности;
4. Елементе за квалитативну оцену научног доприноса кандидата;
5. Елементе за квантитативну оцену научног доприноса кандидата;
6. Списак објављених радова и других публикација разврстан по важећим категоријама прописаним Правилником;
7. Податке о цитираности кандидата;
8. Фотокопију решења о претходном избору у звање;
9. Копије објављених радова и других публикација;
10. Прилоге који документују изнете тврдње

У Београду, 28.05.2024.

Др Тијана Томашевић-Илић
Научни сарадник
Институт за физику Београд

НАУЧНОМ ВЕЋУ
ИНСТИТУТА ЗА ФИЗИКУ БЕОГРАД
УНИВЕРЗИТЕТ У БЕОГРАДУ

Предмет: Мишљење руководиоца лабораторије о реизбору у звање научни сарадник кандидата др Тијане Томашевић-Илић са предлогом комисије која ће писати извештај

Др Тијана Томашевић-Илић је запослена у Лабораторији за 2Д материјале Института за физику Београд, Универзитет у Београду. У истраживачком раду бави се темама везаних за добијање, модификацију и примену 2Д материјала и танких филмова 2Д материјала добијених из раствора, као и њихових хетероструктура.

С обзиром да кандидаткиња испуњава све услове предвиђене Законом о научно-истраживачкој делатности и Правилником о поступку, начину вредновања и квалитативном исказивању научноистраживачких резултата истраживача Министарства науке, технолошког развоја и иновација Републике Србије, сагласна сам са покретањем поступка за реизбор Тијане Томашевић-Илић у звање научни сарадник.

За чланове комисије за реизбор Тијане Томашевић-Илић у звање научни сарадник предлажем:

1. Др Јелену Пешић, виши научни сарадник, Института за физику Београд, Универзитет у Београду
2. Др Ивану Милошевић, научни сарадник, Институт за физику Београд, Универзитет у Београду
3. Др Ненада Лазаревића, научни саветник, Институт за физику Београд, Универзитет у Београду
4. Др Марка Спасеновића, научни саветник, Институт за хемију, технологију и металургију, Универзитет у Београду

У Београду, 28.05.2024.

Др Ивана Милошевић, научни сарадник
Руководилац Лабораторије за 2Д Материјале

1. СТРУЧНА БИОГРАФИЈА

Тијана (Драган) Томашевић-Илић рођена је 19. 10. 1982. године у Београду. Основне студије на Факултету за физичку хемију Универзитета у Београду завршила је 2011. године, одбраном дипломског рада „Испитивање глазура византијске керамике применом микро-раманске спектроскопије". Током 2011. и 2012. године била је учесник програма „Прва Шанса" у Централном институту за конзервацију. Мастер академске студије Факултета за физичку хемију Универзитета у Београду завршила је 2015. године, одбраном мастер рада „Сребрни филмови на нанокристалној TiO_2 подлози: синтеза, карактеризација и антимикробна активност". Исте године уписује докторске студије на Факултету за физичку хемију, Универзитет у Београду, и започиње свој научно-истраживачки рад као волонтер на Институту за физику Београд, Универзитет у Београду, у Лабораторији за 2Д материјале, Центра за чврсто стање и нове материјале. Докторску дисертацију под називом „Површинска модификација танких филмова графена ексфолираних из течне фазе и депонованог Лангмир-Блоцетовом методом" одбранила је 30. септембра 2019. године на Факултету за физичку хемију.

У Институту за физику запослена је од новембра 2016. године, а одлуком Матичног научног одбора за физику 24. јануара 2020. године стекла је звање научни сарадник. Њен рад у Лабораторији за 2Д материјале је фокусиран на ексфолијацију слојевитих, 2Д материјала из раствора, контролисану депозицију наноматеријала у танке филмове, функционализацију/површинску модификацију 2Д материјала различитим ковалентним и нековалентним стратегијама и истраживање примене танких филмова заснованих на 2Д материјалима (сензори, соларне ћелије, заштитне превлаке). Поред графена и дихалкогенида прелазних метала, такође ради на слојевитим изолаторима и низу других 2Д материјала. Учествовала је на националном пројекту ОИ171005 „Физика уређених наноструктура и нових материјала у нанофотоници" (2010-2019; ангажована од 2016. године), два пројекта билатералне сарадње између Србије и Немачке „Контролисана модификација електронских особина танких филмова дихалкогенида прелазних метала за примене у соларним ћелијама – комбиновани теоријско-експериментални приступ" и „Танки филмови ексфолираних ТМД-а из течне фазе за детекцију гаса" (2020-2021), иновационом пројекту „ Употреба наноматеријала за потребе ојачавања дрвета као конструктивног елемента" (2020-2021), као и иновационом пројекту „Доказ концепта" Института за физику Београд „Графеном импрегнирано дрво повећане биолошке отпорности и трајности" (2023-2024). Тренутно је ангажована на иновационом пројекту „Доказ концепта" Института за физику Београд „Оптимизација примене бактерија у синтези бионаночестица гвожђа"(2024).

Др Томашевић-Илић је руководилац националног пројекта „2D Material-based Tiled Network Films for Heritage Protection-2DHeriPro" програма ПРИЗМА Фонда за науку Републике Србије (2023-2026), као и пројекта билатералне сарадње између Републике Србије и Републике Аустрије „Модулација магнетних особина самоорганизованих филмова графена за детекцију загађења и пречишћавање отпадних вода" (2022-2024).

Такође, 2019. године Др Томашевић-Илић је учествовала и у Erasmus+KA 107 програму размене истраживача и међународне сарадње Института за физику у Београду и Универзитета у Хајделбергу, Немачка.

Др Тијана Томашевић-Илић је аутор/коаутор једанаест научних радова са СЦИ-листе (два М21а, четири М21, три М22 категорије, један М23 и један без категорије), као и двадесет саопштења са међународних конференција (деветнаест штампаних у изводу и један штампан у целини).

2. ПРЕГЛЕД НАУЧНЕ АКТИВНОСТИ Др ТИЈАНЕ ТОМАШЕВИЋ-ИЛИЋ

Научно-истраживачки рад, др Томашевић-Илић је првенствено фокусиран на ексфолијацију 2Д материјала из течне фазе, контролисану депозицију и испитивање морфолошких, структурних, оптичких и електронских особина танких филмова самоорганизованих структура 2Д материјала ексфолираних из раствора, њихову функционализацију/површинску модификацију и анализу промена на површини које настају у интеракцији ових материјала са спољашњом средином, укључујући истраживање примене танких филмова заснованих на 2Д материјалима (сензори, соларне ћелије, заштитне превлаке).

Научна активност кандидаткиње, **пре претходног избора у звање**, се грубо може поделити на три целине: испитивање утицаја површинске модификације танких филмова графена ексфолираног из течне фазе; ексфолијација и испитивање танких филмова других 2Д материјала; синтеза и површинска модификација танких филмова TiO2.

Први и најзначајнији део научне активности Др Тијане Томашевић-Илић, пре претходног избора у звање, обухватао је експериментално истраживање утицаја површинске модификације графена ексфолираног из течне фазе и депонованог Лангмир-Блоџетовом методом, на оптоелектронске особине добијених танких филмова. Метода ексфолијације из течне фазе, праћена Лангмир-Блоџетовом методом, која се заснива на (само)организацији наноструктура на течно-гасној међуфази индукованој површинским напоном материјала, представља једноставну, индустријски применљиву и економски исплативу процедуру којом се могу добити велике површине континуалних филмова графена, високе транспарентности на различитим подлогама. Међутим, танки филмови добијени на овај начин имају високу површинску отпорност која је последица самоорганизације љуспица графена у танке филмове која индукује велику густину дефеката филмова. Кандидаткиња је у оквиру резултата свог истраживања идентификовала природу дефеката у добијеним филмовима и показала да се применом агресивних метода површинске модификације/функционализације, као што су фотохемијска оксидација, хемијска функционализација азотном киселином и термално одгревање, површинска отпорност танких филмова графена ексфолираног из течне фазе и депонованог Лангмир-Блоџетовом методом на чврсте, али и транспарентне и флексибилне подлоге, може вишеструко смањити, при чему ниједна од поменутих метода не доводи до значајне промене високе транспаренције филмова. У циљу бољег

разумевања промене електричних својстава до којих долази при интеракцији различитих допаната са формираним филмовима графена испитивана су морфолошка, структурна, оптичка и електронска својства самоорганизованих структура пре и након примене датих метода површинске модификације, методама микроскопије атомских сила, скенирајуће електронске микроскопије, Раманове спектроскопије, инфрацрвене спектрометрије са Фуријеовом трансформацијом, спектрометрије фотоелектрона насталих озрачивањем рендгенским зрацима, УВ/ВИД спектрофотометрије и микроскопије сила Келвиновом пробом. Показано је да велика густина ивица, као доминантни тип дефеката филмова графена ексфолираног из раствора, има пресудну улогу у ефектима које примењене методе модификације имају на филмове. Азотна киселина, као п-тип допанта, примењена на испитиване филмове графена доводи до померања Фермијевог нивоа и смањења површинске отпорности, не утичући на транспаренцију филмова графена. Фотохемијска оксидација озоном из ваздуха примењена на графен добијен хемијском депозицијом из парне фазе, незнатне густине дефеката, проузрокује стварање дефеката у графенској равни и смањење проводности. Насупрот томе, кандидаткиња је показала да фотохемијска оксидација примењена на танке филмове графена са великом густином дефеката, у којима су ивице доминантан тип дефеката, доводи до допирања п-типа и смањењења ефекта ивица, што доприноси смањењу површинске отпорности филмова. Термално одгревање филмова графена не доводи до функционализације материјала, али у филмовима добијених депозицијом графена из раствора може отклонити заостали растварач и евентуално присутне адсорбоване врсте из ваздуха, што доводи до смањења површинске отпорности филмова не утичући на високу транспаренцију филмова. Резултати наведеног истраживања су приказани у оквиру три рада:

- **Tijana Tomašević-Ilić**, Đorđe Jovanović, Igor Popov, Rajveer Fandan, Jorge Pedrós, Marko Spasenović and Radoš Gajić, Reducing sheet resistance of self-assembled transparent graphene films by defect patching and doping with UV/ozone treatment, Applied Surface Science 458 (2018) 446–453.
- Aleksandar Matković, Ivana Milošević, Marijana Milićević, **Tijana Tomašević-Ilić**, Jelena Pešić, Milenko Musić, Marko Spasenović, Djordje Jovanović, Borislav Vasić, Christopher Deeks, Radmila Panajotović, Milivoj R. Belić, and Radoš Gajić, Enhanced sheet conductivity of Langmuir-Blodgett assembled graphene thin films by chemical doping, 2D Materials 3 (2016) 015002.
- **Tijana Tomašević-Ilić**, Jelena Pešić, Ivana Milošević, Jasna Vujin, Aleksandar Matković, Marko Spasenović and Radoš Gajić, Transparent and conductive films from liquid phase exfoliated graphene, Optical and Quantum Electronics 48 (2016) 319.

Поред научног истраживања које је било везано за испитивање танких филмова графена ексфолираног из раствора, кандидаткиња се бавила и анализом нанољуспица и танких филмова и других 2Д материјала, као што су молибден-дисулфид и хекса-борнитрид, ексфолијацијом ових материјала из течне фазе, оптимизацијом формирања филмова из раствора ових материјала, као и могућностима њихове примене у области оптоелектронике или заштитних превлака. Резултати овог истраживања су приказани у оквиру једног рада и презентовани на две конференције:

- Jelena Pešić, Jasna Vujin, **Tijana Tomašević‑Ilić**, Marko Spasenović and Radoš Gajić, DFT study of optical properties of MoS_2 and WS_2 compared to spectroscopic results on liquid phase exfoliated nanoflakes, Optical and Quantum Electronics 50 (2018) 291.
- **T. Tomašević-Ilić**, Đ. Jovanović, R. Panajotović, R. Gajić, M. Spasenović, Large-scale deposition of self-assembled thin films from liquid phase exfoliated h-BN, Photonica 2019, 26-30 Aug 2019, Belgrade, Serbia,, p.114.
- **Tijana Tomašević-Ilić**, Aleksandar Matković, Jasna Vujin, Radmila Panajotović, Marko Spasenović and Radoš Gajić, P-type field-effect transistors based on liquid phase exfoliated MoS_2, Graphene 2017, 28-31 March, 2017, Barcelona, Spain.

Такође, научна активност пре претходног избора у звање је обухватала и истраживање фокусирано на добијање танких филмова наночестичног сребра на нанокристалној подлози титанијум-диоксида и испитивање морфолошких и оптичких својстава добијених хетероструктура, као и њихова фотокаталитичке и антимикробне активности. Показано је да се површинском модификацијом нанокристалне подлоге титанијум-диоксида у виду формирања хетероструктуре филмова сребра и танких филмова титанијум-диоксида депонованог из колоидних раствора могу добити површине са повећаним фотокаталитичким и антимикробним својствима. Резултати овог истраживања су приказани у раду:

- Ivana D Vukoje, **Tijana D Tomašević-Ilić**, Aleksandra R Zarubica, Suzana Dimitrijević, Milica D Budimir, Mila R Vranješ, Zoran V Šaponjić and Jovan M. Nedeljković, Silver film on nanocrystalline TiO2 support: photocatalytic and antimicrobial ability, Materials Research Bulletin 60 (2014) 824-829.

Научна активност кандидата **након претходног избора у звање**, се такође може поделити на три целине: примена танких филмова 2Д материјала за детекцију гасова, површинска модификација танких филмова графена са циљем модулације њихових магнетних особина, и добијање и испитивање 2Д материјала који се могу користити као заштитне превлаке.

Након претходног избора у звање научна активност Др Томашевић-Илић је проширена на истраживање примене танких филмова графена и платина-диселенида ексфолираних из раствора, као сензора за детекцију гасова. Први део истраживања кандидаткиње у оквиру ове тематике фокусиран је на фабрикацију сензора на бази графена. Показано је да се танки филмови графена, ексфолираног из раствора и депонованог Лангмир-Блоцетовом методом, услед присуства велике густине дефеката-ивица на површини датог материјала могу ефикасно користити за детекцију влаге и фабрикацију флексибилних и транспарентних хемирезистора са брзим одзивом од 30 ms. Такође, показано је да сам процес ексфолијације графена утиче на перформансе добијених сензора. Други део истраживања кандидаткиње у оквиру ове тематике је био фокусиран на добијање хомогених филмова PtSe2 из раствора, ниске храпавости и контролисане дебљине. У оквиру овог истраживања кандидаткиња је променом површинског напона на фазној граници формирања танких филмова PtSe2 омогућила постизање површинског притиска за компресију насумично распоређених нанољуспица у организовану и умрежену наноструктуру. АФМ и СЕМ су потврдили фино

умрежавање нанољуспица у танак филм, а Раманска спектроскопија структуру карактеристичну за танак филм PtSe2. Својства и перформансе овако добијених филмова су тестирана у односу на филмове PtSe2 из раствора формираних насумичним распоређивањем нанољуспица. Добијени филмови су показали знатно већу проводљивост која је приписана бољој умрежености нанољуспица у филму. Добијени филмови су коришћени за фабрикацију сензора и тестирани за детекцију амонијака. Резултати овог истраживања показали су да се дати филмови могу користити као сензори са високом осетљивошћу (0.100 ppm) и брзим одзивом при излагању амонијаку. Такође, показано је да добијени филмови задржавају дугорочну стабилност, остајући функционални и ефикасни током периода од 15 месеци. Резултати истраживања у оквиру тематике везане за примену танких филмова 2Д материјала за детекцију гасова приказани су у оквиру три рада и једног саопштења на међународној конференцији:

- Stevan Andrić, **Tijana Tomašević-Ilić**, Marko V Bošković, Milija Sarajlić, Dana Vasiljević-Radović, Milče M Smiljanić, Marko Spasenović, Ultrafast humidity sensor based on liquid phase exfoliated graphene, Nanotechnology 32 (2020) 025505.
- Marko Spasenović, S Andrić, **Tijana Tomašević-Ilić**, Graphene-based Chemiresistive Gas Sensors, 2021 IEEE 32nd International Conference on Microelectronics (MIEL), 12-14 September 2021, Nis, Serbia, p 25-28
- Stevan Andrić, **Tijana Tomašević-Ilić**, Lazar Rakočević, Dana Vasiljević-Radović, Marko Spasenović, Three Types of Films from Liquid-phase-exfoliated Graphene for Use as Humidity Sensors and Respiration Monitors, Sensors and Materials 34 (2022) 3933-3947.
- Kangho Lee, Beata M Szydłowska, Oliver Hartwig, Kevin Synnatschke, Bartlomiej Tywoniuk, Tomáš Hartman, **Tijana Tomašević-Ilić**, Cian P Gabbett, Jonathan N Coleman, Zdeněk Sofer, Marko Spasenović, Claudia Backes, Georg S Duesberg, Highly conductive and long-term stable films from liquid-phase exfoliated platinum diselenide, Journal of Materials Chemistry C 11 (2023) 593-599.

Такође, научна активност кандидаткиње, након претходног избора је обухватала осмишљавање и извођење истраживања које укључује модулацију магнетних особина танких филмова графена њиховом хемијском функционализацијом наночестицама гвожђа. У оквиру овог истраживања, који је део билатералног пројекта којим кандидаткиња руководи, графен је ексфолиран методом ексфолијације из течне фазе, и допиран наночестицама гвожђа у току формирања филма. Површинска модификација графена је потврђена Раманском спектроскопијом, Инфрацрвеном спектроскопијом са Фуријеовом трансформацијом и XPS-ом, а МФМ фазне слике и профили су показали да допирање доводи до индукције локалног магнетног момента. Испитивана је примена добијених филмова за детекцију и адсорпцију тешких метала из водених раствора. XPS -мерења су показала да при интеракцији ових филмова са јонима тешких метала долази до њихове адсорпције, што указује да се магнетно модификовани филмови графена ексфолираног из раствора и депонованог Лангмир-Блоцетовом методом могу користити као магнетни адсорбери за детекцију метала и пречишћавање вода. Резултати овог истраживања су приказани на међународној конференцији:

1. Milošević Ivana, Vujin, Jasna, Muhammad Zubair Khan, Thomas Griesser, Christian Teichert, **Tomašević-Ilić Tijana**, Fe-nanoparticle-modified Langmuir-Blodgett Graphene Films for Pb(II) Water Purification, The 21th Symposium on Condesed Matter Physics-SFKM 2023, 26-30 June, Belgrade, Serbia, p.87

Поред поменутог, кандидаткиња је након претходног избора у звање започела истраживање које укључује ексфолијацију хекса-бор нитрида, и природних минерала, депозицију ексфолираног материјала у танке филмове и њихову примену као заштитних превлака за очување културне баштине. Дато истраживање се реализује у оквиру 2DHeriPro пројекта, чија је реализација започела 01. децембра 2023. године.

3. ЕЛЕМЕНТИ ЗА КВАЛИТАТИВНУ ОЦЕНУ НАУЧНОГ ДОПРИНОСА

3.1.Квалитет научних радова

3.1.1. Научни ниво и значај научних резултата, утицај научних радова

Др Тијана Томашевић-Илић је у досадашњој каријери била аутор/коаутор 10 научних радова у међународним часописима. Два рада су објављена у међународним часописима изузетних вредности (категорија М21а), четири у врхунским међународним часописима (категорија М21), два у истакнутим међународним часописима (категорија М22) и два у међународним часописима (категорија М23). Кандидаткиња је до сада учествовала на више међународних конференција у земљи и иностранству.

У периоду **након одлуке Научног већа о утврђивању предлога за претходни избор у звање**, Др Томашевић-Илић је била аутор/коаутор 4 научна рада у међународним часописима (три М21 и један М23 категорије) и 5 саопштења на међународним конференцијама (један М33 и четири М34 категорије).

Два рада се могу сматрати најзначајнијим радовима кандидаткиње у периоду за реизбор:

1. Kangho Lee, Beata M Szydłowska, Oliver Hartwig, Kevin Synnatschke, Bartlomiej Tywoniuk, Tomáš Hartman, **Tijana Tomašević-Ilić**, Cian P Gabbett, Jonathan N Coleman, Zdeněk Sofer, Marko Spasenović, Claudia Backes, Georg S Duesberg, Highly conductive and long-term stable films from liquid-phase exfoliated platinum diselenide, Journal of Materials Chemistry C 11 (2023) 593-599. https://doi.org/10.1039/D2TC03889G

Рад приказује прво успешно формирање хомогених филмова $PtSe_2$ из раствора, ниске храпавости и контролисане дебљине, детаљно описује процедуру добијања, хемијску структуру, морфологију, и електричне особине ових филмова, као и могућност њихове примене за детекцију амонијака. Иако није међу првим ауторима, кандидаткиња је применила модификовану Лангмир-Блоцетову методу за формирање филмова 2Д материјала и предложила методологију којим се омогућава добијање танких филмова $PtSe2$ из раствора и фабрикација испитиваних сензора, и стога се њен допринос у овом раду може сматрати кључним. Наиме, кандидаткиња је променом површинског напона на фазној граници формирања танких филмова $PtSe2$ омогућила постизање површинског притиска за компресију насумично распоређених нанољуспица у организовану и умрежену наноструктуру. АФМ и СЕМ су потврдили фино умрежавање нанољуспица у танак филм, а Раманска спектроскопија структуру карактеристичну за танак филм $PtSe_2$.

Добијени филмови су коришћени за фабрикацију сензора и тестирани за детекцију амонијака. Резултати овог истраживања показали су да се дати филмови могу користити као сензори са високом осетљивошћу (0.100 ppm) и брзим одзивом при излагању амонијаку. Такође, показано је да добијени филмови задржавају дугорочну стабилност, остајући функционални и ефикасни током периода од 15 месеци. Кључни рад у коме се огледа оригинални допринос кандидаткиње, до сада није био коришћен при избору у звање ни једног другог кандидата, што је у складу са условима прописаним Правилником о стицању истраживачких и научних звања Министарства науке, технолошког развоја и иновација Републике Србије.

2. Stevan Andrić, **Tijana Tomašević-Ilić**, Lazar Rakočević, Dana Vasiljević-Radović, Marko Spasenović, Three Types of Films from Liquid-phase-exfoliated Graphene for Use as Humidity Sensors and Respiration Monitors, Sensors and Materials 34 (2022) 3933-3947. https://doi.org/10.18494/SAM4092

У овом раду испитиване су перформансе танких филмова графена, депонованих Лангмир-Блоџетовом методом, као активних површина сензора за детекцију влаге и мониторинг дисања, при чему су се за формирање филмова користиле три различите врсте дисперзија графена. Графен је за потребе овог рада добијен ексфолијацијом из течне фазе, при чему је сам процес ексфолијације индукован на три различита начина (ултразвуком, електрохемијски и мешањем-смицањем). Структура, транспарентност, дебљина и морфологија ових филмова су испитиване спектрометријом фотоелектрона насталих озрачивањем рендгенским зрацима, УВ-ВИД спектрофотометријом и микроскопијом атомских сила. Показано је да процес ексфолијације графена у раствору може значајно утицати на перформансе добијеног сензора услед разлике у хомогености, дебљини и присуства адсорбованих функционалних група. Такође, иако је све три врсте сензора могуће користити за детекцију влаге и мониторинг дисања, показано је да сваки од њих има своје предности и мане. Сензори за које је коришћена дисперзија код које је ексфолијација индукована електрохемијски је најпоузданији, док је сензор за које је коришћена дисперзија код које је ексфолијација индукована ултразвуком најосетљивији. У оквиру овог рада Др Томашевић-Илић је дала допринос у виду ексфолијације графена и фабрикацији сензора, тумачењу и интерпретацији добијених резултата и писању оригиналног рукописа.

3.1.3. *Параметри квалитета часописа*

Кандидаткиња др Тијана Томашевић-Илић је објавила радове у следећим међународним часописима, при чему су подвучени они часописи у којима је кандидаткиња објавила радове након стицања претходног научног звања:

- 1 рад у часопису Solar Energy Materials and Solar Cells(ИФ$_{2023/2022}$=6,900; СНИП=1,56)
- 1 рад у часопису Journal of Materials Chemistry C (ИФ$_{2022}$=6,400; СНИП=1,23)
- 1 рад у часопису 2D Materials (ИФ$_{2016}$=6,937; СНИП=1,04)
- 1 рад у часопису Applied Surface Science (ИФ$_{2018}$=5,155; СНИП=1,35)
- 1 рад у часопису Nanotechnology (ИФ$_{2020}$=3,874; СНИП=0,81)
- 1 рад у часопису Materials Research Bulletin (ИФ$_{2014}$=2,288; СНИП=1,01)
- 1 рад у часопису Microelectronic Engineering (ИФ$_{2017}$=2,020; СНИП=0,95)

- 2 рада у часопису Optical and Quantum Electronics (ИФ$_{2016}$=1,055; СНИП=0,62; ИФ$_{2017}$=1,547; СНИП=0,63)
- 1 рад у часопису Sensors and Materials (ИФ$_{2022}$=1,200; СНИП=0,39)

Укупан импакт фактор објављених радова је 37,376, а након а након одлуке Научног већа о стицању претходног научног звања импакт фактор износи 18.374. Др Томашевић-Илић је објављивала радове у часописима угледних издавача (Elsevier, The Royal Society of Chemistry, IOP Publishing).

Додатни библиометријски показатељи квалитета часописа у којима је кандидаткиња објављивала радове (категорије М20) у периоду након одлуке Научног већа о претходном избору у научно звање приказано је у следећој табели:

	ИФ	М	СНИП
Укупно	18,374	27	3,990
Усредњено по чланку	4,594	6,750	0,998
Усредњено по аутору	2,253	3,085	0,430

3.1.2. Позитивна цитираност научних радова кандидата

Према подацима из базе Web of Science, радови др Тијане Томашевић-Илић су цитирани укупно 108 пута, од чега 84 пута изузимајући аутоцитате. Хиршов индекс је 6.

3.1.3. Међународна сарадња

Др Томашевић-Илић активно сарађује са групом за Микроскопију Скенирајућом Пробом Института за физику у Леобену, (СПМ-МУЛ), у оквиру билатералног пројекта између Србије и Аустрије, којим кандидаткиња руководи. Такође проф. Др Christian Teichert, (СПМ-МУЛ) је спољни сарадник 2DHeriPro пројекта Фонда за науку, чији је кандидаткиња руководилац.

3.2. Нормирање коауторских радова, патената и техничких решења

Сви радови спадају у категорију експерименталних радова у природно-математичким наукама, тако да се радови са 7 и мање коаутора узимају са пуном тежином, а радови са више коаутора (један М21 рад са 13 коаутора и један М21 рад са 11 коаутора) нормирају се по формули датој у Правилнику о поступку и начину вредновања и квантитативном исказивању научноистраживачких резултата истраживача.

3.3. Руковођење пројектима, потпројектима и пројектним задацима

Др Томашевић-Илић је руководилац два текућа пројекта:

- Национални пројекат Фонда за науку Републике Србије - програм ПРИЗМА „2D Material-based Tiled Network Films for Heritage Protection-2DHeriPro" (2023-2026)
- Билатерални пројекат између Републике Србије и Републике Аустрије „Magnetism Modulation of Self-Assembled Graphene Films for Wastewater Treatment" (2022-2024)

3.4. Активност у научним и научно-стручним друштвима

Др Томашевић-Илић је била члан организационог одбора 21. симпозијума физике кондензоване материје, одржаног у Београду, од 26-30 јуна 2023. године.

3.5. Утицај научних резултата

Утицај научних резултата кандидата описани су у тачкама 3.1.1, 3.1.2 и 3.1.3 овог одељка, као и у прилогу о цитираности.

3.6. Конкретан допринос кандидата у реализацији радова у научним центрима у земљи и иностранству

Кандидаткиња је највећи део своје истраживачке делатности реализовала у Институту за физику Београд. Значајно је допринела свим радовима у којима је коаутор. Допринос се огледа у синтези узорака, у анализи података добијених одговарајућим методама карактеризације, као и у презентацији и интепретацији резултата и писању радова. Такође, кандидаткиња је последњи аутор на два рада М30 категорије у оквиру којих је дала допринос у осмишљавању и извођењу истраживања, као и презентацији резултата. Наставила је постојећу сарадњу Лабораторије за 2Д материјале са групом за Микроскопију Скенирајућом Пробом, Института за физику у Леобену, у оквиру билатералниог пројекта између Србије и Аустрије, којим кандидаткиња руководи. Остварила је сарадњу са Факултетом примењених уметности, Универзитет уметности у Београду у оквиру сарадње на пројекту Фонда за науку Републике Србије којим кандидаткиња руководи. Током свог рада кандидаткиња је показала завидан ниво самосталности и способности за научни рад.

3.7. Предавања на конференцијама, друга предавања и активности

Након претходног избора у звање Др Томашевић-Илић је одржала предавање на међународној конференцији „71st Annual Meeting of the Austrian Physical Society", OPG 2022, 2022. године у Леобену, Аустрија.

Такође, кандидаткиња је одржала и Progress Report на међународној конференцији „VIII International School and Conference on Photonic", Photonica 2021, 2021 године у Београду, Србија.

4. ЕЛЕМЕНТИ ЗА КВАНТИТАТИВНУ ОЦЕНУ НАУЧНОГ ДОПРИНОСА

Остварени М-бодови по категоријама публикација

Категорија	М-бодова по публикацији	Број публикација	Укупно М-бодова	Укупно М-бодова **Нормирано**
М21	8	3	24	16,08
М23	3	1	3	3
М33	1	1	1	1
М34	0,5	4	2	2

Поређење оствареног броја М-бодова са минималним условима потребним за избор у звање научни сарадник

	Потребно	Остварено М-бодова	Остварено М-бодова **Нормирано**
Укупно	16	30	22,08
М10+М20+М31+М32+М33+М41+М42	10	28	20,08
М11+М12+М21+М22+М23	6	27	19,08

5. СПИСАК РАДОВА И ОСТАЛИХ ПУБЛИКАЦИЈА

Радови у међународном часопису изузетних вредности (М21а)

- објављени пре претходног избора у звање-

1. **Tijana Tomašević-Ilić**, Đorđe Jovanović, Igor Popov, Rajveer Fandan, Jorge Pedrós, Marko Spasenović and Radoš Gajić, Reducing sheet resistance of self-assembled transparent graphene films by defect patching and doping with UV/ozone treatment, Applied Surface Science 458 (2018) 446–453.
2. Aleksandar Matković, Ivana Milošević, Marijana Milićević, **Tijana Tomašević-Ilić**, Jelena Pešić, Milenko Musić, Marko Spasenović, Djordje Jovanović, Borislav Vasić, Christopher Deeks, Radmila Panajotović, Milivoj R. Belić, and Radoš Gajić, Enhanced sheet conductivity of Langmuir-Blodgett assembled graphene thin films by chemical doping, 2D Materials 3 (2016) 015002.

Радови у врхунском међународном часопису (М21)

- објављени након претходног избора у звање-

1. Djordje Jovanović, Miloš Petrović, **Tijana Tomašević-Ilić**, Aleksandar Matković, Matevž Bokalič, Marko Spasenović, Konstantinos Rogdakis, Emmannuel Kymakis, Dragan Knežević, Lucio Cinà, Radoš Gajić, Long-term stability of graphene/c-Si Schottky-junction solar cells, Solar Energy Materials and Solar Cells 258 (2023) 112414.
2. Kangho Lee, Beata M Szydłowska, Oliver Hartwig, Kevin Synnatschke, Bartlomiej Tywoniuk, Tomáš Hartman, **Tijana Tomašević-Ilić**, Cian P Gabbett, Jonathan N Coleman, Zdeněk Sofer, Marko Spasenović, Claudia Backes, Georg S Duesberg, Highly conductive and long-term stable films from liquid-phase exfoliated platinum diselenide, Journal of Materials Chemistry C 11 (2023) 593-599.
3. Stevan Andrić, **Tijana Tomašević-Ilić**, Marko V Bošković, Milija Sarajlić, Dana Vasiljević-Radović, Milče M Smiljanić, Marko Spasenović, Ultrafast humidity sensor based on liquid phase exfoliated graphene, Nanotechnology 32 (2020) 025505.

- објављени пре претходног избора у звање-

1. Ivana D Vukoje, **Tijana D Tomašević-Ilić**, Aleksandra R Zarubica, Suzana Dimitrijević, Milica D Budimir, Mila R Vranješ, Zoran V Šaponjić and Jovan M. Nedeljković, Silver film on nanocrystalline TiO2 support: photocatalytic and antimicrobial ability, Materials Research Bulletin 60 (2014) 824-829.

Радови у истакнутом међународном часопису (М22)

- објављени пре претходног избора у звање-

1. S. Djurić, G. Kitić, J. Dubourg, R. Gajić, **T. Tomašević-Ilić**, V. Minić and M. Spasenović, Miniature graphene-based supercapacitors fabricated by laser ablation, Microelectronic Engineering 182 (2017) 1-7.

2. **Tijana Tomašević-Ilić**, Jelena Pešić, Ivana Milošević, Jasna Vujin, Aleksandar Matković, Marko Spasenović and Radoš Gajić, Transparent and conductive films from liquid phase exfoliated graphene, Optical and Quantum Electronics 48 (2016) 319.

Радови у међународном часопису (М23)

- објављени након претходног избора у звање-

1. Stevan Andrić, **Tijana Tomašević-Ilić**, Lazar Rakočević, Dana Vasiljević-Radović, Marko Spasenović, Three Types of Films from Liquid-phase-exfoliated Graphene for Use as Humidity Sensors and Respiration Monitors, Sensors and Materials 34 (2022) 3933-3947

- објављени пре претходног избора у звање-

5. Jelena Pešić, Jasna Vujin, **Tijana Tomašević-Ilić**, Marko Spasenović and Radoš Gajić, DFT study of optical properties of MoS2 and WS2 compared to spectroscopic results on liquid phase exfoliated nanoflakes, Optical and Quantum Electronics 50 (2018) 291.

Саопштења са међународног скупа штампана у целини (М33)

- објављени након претходног избора у звање-

1. Marko Spasenović, S Andrić, **Tijana Tomašević-Ilić**, Graphene-based Chemiresistive Gas Sensors, 2021 IEEE 32nd International Conference on Microelectronics (MIEL), 12-14 September 2021, Nis, Serbia, p 25-28

Саопштење са међународног скупа штампано у изводу (М34)

- објављени након претходног избора у звање-

2. Milošević Ivana, Vujin, Jasna, Muhammad Zubair Khan, Thomas Griesser, Christian Teichert, **Tomašević-Ilić Tijana**, Fe-nanoparticle-modified Langmuir-Blodgett Graphene Films for Pb(II) Water Purification, The 21th Symposium on Condesed Matter Physics-SFKM 2023, 26-30 June, Belgrade, Serbia, p.87
3. **Tijana Tomasevic-Ilic**, Langmuir-Blodgett films from liquid phase exfoliated 2D materials, 71st Annual Meeting of the Austrian Physical Society, OPG 2022, 26-30 September 2022, Leoben, Austria, p. 96-97
4. **T. Tomasević-Ilić**, N. Škoro, N. Puač, M. Spasenović, Plasma-assisted nitrogen doping of Langmuir-Blodgett self-assembled graphene films, VIII International School and Conference on Photonic, Photonica 2021, 23-27 Aug 2021, Belgrade, Serbia, p. 86.
5. **T. Tomasević-Ilić**, M. Spasenović, Langmuir-Blodgett films from liquid phase exfoliated 2D materials: surface modification and optoelectronic properties, VIII International School and Conference on Photonic, Photonica 2021, 23-27 Aug 2021, Belgrade, Serbia, p. 49.

- објављени пре претходног избора у звање-

1. **T. Tomašević-Ilić**, Đ. Jovanović, R. Panajotović, R. Gajić, M. Spasenović, Large-scale deposition of self-assembled thin films from liquid phase exfoliated h-BN, Photonica 2019, 26-30 Aug 2019, Belgrade, Serbia,, p.114.

2. S. Andrić, **T. Tomašević-Ilić**, D. Vasiljević-Radović, M. Spasenović, The influence of nanosheet size on formation of graphene films by Langmuir-Blodgett deposition from the liquid phase, Photonica 2019, 26-30 Aug 2019, Belgrade, Serbia, p. 107.

3. S. Andrić, **T. Tomašević-Ilić**, M. Sarajlić, Ž. Lazić, K. Cvetanović Zobenica, M. Rašljić, M. Smiljanić, and M. Spasenović, Humidity sensing with Langmuir-Blodgett assembled graphene films from liquid phase, chem2Dmater, 03-06 September 2019, Dresden, Germany, p. 116.

4. Djordje Jovanović, **Tijana Tomašević-Ilić**, Nikola Tasić, Aleksandar Matković, Marko Spasenović and Radoš Gajić, Emmanuel Kymakis, Silicon going indoors, NanoBio 2018, 24-28 September, 2018, Heraclion, Crete, p.119

5. **Tijana Tomašević-Ilić**, Aleksandar Matković, Jasna Vujin, Radmila Panajotović, Marko Spasenović and Radoš Gajić, P-type field-effect transistors based on liquid phase exfoliated MoS2, Graphene 2017, 28-31 March, 2017, Barcelona, Spain.

6. **T. Tomašević-Ilić**, Dj. Jovanović, J. Pešić, A. Matković, M. Spasenović and R. Gajić, Enhancing conductivity of self-assembled transparent graphene films with UV/Ozone Treatment, Photonica 2017, 28. Aug - 1. Sep, 2017, Belgrade, Serbia, p. 80.

7. J. Pešić, J. Vujin, **T. Tomašević-Ilić**, M. Spasenović and R. Gajić, Ab-initio study of optical properties of MoS2 and WS2 compared to spectroscopic results of liquid phase exfoliated nanoflakes, Photonica 2017, Aug - 1. Sep, 2017, Belgrade, Serbia, p.94.

8. T. Szabó, J. Vujin, **T. Tomaševic**, R. Panajotović, A. E. Sarrai, Sz. Zsolt, G. Váró, K. Hajdu, M. Botond, K. Hernádi and L. Nagy, Posiible applications of carbon based bio-nanocomposites in optoelectronics, XXVIst Congress of the Hungarian Biophysical Society, August 22-25 2017, Szeged, p.54.

9. T. Szabó, **T. Tomaševic**, R. Panajotović, J. Vujin, A. E. Sarrai, G. Váró, Zs. Szegletes, G. Garab, K. Hajdu and L. Nagy, Photosynthetic reaction-center/graphene biohybrid for optoelectronics, 5th International Conference on Biosensing Technology, 7-10 May 2017, Riva del Garda, Italy, p.121.

10. Marko Spasenović, **Tijana Tomašević-Ilić**, Aleksandar Matković and Radoš Gajić, Transparent and Conductive Films From Liquid Phase Exfoliated Graphene, EuroScience Open Forum – ESOF 2016, 24-27 July 2016, Manchester, United Kingdom, p. 40-41.

11. Djordje Jovanović, **Tijana Tomašević**, Aleksandar Matković, Nikola Tasić and Rados Gajić, Low light solar cells, 13th International Conference on Nanosciences and Nanotechnologies, NN16, 5-8 July 2016, Thessaloniki, Greece, p.289.

12. D. Jovanović, **T. Tomašević**, A. Matković, M. Musić, N. Tasić, M. Spasenović and R. Gajić, Low light low cost solar cells, 3rd International School and Conference on Optoelectronics, Photonics, Engineering and Nanostructures, Saint Petersburg OPEN 2016, 28 – 30 March 2016, St Petersburg, Russia, p.205.

13. **T. Tomašević-Ilić**, J. Pešić, I. Milošević, J. Vujin, A. Matković, M. Spasenović and R. Gajić, Transparent and conductive films from liquid phase exfoliated graphene, the Fifth international school and conference on photonics, Photonica 2015, 24-28 August 2015, Belgrade, Serbia, p.191.

14. A. Matković, I. Milošević, M. Milićević, **T. Tomašević-Ilić**, J. Pešić, M. Musić, M. Spasenović, Dj. Jovanović, B. Vasić, M. R. Belić and R. Gajić, Chemical Doping of Langmuir-Blodgett Assembled Graphene Films for Flexible Transparent Conductive

Electrodes, the 19th Symposium on Condensed Matter Physics - SFKM 2015, 7 – 11 September 2015, Belgrade, Serbia, p.93.

15. A. Matković, I. Milošević, M. Milićević, A. Beltaos, **T. Tomašević-Ilić**, J. Pešić, M. M. Jakovljević, M. Musić, U. Ralević, M. Spasenović, Dj. Jovanović, B. Vasić, G. Isić and R. Gajić, Spectroscopic and Scanning Probe Microscopic Investigations and Characterization of Graphene, the 19th Symposium on Condensed Matter Physics - SFKM 2015, 7 – 11 September 2015, Belgrade, Serbia, p.32.

MENU

Citation Report

Tijana Tomasevic-Ilic (Author)

Analyze Results | 🔔 Create Alert

⬇ Export Full Report

Publications

10
Total

From 1996 ⌄ to 2024 ⌄

Citing Articles

79 Analyze
Total

70 Analyze
Without self-citations

Times Cited

108
Total

84
Without self-citations

10.8
Average per item

6
H-Index

Times Cited and Publications Over Time

DOWNLOAD

Publications	Citations
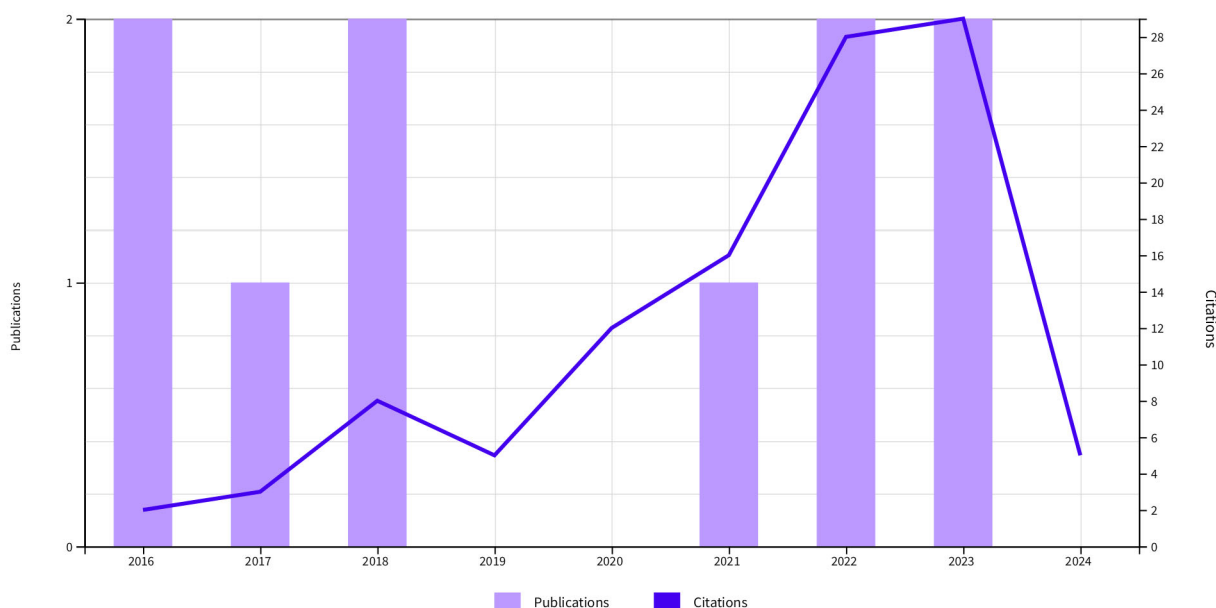
10 Publications	Sort by: Citations: highest first ▼	‹ 1 of 1 ›	Citations						
			‹ Previous year			Next year ›	Average per year	Total
			2020	2021	2022	2023	2024		
	Total		12	16	28	29	5	12	108
1	Enhanced sheet conductivity of Langmuir-Blodgett assembled graphene thin films by chemical doping Matkovic, A; Milosevic, I; (...); Gajic, R Mar 2016 | 2D MATERIALS 3 (1)		4	2	5	4	2	2.89	26
2	Reducing sheet resistance of self-assembled transparent graphene films by defect patching and doping with UV/ozone treatment Tomasevic-Ilic, T; Jovanovic, D; (...); Gajic, R Nov 15 2018 | APPLIED SURFACE SCIENCE 458 , pp.446-453		4	6	7	7	0	3.57	25
	Transparent and conductive films from liquid phase exfoliated graphene								

#	Title						Average	Total
3	Tomasevic-Ilic, T; Pesic, J; (…); Gajic, R Jun 2016 | OPTICAL AND QUANTUM ELECTRONICS 48 (6)	3	3	5	4	0	2.11	19
4	**Miniature graphene-based supercapacitors fabricated by laser ablation** Djuric, SM; Kitic, G; (…); Spasenovic, M Oct 5 2017 | MICROELECTRONIC ENGINEERING 182 , pp.1-7	1	3	3	3	0	1.75	14
5	**Ultrafast humidity sensor based on liquid phase exfoliated graphene** Andric, S; Tomasevic-Ilic, T; (…); Spasenovic, M Jan 8 2021 | NANOTECHNOLOGY 32 (2) Enriched Cited References	0	2	5	3	1	2.75	11
6	**DFT study of optical properties of MoS_2 and WS_2 compared to spectroscopic results on liquid phase exfoliated nanoflakes** PeiAç, J; Vujin, J; (…); Gajic, R Jul 2018 | OPTICAL AND QUANTUM ELECTRONICS 50 (7)	0	0	3	3	1	1	7
7	**Highly conductive and long-term stable films from liquid-phase exfoliated platinum diselenide** Lee, KH; Szydlowska, BM; (…); Duesberg, GS Jan 5 2023 | JOURNAL OF MATERIALS CHEMISTRY C 11 (2) , pp.593-599 Enriched Cited References	0	0	0	4	0	1.33	4
8	**Three Types of Films from Liquid-phase-exfoliated Graphene for Use as Humidity Sensors and Respiration Monitors** Andric, S; Tomasevic-Ilic, T; (…); Spasenovic, M 2022 | SENSORS AND MATERIALS 34 (11)	0	0	0	1	1	0.67	2
9	**Long-term stability of graphene/c-Si Schottky-junction solar cells** Jovanovic, D; Petrovic, M; (…); Gajic, R Aug 15 2023 | SOLAR ENERGY MATERIALS AND SOLAR CELLS 258 Enriched Cited References	0	0	0	0	0	0	0
10	**Plasma-Assisted Nitrogen Doping of Langmuir-Blodgett Self-Assembled Graphene Films** Tomasevic-Ilic, T; Skoro, N; (…); Spasenovic, M Jun 2023 | CONDENSED MATTER 8 (2)	0	0	0	0	0	0	0

Citation Report Publications Table

Република Србија
**МИНИСТАРСТВО ПРОСВЕТЕ,
НАУКЕ И ТЕХНОЛОШКОГ РАЗВОЈА**
Матични научни одбор за физику

Број: 660-01-00057/2019-14/5
24.01.2020. године
Б е о г р а д

На основу члана 27. став 1 тачка 1) и члана 76. став 5. Закона о науци и истраживањима („Службени гласник Републике Србије", бр. 49/2019) и Правилника о поступку, начину вредновања и квантитативном исказивању научноистраживачких резултата истраживача („Службени гласник Републике Србије", број 24/16, 21/17 и 38/17) и захтева који је поднео

Институт за физику у Београду

Матични научни одбор за физику на седници одржаној 24.01.2020. године, донео је

ОДЛУКУ
О СТИЦАЊУ НАУЧНОГ ЗВАЊА

Др Тијана Томашевић Илић

стиче научно звање
Научни сарадник

у области природно-математичких наука - физика

О Б Р А З Л О Ж Е Њ Е

Институт за физику у Београду

утврдио је предлог број 2075/1 од 17.12.2019. године на седници Научног већа Института за физику и поднео захтев Матичном научном одбору за физику број 2086/1 од 18.12.2019. године за доношење одлуке о испуњености услова за стицање научног звања **Научни сарадник.**

Матични научни одбор за физику на седници одржаној 24.01.2020. године разматрао је захтев и утврдио да именована испуњава услове из члана 76. став 5. Закона о науци и истраживањима („Службени гласник Републике Србије", бр. 49/2019) и Правилника о поступку, начину вредновања и квантитативном исказивању научноистраживачких резултата истраживача („Службени гласник Републике Србије", број 24/16, 21/17 и 38/17) за стицање научног звања **Научни сарадник** па је одлучио као у изреци ове одлуке.

Доношењем ове одлуке именовани стиче сва права која му на основу ње по закону припадају.

Одлуку доставити подносиоцу захтева, именованом и архиви Министарства просвете, науке и технолошког развоја у Београду.

МИНИСТАР

Младен Шарчевић

**МАТИЧНИ НАУЧНИ ОДБОР ЗА ФИЗИКУ
ПРЕДСЕДНИК**

проф. др Милан Дамњановић
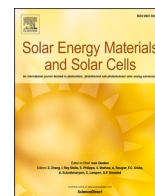
Long-term stability of graphene/c-Si Schottky-junction solar cells

Djordje Jovanović [a,*], Miloš Petrović [b], Tijana Tomašević-Ilić [a], Aleksandar Matković [c], Matevž Bokalič [d], Marko Spasenović [e], Konstantinos Rogdakis [b,f], Emmannuel Kymakis [b,f], Dragan Knežević [g], Lucio Cinà [h], Radoš Gajić [a]

[a] *Institute of Physics Belgrade, University of Belgrade, Pregrevica 118, 11000, Belgrade, Serbia*
[b] *Department of Electrical & Computer Engineering, Hellenic Mediterranean University (HMU), Heraklion, 71410, Crete, Greece*
[c] *Institute of Physics, Montanuniversität Leoben, Franz Josef Strasse 18, 8700, Leoben, Austria*
[d] *Faculty of Electrical Engineering, University of Ljubljana, Trzaska cesta 25, SI-1000, Ljubljana, Slovenia*
[e] *Center for Microelectronic Technologies, Institute of Chemistry, Technology and Metallurgy, University of Belgrade, 11000, Belgrade, Serbia*
[f] *Institute of Emerging Technologies (i-EMERGE) of HMU Research Center, Heraklion, 71410, Crete, Greece*
[g] *Military Technical Institute, Ratka Resanovića 1, 11000, Belgrade, Serbia*
[h] *Cicci Research s.r.l., Via Giordania 227, 58100, Grosseto, GR, Italy*

A R T I C L E   I N F O

A B S T R A C T

A long operational lifetime is required for the use of solar cells in real-life photovoltaic applications. The optimization of operational lifetimes is achieved through understanding the inherent degradation phenomena in solar cells. In this study, graphene/Si Schottky-junction solar cells were produced, utilizing liquid-phase-exfoliated graphene as an active surface. The operational and interface stability of these solar cells over a period of 5 years in ambient conditions (following ISOS-D protocols: dark storage/shelf life) was examined, and the origin of their degradation was reported. It was found that the dominant degradation mechanism could be attributed to the degradation of silver contacts. This was indicated by a decrease in shunt resistance, an increase in the ideality factor (due to a higher carrier recombination), and a constant defect density in graphene films for up to 4 years. Measurements across the solar cell's active area during the 5-year period revealed neither significant spatial inhomogeneity, nor shunt channel defects.

1. Introduction

As global energy demands increase annually in conjunction with technological advancements and a rising trend in connectivity, there is a clear need for compact and reliable clean energy sources [1]. Presently, solar energy harvesting competes favorably with other energy sources worldwide and no longer requires subsidies to remain competitive [2]. This represents a significant de-globalization trend in the energy field, driven by countries seeking solutions for energy resilience. Photovoltaic (PV) technologies have already made considerable commercial progress and are projected to contribute more than 5% of the global energy demand by 2025 [3]. Scaling up to 5 TW of solar energy production (~15% of global demand) by 2030, or even achieving 30% of the world's energy demand (~10 TW), in accordance with the EU Strategic Energy Technology Plan target by 2040–2050 [3–5], appears to be attainable. To accomplish these goals, investments in new solar/coal facilities should currently follow a ratio of 9:1 [6]. This serves as a compelling argument

for additional research and development on emerging PV absorbers to diversify the existing portfolio of solar technologies [7]. Inorganic crystalline silicon (c-Si)-based single-junction PV cells currently dominate terrestrial solar energy conversion due to their high efficiency (>20%), low cost (<0.5 $/W), and good reliability (approximately 25 years) [7,8]. However, organic devices such as organic solar cells (OSC or OPV) [9], dye-sensitized solar cells (DSSC) [10], and perovskite solar cells (PSC) [11] need to achieve improved stability, environmentally safe materials, and production processes to become technologically viable [12–14].

In addition to power conversion efficiency (PCE), there are other crucial aspects to consider in PV energy harvesting, such as stability, manufacturing cost, and ease of processing [15,16]. When it comes to commercial applications, the long-term stability of solar cell (SC) devices in relation to air, humidity, temperature, and light exposure over an extended period is of utmost importance. Real-life applications necessitate long operational lifetimes for solar cell devices, and

---

understanding and mitigating degradation phenomena are prerequisites for the successful implementation of promising technologies beyond silicon [12].

Additionally, the development of small-scale, lightweight, and portable PV devices for indoor usage, known as iPV (indoor Photovoltaic) [17,18], presents an attractive direction for meeting the energy demands of low-power consumption devices. The future market for self-powered electronics as part of the Internet of Things (IoT), including distributed sensors, remote actuators, and communication devices, holds significant potential for iPV applications [19,20]. When integrated into solar cells, graphene serves multiple functions owing to its high transparency and charge mobility, making it a viable alternative to conventional transparent electrodes such as indium tin oxide (ITO) and fluorine doped tin oxide (FTO) [21]. Moreover, a built-in electric field is developed at the graphene/silicon (Gr/Si) interface, aiding in the collection of photogenerated charge carriers [22].

Groundbreaking research on graphene/silicon (Gr/Si) junctions [23] demonstrates the integration of graphene into a Schottky junction with n-doped Si, achieving a power conversion efficiency (PCE) of 1.5%. Substantial improvements exceeding 2% have been observed under low-illumination conditions (0.15 Sun). However, a major obstacle that hampers the performance of graphene/Si solar cells is the poor fill factor [23]. This indicates that charge transport and recombination rates occur on a similar timescale, leading to competitive processes often visually represented by the appearance of an "s-kink" in the current–voltage curves [24]. To address this challenge, one approach is chemical doping, such as using trifluoromethanesulfonic acid (TFSA), which has yielded a PCE of 8.6% [25]. Another strategy involves the inclusion of a buffer oxide layer to reduce the transport barrier, resulting in a PCE surpassing 10% [24]. A more complex method for enhancing PCE involves fine-tuning the graphene Fermi level. This can be accomplished by employing graphene as a gating electrode, covering the dielectric barrier over the semiconductor substrate, leading to a high open-circuit voltage (>0.9 V) and a remarkably high PCE (18.5%) [26].

The study of graphene/Si Schottky junctions for indoor light harvesting has been limited [23], but there are reports focusing on stability. These reports indicate an operational stability of 90%, 80%, and 70% for 7, 30, and 90 days, respectively [14]. On the other hand, the performance and stability of solar cell architectures, other than graphene, in indoor applications [19,20] or stability field [9–11,27,28] have been extensively studied. Indoor photovoltaics (iPV) based on a-Si:H demonstrate a suppression of the fill factor (FF) from 56% to 53%, which then remains constant for 7 days, achieving up to 21% efficiency [29]. Commercial a-Si:H iPV under white LED or fluorescent light (FL) lighting ranges from 4.4% to 9.2% efficiency. Dye-sensitized solar cells (DSSCs) have achieved 51.6% operational stability (efficiency) after 273 h of continuous one-sunlight soaking in hybrid devices [10]. In iPV, DSSCs exhibit 34% efficiency for 1000 lx FL, with extrapolated lifetimes of 25–40 years for DSSCs with hydrophobic dyes. Organic photovoltaics (OPVs) have demonstrated 1330 h of operational stability at the maximum power point (MPPT) [30], and 31% power conversion efficiency (PCE) for 1650 lx white LED (WLED). Quantum dot solar cells (QDSCs) have achieved 9.7% efficiency under 1000 lx LED light for Si QD-based hybrid PVs and 19.5% efficiency under 2000 lux FL for colloidal metal chalcogenide quantum dots (QDs). Perovskite solar cells (PSCs) maintain 90% of initial efficiency over a 2400-h test in ambient conditions with 25% humidity [27]. Encapsulated PSCs have demonstrated 18.7% PCE with 95% operational stability after 3 months of outdoor exposure [28]. Lead–halide perovskite (MAPbI3) has achieved an iPV PCE of 37.2% under 1000 lx WLED.

Our study aims to validate the long-term environmental operational stability of these devices over a 5-year period and identify the critical structural mechanisms responsible for performance degradation during the aging process. Additionally, a proposed low-cost fabrication method for graphene-based electrodes is presented, highlighting its potential for stable graphene/Si Schottky-junction solar cells. Finally, suggestions are made on mitigating these negative effects by adjusting the trade-off between device design and fabrication cost, particularly through the use of solution-based graphene fabrication. The prospective applications of such devices were found to be suitable for the compact off-grid (without battery) supply of IoT sensors in indoor conditions.

2. Experimental section

2.1. Material, production, and chemicals

2.1.1. Graphene film synthesis and fabrication

Stock graphene dispersions were produced from commercially available graphite powder (Sigma Aldrich) with an initial concentration of 18 mg/ml by liquid phase exfoliation in N-methyl-2-pyrrolidone (NMP, Sigma Aldrich, product no. 328634), following the same procedure as previously reported [31–33]. Dispersions of liquid-phase-exfoliated (LPE) graphene were used for thin film formation by Langmuir-Blodgett self-assembly (LBSA) at the toluene-water interface [34]. Quartz, Si/SiO_2, and prepatterned Si/SiO_2 wafers were used as substrates. Surface modification of the prepared films was realised by annealing and UV/O_3 treatment. The annealing was carried out in a tube furnace at 300 °C in an argon atmosphere for 2 h. UV/ozone treatment was performed by exposing the graphene films to ultraviolet radiation and ozone for 5 min at 50 °C chamber temperature in a Novascan UV/Ozone Cleaner.

2.1.2. Silicon wafers

We used Si/SiO2 <100> c-Si wafers (525 μm thick) with an SiO_2 (300 nm thick) layer on top. The Si wafers are doped with As to a concentration of $N_d = 1.2–7.4e^{19}$ cm^{-3}. They have R = 0.001–0.01 Ω-cm, electron affinity Xsi = 4.05 eV, electron mobility = ~45 cm^2/Vs, Kr effective Richardson constant = 120 A/cm^{2}K^2, relative permittivity ε = 11.7 [35] −11.9 [23], $\varepsilon_0 = 8.854 \times 10^{-12}$ F cm−1, dEgap ~75 meV, and an optical band gap Eg,1 = 1.03 [36] with a work function = 4.4 eV. The data are provided by the wafer manufacturer (Inseto, UK).

2.2. Solar cell fabrication, functionalization, and storage

SCs are formed by Schottky junctions between graphene films and highly n-doped c-Si, as schematically shown in Fig. 1a. Graphene films are deposited on pre-patterned Si/SiO$_2$ wafers (with different Si-junction (active) square areas ranging from 0.8 mm^2 to 1.2 mm^2). Contacts of the front (graphene anode) and back (Si cathode) electrodes were made with a silver paste. In order to increase device performance, the obtained graphene films were thermally annealed (A films) and then exposed to photochemical oxidation (AO films) [31]. Two different types of solar cells were assembled using A and AO graphene films. The annealing process is utilized to remove residual solvents and increase connections between the graphene layers, while the UV/ozone treatment decreased the density of the defects [31]. Solar cells were kept for 5 years on the shelf, i.e., in environmental conditions, according to ISOS-D protocols: dark storage/shelf life [37].

2.3. Material analysis

The optical and electrical characterization of A and AO graphene films was performed with UV-VIS spectrophotometry, Raman spectroscopy, and two-point probe resistance measurements. An additional analysis of pristine graphene films was performed with atomic force microscopy (AFM) and Kelvin Probe Force Microscopy (KPFM).

Optical transmittance was obtained with a UV-VIS spectrophotometer (PerkinElmer Lambda 4B UV-VIS) on quartz wafers. Raman was performed with a TriVista 557 S&I GmbH Micro Raman spectrometer (λ = 532 nm) at room temperature, with a Coherent laser power of 20 mW, using a 50X objective. The two-point resistance of each graphene film, R$_{sheet}$, was calculated by considering sample geometry factors.
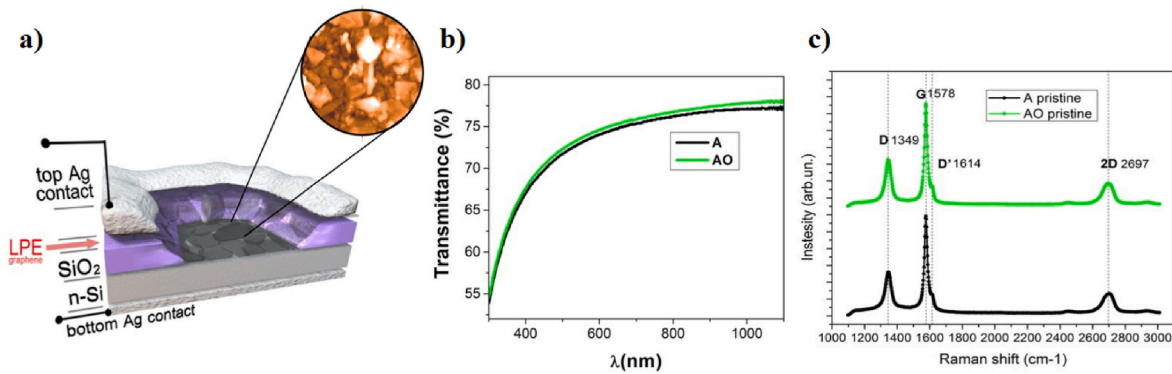
Fig. 1. a) Graphene/c-Si Schottky-junction solar cell with an AFM topography image in the inset (inset diameter 1 μm, z scale 100 nm), b) optical transmittance of graphene films on quartz substrates, c) Raman spectra of pristine A and AO graphene films on the Si/SiO$_2$ substrate.

The surface morphology of the films was characterized with a Horiba/AIST-NT Omegascope atomic force microscope (AFM) in tapping mode. Aseylec probes were employed (spring constant ~ 42 N/m, resonant frequency ~ 70 kHz, tip radius below 30 nm). Amplitude-modulated (AM)-KPFM measurements were carried out in a two-pass mode under ambient conditions, with the probe lifted 25 nm during the second pass. Topography and contact potential difference (CPD) images were processed in the open-source software, Gwyddion v2.56. In the case of topography images, zero-order line-filtering was applied, as well as leveling of the base plane. In the case of CPD images, only zero-order line-filtering was applied and the data were summed in a histogram. For KPFM measurements, the graphene films were grounded and supported by SiO$_2$. Before and after the work function (WF) of each graphene film was measured, a freshly cleaved HOPG surface (scanned within 5 min from cleaving) was probed with an identical set of parameters [38]. The HOPG measurements were used to calibrate the probe and confirm that the WF of the probe did not change during the measurements of the graphene films.

2.4. Device characterization and measurements

I–V measurements in dark and light conditions were performed with a modular testing platform (Arkeo – Cicci research s.r.l.) composed of a white LED array (4200 K) with optical power density tuneable from 10 to 100 mW/cm^2 (0.1–1 Sun), and a high-speed source meter unit (600 k samples/s) in a four-wire configuration under ambient conditions. The LED intensity was calibrated at the equivalent of 1 Sun intensity by adjusting the J$_{sc}$ value to be equal to the measured in the J–V curve using the solar simulator.

Small-perturbation transient photovoltage (TPV) measurements were conducted using the transient module of the commercial system Arkeo (Cicci Research s.r.l.). The open circuit mode was controlled via differential voltage amplifiers and short photogeneration pulses were generated using a fast LED (470 nm) with a Lambertian radiation pattern and 120° viewing angle limited at 100 mA current. The background bias was set close to the open circuit voltage (V$_{oc}$) in order to avoid the resistor–capacitor (RC) effect.

The external quantum efficiency (EQE) measurements were conducted using an integrated system (Enlitech, Taiwan), with a lock-in amplifier and a current preamplifier under short-circuit conditions. The light spectrum was calibrated using a monocrystalline photodetector of a known spectral response.

Thermal images were taken with a thermovision camera, SC 7200 FLIR, with a spectral range from 1.5 μm to 5.1 μm, an instantaneous field of view (IFOV) of 0.6 mrad, a focal plane array of 320×240, an objective of 50 mm, and with a distance to sample of 1 m.

Light Beam Induced Current (LBIC) measurements were carried out using an in-house developed LBIC system. Laser diodes with a 642 and 1060 nm wavelength were used. The response was measured using the lock-in technique at excitation frequency of 1023 Hz. The measurement step was 25 μm and 10 μm for AO and A sample types, respectively. The beam spot was estimated to a few measurement steps maximum, since there were no sharp features in the samples.

3. Results and discussion

According to UV-VIS spectroscopic measurements presented in Fig. 1b., A and AO graphene films both exhibited high optical transparency T>70% at a wavelength of 660 nm with constant sheet resistance R$_{sheet}$ (~10 kΩ/sq). It should be noted that the measured optical absorbance is due to graphene only, because the measurements are performed on graphene supported by transparent quartz wafers. Despite the absorbance of the film itself, the graphene does not affect the Si absorption. The multilayer graphene structure was confirmed with Raman spectroscopy (Fig. 1c). The spectra feature all pronounced bands characteristic of the LPE graphene films [31]. An additional analysis of graphene films, obtained with AFM and KPFM techniques, is presented in Fig. S1 of Supporting Information (SI).

In order to obtain the complete set of operational solar cell parameters, we performed dark I–V and transient photovoltage (TPV) measurements on the same samples at the time of fabrication, pristine (t = 0) and after 1.5 years (dark storage/shelf life conditions). For the calculation of the SC parameters, we used standardized different methods [39], with the most important parameters being the series resistance (R$_s$), shunt resistance (R$_{sh}$), and ideality factor (n, used to identify the dominant form of recombination). The dark I–V measurements of pristine and 1.5 year old A and AO samples are presented in Fig. 2. R$_{sh}$ was obtained from the inverse slope of the dark I–V curve in the linear regime at V~0, when the current is at its maximum. R$_s$ was obtained from the part of the dark I–V curve with a high slope on the semi-log scale which corresponds to Fermi level alignment that occurs with adding electrons during voltage increase. Mathematically, this ratio is defined as dV/d(lnI) = R$_s$•I + n•(k$_B$•T)/q, where n is the diode ideality factor, q is elementary charge, T is absolute temperature, and k$_B$ is Boltzmann's constant. A plot of d(V)/d(lnI) vs. I will give R$_s$ as the slope and n as the y-axis intercept. n was obtained from the slope q/(nk$_B$T), i. e., a linear fit of the [ln(I)–V] curve (Fig. 2a and b), which has a nearly linear part in the range of 0.1–0.4 V of the forward bias regime. As evident from the semi-log IV curves (Fig. 2a) and b)), the SC leakage current increased over time, observed from the rise in the negative section of the curve. This behavior indicates that R$_{sh}$ decreases with aging because of the creation of unwanted pathways for the current leakage [40], and it would be expected to decrease more with further cell aging. As seen in Table 1, R$_{sh}$ increases in pristine AO over A cells and decreases more rapidly in aged cells (double in A and 10 times in AO cells). Furthermore, we can see that our SC has high values of R$_{sh}$, which
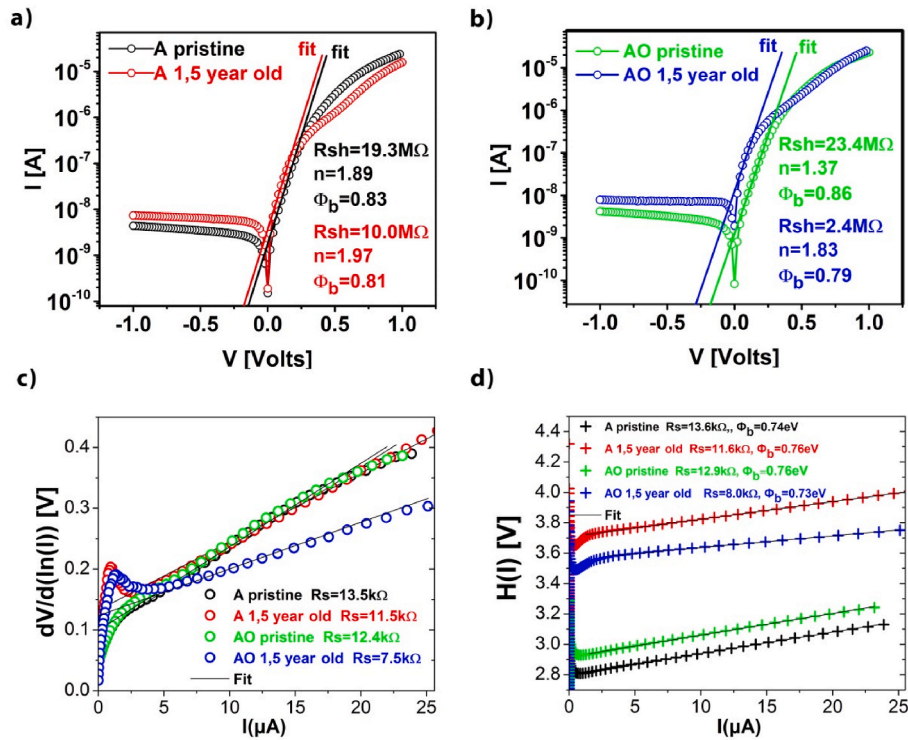
Fig. 2. Dark I–V measurements for pristine and 1.5-year-old A and AO solar cells. The fitted values of R_{sh} and Φ_b are extrapolated from lnI(V) for a) A and b) AO cells. c) The fitted values of R_s are extrapolated from dV/dlnI(I), and d) validated values of R_s and Φ_b are extrapolated from H(I).

Table 1
Dark measurement parameters of pristine t = 0 and aged t = 1.5 year old A and AO cells obtained with different theoretical methods.

Parameter (Method)	Cell			
	A		AO	
Year	pristine	1.5	pristine	1.5
R_s (dV/dlnI)[kΩ]	13.50	11.54	12.39	7.46
R_s (H(I) validate) [kΩ]	13.61	11.58	12.89	8.05
R_{sh} [MΩ]	19.3	10.0	23.4	2.4
n(lnI(V))	1.89	1.97	1.37	1.83
Φ_b (lnI(V)) [eV]	0.83	0.81	0.86	0.79
Φ_b (H(I) validate) [eV]	0.74	0.76	0.76	0.73

could be very important for indoor (low-light) performance [41–44]. In order to validate the results for R_s and obtain the Schottky barrier height (Φ_b), the voltage drop can be related to the deviation from an ideal diode as the Schottky barrier function: $H(I) = V - n(k_B \bullet T/q) \bullet \ln(I/(A \bullet K_r \bullet T^2) = R_s \bullet I + n \bullet \Phi_b$, where K_r is Richardson's constant for n-Si [120 A/cm²K²], A is the active area of the cell, and Φ_b is the Schottky barrier height [34]. Using the values of n obtained in previous dV/dlnI(I) vs. I analysis, the y-intercept gives Φ_b and the slope validates R_s. On the other hand, R_s, obtained via two complementary methods, is maintained almost constant with values ~10 kΩ, with a little drop over time, more so in doped AO cells (Fig. 2c) and d)). The R_s value of ~10 kΩ of solar cells is exclusively connected to the high resistance of graphene films (R_{sheet} ~10 kΩ/sq). Constant R_s over time is associated with stable charge transport across interfaces within the PV cell. The constant R_s is a good indicator that there was no interface degradation in time between the Si, graphene, and silver (Ag) contacts. R_s was smaller in AO than in A cells, both for pristine and aged cells, pointing toward better electrical properties of the AO cells. It should be noted that a small divergence in R_s between the cells can also arise from the fabrication of the cell (incomplete removal of native oxide), and intrinsic defects close to the surface of the Si wafer. Small divergences are not always related to the

graphene R_{sheet} being constant in both samples; hence, an insufficiently clean Si surface may leave an inhomogeneous native SiO_2 layer on the Si surface, or there may occur incomplete removal of the wafer cleaner, i. e., acetone. It must be pointed out that the obtained values for R_s are three orders of magnitude higher than in other graphene/Si solar cells made with high-quality CVD graphene [23–26]. The high R_s could be the consequence of the cost-effective solution-based LPE process that results in films made of interconnected small flakes of graphene, rather than a clean homogeneous film such as CVD graphene. From Fig. 2, we can also observe that the ideality factor decreases in AO relative to the A pristine solar cells (1.89–1.37), which are values that are in agreement with literature reports for non-treated A cells (range of 1.6–2.0) and doped AO cells (range of 1.3–1.5) [24]. Over time, n increases in both cells, but more so in AO-treated cells. As the ideality factor is very sensitive on surface recombination [45,46], we can hypothesize that the level of recombination could be affecting the change in the ideality factor.

The assumption of stable charge transport across interfaces within the PV cell, based on the stable R_s in time, is further supported by the obtained values of Φ_b (see Table 1 and Fig. 2a), b), and d)). The Φ_b is obtained from the saturated current (I_s) as the y-intercept of the linear part of the semi-log I–V curve according to the formula $\Phi_b = (k_B \bullet T/q) \bullet \ln(A \bullet K_r \bullet T^2/I_s)$ [39]. From Fig. 2 and Table 1, we can see that Φ_b remains almost the same in both diodes and in time (0.79–0.86eV). This indicates that aging did not impact the materials at the interfaces [40]. Φ_b is estimated to be 0.83 and 0.86 for pristine, and 0.81 and 0.79 for aged cells. The small rise in Φ_b with the UV/ozone for pristine samples could be associated with hole-doping [25,32]. A decreasing trend for Φ_b is observed in both cells, but more so in AO-treated cells as a consequence of a higher degradation of AO graphene films. Contrary to this, if we use values for the graphene work function, W_{gr}, obtained from KPFM (4.98 and 4.81 for A and AO films, Fig. S1), and based on the Schottky–Mott model, where $\Phi_b = W_{gr} - \chi_{Si}$ (χ_{Si} = 4.05, electron affinity of Si), we have the opposite trend for Φ_b. Φ_b decreases by ozone-doping from 0.93 to 0.76 for AO and A pristine samples, respectively [23,25]. Due to electron-doping of graphene films in environmental conditions and the

work function in metals, in practice, exposure to ozone does not have a real impact on Φ_b. The reason for this is that the Schottky theory neglects the impact of the different surface states on Φ_b (additional interfaces formed because of incomplete covalent bonds, existence of impurities, patina, and basically everything which generates additional charges on phases boundaries) [47]. Constant Φ_b in time does not mean that the material did not degrade. As we mentioned earlier, it could be from the SiO$_2$ or remaining impurities that result in a relatively high Φ_b. Aging degradation does not have enough influence to perturb the Φ_b value. Furthermore, Φ_b can be unstable, varying during an applied voltage scan as a consequence of the varying Fermi level. A high-defect population or existence of impurities can impact carrier accumulation. This carrier accumulation can occur on the Si surface because of the forming of SiO$_2$ or a high mobility difference between the Si and graphene. On the other hand, since Φ_b and the built-in potential V_{bi} are connected by the formula $\Phi_b = V_{bi} + e^{-1}k_BT \ln(N_c/N_d)$ [48,49], where N_c is the effective density of the states in the conduction band and N_d is the doping level of the semiconductor, the increase in Φ_b could be a consequence of the increase in V_{oc} and V_{bi}. This Φ_b increase leads to an increased charge transfer across the metal–semiconductor interface, creating a larger potential drop V_{bi} across the depletion region, and allowing for a more efficient collection of electrons and holes [25]. This requires additional attention, since the difference between the metal–semiconductor Fermi level does not mean that is the real value for V_{bi}. In highly doped materials, as in our case ($N_d \sim 10^{19}$cm^{-3}), electrons and holes can tunnel through this layer, decreasing the total potential below the theoretical expected value. Furthermore, the structure of graphene has a big impact on Φ_b, since defects can ruin the ideality factor [50].

In order to validate the conclusion that the ideality factor increases as a consequence of more intense recombination, TPV measurements were implemented. Small-perturbation measurements were used to probe the bimolecular charge recombination rate and estimate the carrier lifetime. In general, a longer carrier lifetime means that the recombination order is reduced (recombination speed is inversely proportional to the lifetime) [25]. This leads to higher-quality cells in operational terms. In Fig. 3, the results for the lifetime of both sample types and aging periods are presented. We observe a drop in lifetime (about 50%) between the pristine and aged devices in both UV/ozone and non-treated devices. These results are in agreement with the I–V dark measurements (R_{sh} and n), where, in time, the recombination increases as a consequence of the degradation of material (most probably of silver contacts). The drop in lifetime is smaller between A and AO cells (~30%), and lower in A cells that have a longer lifetime than AO cells. A little shorter AO lifetime is related to the oxygen treatment of graphene [31], where oxygen is introduced as a recombination centre. As mentioned earlier, the carrier lifetime is linked with the direct non-radiative recombination of carriers, which means that in the case of aged cells, we have suppressed carrier transport between the electrodes and a more intense recombination. According to the experimental conditions, the shallow defects do not have an impact on this because their population is filled before the TPV measurements. It could be expected that the carrier lifetime decreases further as the cells are aged even more.

The insets of Fig. 3c) and d) present the spread of the voltage signal that increases in real conditions, potentially originating from the low electrode contact quality (silver paste). In both cases, the charge carrier lifetime is about 20 μs for pristine and 10 μs for aged samples. The smaller slope in aged cells confirms a small variation in R_s obtained from dark current analysis. This means that pristine devices have more surface defects and the aging process accelerates some kind of ''passivation process'' that enables the decreasing in defects. The effect is most likely caused by either the carrier's reservoir generation or the space charge region at the interface.

With I–V dark and TPV solar cell measurements on pristine and 1.5-year-aged solar cells, we can conclude that there was material degradation without an interface degradation between the graphene and Si (R_s, $\Phi_b \sim$ const., Table 1). We assume that the primary material degradation bottleneck could come from the degradation of silver contacts (R_{sh} decreases, ideality factor increases (higher carrier recombination), and the slopes of voltage are higher over time (Figs. 2 and 3).

By utilizing highly n-doped c-Si wafers, a higher concentration of carriers can be achieved. This effect becomes more prominent in dark
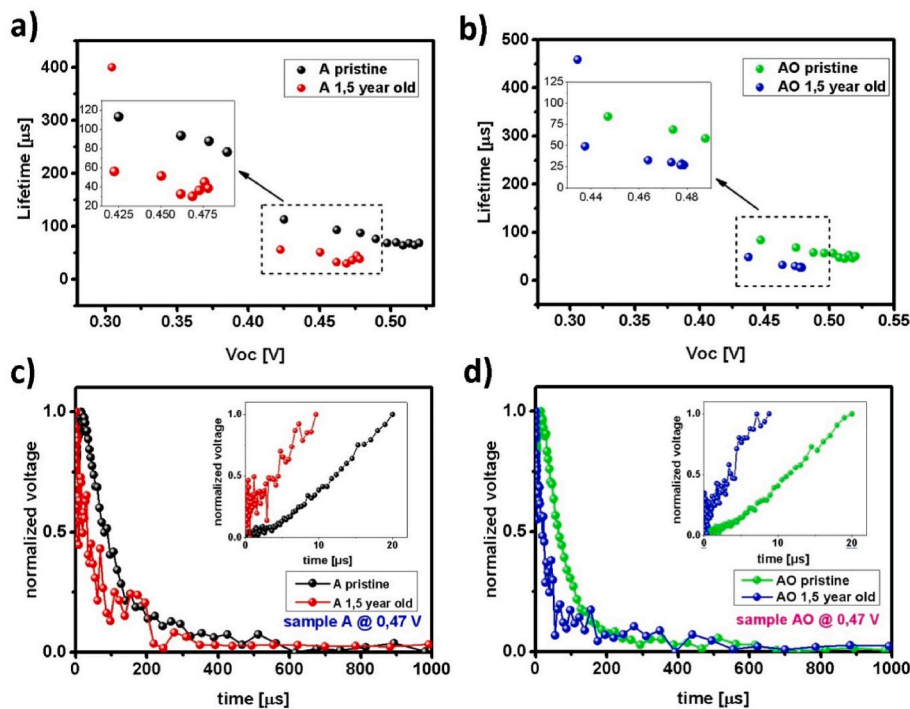

Fig. 3. TPV measurements for A and AO pristine and 1.5-year-old samples. a) and b) lifetime as a function of V_{oc}; c) and d) photovoltage as a function of time. Insets-speeds of voltage signal.

conditions, where photogeneration phenomena are absent. The increased carrier concentration enhances mobility. However, at higher intensities, when the concentration of electrons/holes rises, recombination also increases, leading to a rapid decrease in power conversion efficiency (PCE), primarily due to a decrease in the fill factor (FF). The FF represents the balance between electrode transport and lifetime. Fig. S2 illustrates that mobility exponentially declines as N_d (carrier concentration) increases, impacting recombination as a result of an increased number of free electrons. Essentially, there exists a trade-off between these two processes. Consequently, it can be suggested that for indoor low-light applications such as IoT devices, employing highly doped Si wafers with high-resistivity (R_s) graphene films could be a suitable option for solar cells.

The tested devices, which were stored in accordance with ISOS-D protocols (dark storage/shelf life [37]), demonstrated operational stability for a minimum of 4 years. The stability of the graphene films was assessed using Raman spectroscopy, specifically by examining the ratio of the peak intensities D/G and D/D′ (calculated from the peak maximum intensity), as shown in Fig. 4. For the pristine samples, we observed a consistent value for defect density (D/G ~0.4) and the D/D′ ratio, which was approximately 4. The value of the D/D′ ratio is indicative of the predominant defect type in the graphene samples [51,52]. The D/D′ ratio suggests that edges are the primary defect type, aligning with our previous findings for the thin films derived from liquid-phase-exfoliated graphene [31]. However, after 4 years, there was an increase in both the D/G and D/D′ ratios, indicating the onset of film degradation [31,47,48]. Further film degradation may occur with time, which leads to an estimated lifetime of these solar cells on the order of 10 years.

Additionally, the spatial homogeneity of the 4-year-old devices was assessed using Light Beam Induced Current (LBIC) measurements. The results, depicted in Fig. 5, illustrate the LBIC scans of two devices of different types (top: A–thermally annealed, bottom: AO–thermally annealed and UV/ozone-treated) conducted at two laser wavelengths (left: 642 nm, right: 1060 nm). Notable inhomogeneities are not observed within the active area of the devices, indicating a relative spatial stability. However, minor inhomogeneities are present in the 1060 nm scan of device A, which are absent in the 642 nm scan. These discrepancies may originate from the inhomogeneities on the back side of the device. Since LBIC scans were not conducted in the beginning of experiment, it is not possible to determine their temporal origin.

An additional analysis of the stability of solar cells aged for 3 and 5 years was performed using thermovision (further details in Supplementary Information), as shown in Fig. S3. Furthermore, the effect of ageing is explored by measuring of external quantum efficiency (EQE) in pristine and 5 years old A and AO cells (Fig. S4). We can see that EQE decreased about 50% in both cells (more in A then AO cells) as the effect of ageing of graphene films and silver contacts (see Fig. 4 and Fig. S5). Since the operation of our novel solar cells in bright conditions is not the main subject of this paper, we have measured the photovoltaic response

only on the two cells discussed above.

Finally, the current–voltage response of both the fresh and aged devices (pristine and 1.5 year old) under variable light bias (0.13–1.0 Sun, white LED 4200 K source) is presented in Fig. S5 in Supplementary Information. It is evident that the aged cells exhibit about 50% degradation in efficiency and JV compared to the fresh cells. Additionally, we observe that the efficiency increases as solar intensities decrease, particularly in indoor conditions. This phenomenon can be attributed to factors such as a high R_{sh}, lower recombination intensities in solar cells, and the high N_d of the Si wafers [41–43].

4. Conclusion

In summary, we have validated the operational stability of graphene/Si Schottky-junction solar cells over 5 years, and graphene/Si interface stability over 1.5 years in air (R_s and $\Phi_b \sim$ const.), respectively. A critical structural mechanism responsible for the performance degradation during the aging process was identified to be the degradation of Ag contacts (R_{sh} decreases, n increases, and the slopes of voltage are higher over time). LBIC and FLIR techniques validated the spatial stability, homogeneity, and the absence of shunt channel defect places over a 5-year period, while Raman spectroscopy confirmed the low defect density of graphene films over 4 years. The use of highly doped Si wafers with high R_s graphene films could be a good option for IoT Gr/Si solar cell indoor applications. This study therefore proposes a facile, simple, and low-cost fabrication approach of graphene-based electrodes with long-term stability. Our work highlights the long-term stability of liquid-phase-exfoliated materials in an operational environment, which was observed before [34] and indicates that LPE followed by Langmuir–Blodgett assembly is an efficient fabrication method for real-world devices.

CRediT authorship contribution statement

Djordje Jovanović: Writing – review & editing, Visualization, Validation, Supervision, Software, Resources, Project administration, Investigation, Funding acquisition, Formal analysis, Data curation, Conceptualization. **Miloš Petrović:** Writing – review & editing, Writing – original draft, Visualization, Validation, Software, Methodology, Investigation, Formal analysis, Data curation, Conceptualization. **Tijana Tomašević-Ilić:** Writing – review & editing, Visualization, Validation, Methodology, Investigation, Formal analysis, Conceptualization. **Aleksandar Matković:** Writing – review & editing, Visualization, Validation, Supervision, Methodology, Investigation, Formal analysis, Conceptualization. **Matevž Bokalič:** Writing – review & editing, Visualization, Methodology, Investigation, Data curation. **Marko Spasenović:** Writing – review & editing, Methodology, Investigation, Data curation. **Konstantinos Rogdakis:** Writing – review & editing, Investigation, Formal analysis, Data curation. **Emmannuel Kymakis:** Writing – review & editing, Resources, Project administration. **Dragan Knežević:** Writing –
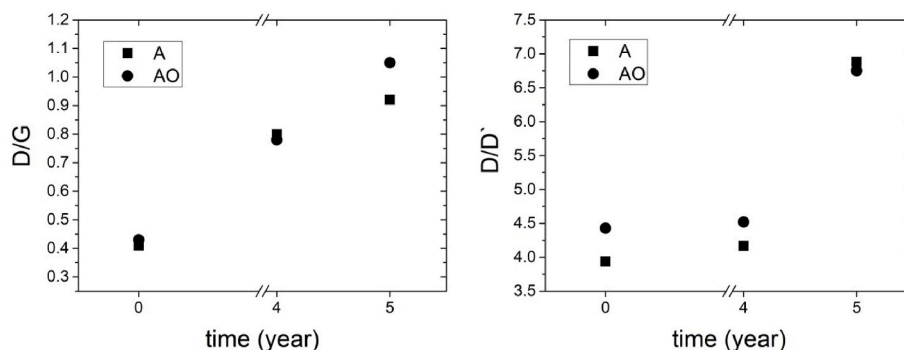
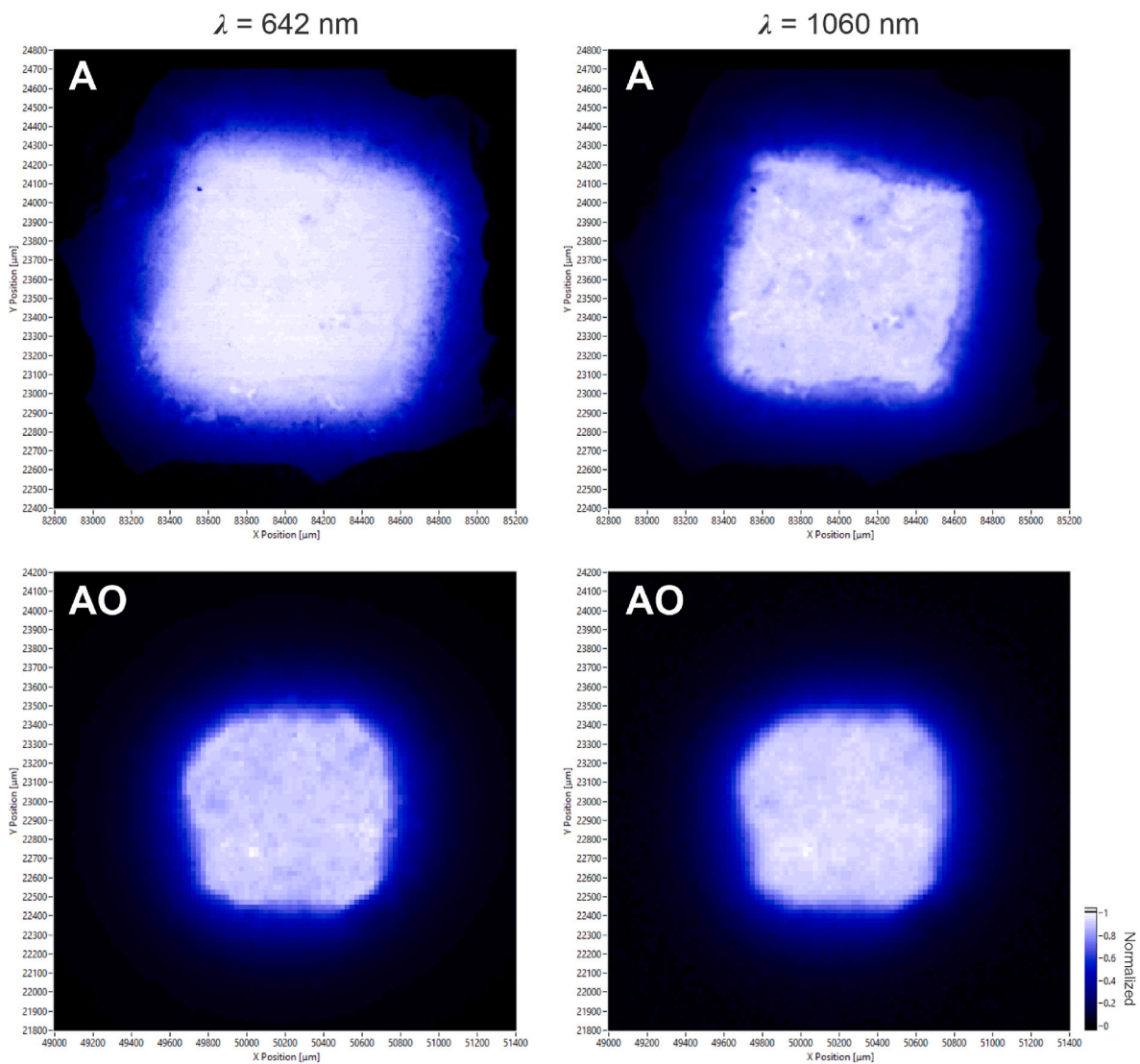**Fig. 4.** D/G and D/D′ ratios over time for A and AO graphene films.

Fig. 5. LBIC spatial maps of 4-year-old A and AO solar cells, measured at 642 and 1060 nm laser wavelength.

review & editing, Visualization, Validation, Formal analysis, Data curation. **Lucio Cinà:** Formal analysis, Investigation, Visualization, Writing – review & editing. **Radoš Gajić:** Writing – review & editing, Validation, Supervision, Funding acquisition, Data curation.

Declaration of competing interest

The authors declare that they have no known competing financial interests or personal relationships that could have appeared to influence the work reported in this paper.

Data availability

Data will be made available on request.

Acknowledgments

Appendix A. Supplementary data

Supplementary data to this article can be found online at https://doi.org/10.1016/j.solmat.2023.112414.

References

[1] European Green Deal, European Union, 2021.

[2] Borge Brende, Biotech Future Forum, 2022. Belgrade, Serbia, https://biotechff.gov.rs.

[3] A European Green Deal. https://ec.europa.eu/info/strategy/priorities-2019-2024/european-green-deal_en.

[4] The European Strategic Energy Technology Plan, European Commission, 2014. https://ec.europa.eu/energy/topics/technology-and-innovation/strategic-energy-technology-plan_en.

[5] EU Energy Roadmap 2050. https://ec.europa.eu/energy/sites/ener/files/documents/2012_energy_roadmap_2050_en_0.pdf.

[6] World Economic Forum. Annual Meeting 2023, January 2023. Davos, Switzerland, https://www.weforum.org/events/world-economic-forum-annual-meeting-2023.

[7] Cost Action CA21148, Research and International Networking on Emerging Inorganic Chalcogenides for Photovoltaics, 2022.

[8] D.C. Jordan, S.R. Kurtz, Photovoltaic degradation rates—an analytical review, Prog. Photovoltaics 21 (2013) 12–29, https://doi.org/10.1002/pip.1182.

[9] Sungwoo Jung, Yongjoon Cho, So-Huei Kang, Seong-Jun Yoon, Changduk Yang, Effect of third component on efficiency and stability in ternary organic solar cells: more than a simple superposition, Solar RRL 6 (2022), 21008192022, https://doi.org/10.1002/solr.202100819.

[10] Rusoma Akilimali, Gurpreet Singh Selopal, Mahyar Mohammadnezhad, Ka Ibrahima, M. Zhiming, Gregory P. Lopinski Wang, Haiguang Zhao, Federico Rosei, Structural effect of Low-dimensional carbon nanostructures on Long-term stability of dye sensitized solar cells, Chem. Eng. J. 435 (2022), 135037, https://doi.org/10.1016/j.cej.2022.135037.

[11] K.H. Girish, K.A. Vishnumurthy, T.S. Roopa, Role of conducting polymers in enhancing the stability and performance of perovskite solar cells: a brief review, Materials Today Sustainability17 (2022), 100090, https://doi.org/10.1016/j.mtsust.2021.100090.

[12] Mikkel Jørgensen, Kion Norrman, Frederik C. Krebs, Stability/degradation of polymer solar cells, Sol. Energy Mater. Sol. Cell. 92 (2008) 686–714, https://doi.org/10.1016/j.solmat.2008.01.005.

[13] Dong In Kim, Ji Won Lee, Rak Hyun Jeong, Jin-Hyo Boo, A high-efficiency and stable perovskite solar cell fabricated in ambient air using a polyaniline passivation layer, Sci. Rep. 12 (2022) 697, https://doi.org/10.1038/s41598-021-04547-3.

[14] Eric Singh, Hari Singh Nalwa, Stability of graphene-based heterojunction solar cells, RSC Adv. 5 (2015) 73575–73600, https://doi.org/10.1039/C5RA11771B.

[15] J. Brabec, J.A. Hauch, P. Schilinsky, C. Waldauf, Production aspects of organic photovoltaics and their impact on the commercialization of devices, MRS Bull. 30 (2005) 50–52, https://doi.org/10.1557/mrs2005.10.

[16] C.J. Brabec, Organic photovoltaics: technology and market, Sol. Energy Mater. Sol. Cells 83 (2004) 273–292, https://doi.org/10.1016/j.solmat.2004.02.030.

[17] Christos Polyzoidis, Konstantinos Rogdakis, Emmanuel Kymakis, Indoor perovskite photovoltaics for the Internet of Things - challenges and opportunities toward market uptake, Adv. Energy Mater. 11 (2021), 2101854, https://doi.org/10.1002/aenm.202101854.

[18] Konstantinos Rogdakis, Nikolaos Karakostas, Emmanuel Kymakis, Up-scalable emerging energy conversion technologies enabled by 2D materials: from miniature power harvesters towards grid-connected energy systems, Energy Environ. Sci. 14 (2021) 3352–3392, https://doi.org/10.1039/D0EE04013D.

[19] I. Mathews, S.N. Kantareddy, T. Buonassisi, I.M. Peters, Technology and market perspective for indoor photovoltaic cells, Joule 3 (2019) 1415–1426, https://doi.org/10.1016/j.joule.2019.03.026.

[20] Vincenzo Pecunia, Luigi G. Occhipinti, Robert L.Z. Hoye, Emerging indoor photovoltaic technologies for sustainable Internet of Things, Adv. Energy Mater. 11 (2021), 2100698, https://doi.org/10.1002/aenm.202100698.

[21] W.S. Koh, C.H. Gan, W.K. Phua, Y.A. Akimov, P. Bai, The potential of graphene as an ITO replacement in organic solar cells: an optical perspective, IEEE J. Sel. Top. Quant. Electron. 14 (2020), 4000107, https://doi.org/10.1109/JSTQE.2013.2247976.

[22] Muhammad Fahad Bhopal, Doo Won Lee, Atteq ur Rehman and Soo Hong Lee, Past and future of graphene/silicon heterojunction solar cells: a review, J. Mater. Chem. C 5 (2017) 10701–10714, https://doi.org/10.1039/C7TC03060F.

[23] Xinming Li, Hongwei Zhu, Kunlin Wang, Anyuan Cao, Jinquan Wei, Chunyan Li, Yi Jia, Zhen Li, Li Xiao, Dehai Wu, Graphene-on-silicon Schottky junction solar cells, Adv. Mater. 22 (2010) 2743–2748, https://doi.org/10.1002/adma.200904383.

[24] Yi Song, Xinming Li, Charles Mackin, Xu Zhang, Wenjing Fang, Tomás Palacios, Hongwei Zhu, Jing Kong, Role of interfacial oxide in high-efficiency graphene–silicon Schottky barrier solar cells, Nano Lett. 15 (2015) 2104–2110, https://doi.org/10.1021/nl505011f.

[25] Xiaochang Miao, Sefaattin Tongay, Maureen K. Petterson, Berke Kara, Andrew G. Rinzler, Bill R. Appleton, Arthur F. Hebard, High efficiency graphene solar cells by chemical doping, Nano Lett. 12 (2012) 2745–2750, https://doi.org/10.1021/nl204414u.

[26] Xiaoqiang Li, Wenchao Chen, Shengjiao Zhang, Zhiqian Wu, Peng Wang, Zhijuan Xu, Hongsheng Chen, Wenyan Yin, Huikai Zhong, Shisheng Lin, 18.5% efficient graphene/GaAs van der Waals heterostructure solar cell, Nano Energy 16 (2015) 310–319, https://doi.org/10.1016/j.nanoen.2015.07.003.

[27] Qiang Lou, Gang Lou, Hailing Guo, Tian Sun, Chunyun Wang, Gaoda Chai, Xia Chen, Guoshen Yang, Yuzheng Guo, Hang Zhou, Enhanced efficiency and stability of n-i-p perovskite solar cells by incorporation of fluorinated graphene in the spiro-OMeTAD hole transport layer, Adv. Energy Mater. 12 (2022), 2201344, https://doi.org/10.1002/aenm.202201344.

[28] F. Bella, G. Griffini, J.P. Correa-Baena, G. Saracco, M. Gratzel, A. Hagfeldt, S. Turri, C. Gerbaldi, Improving efficiency and stability of perovskite solar cells with photocurable fluoropolymers, Science 354 (2016) 203–206, https://doi.org/10.1126/science.aah4046.

[29] K. Ohkawa, S. Shimizu, H. Sato, T. Komaru, W. Futako, T. Kamiya, C.M. Fortmann, I. Shimizu, Stability of a-Si:H solar cells deposited by Ar-treatment or by ECR techniques, Sol. Energy Mater. Sol. Cells 66 (2001) 297–303, https://doi.org/10.1016/S0927-0248(00)00187-2.

[30] Youyu Jiang, Xinyun Dong, Lulu Sun, Tiefeng Liu, Fei Qin, Cong Xie, Pei Jiang, Hu Lu, Xin Lu, Xianmin Zhou, Wei Meng, Li Ning, Brabec Christoph J., and Zhou Yinhua, An alcohol-dispersed conducting polymer complex for fully printable organic solar cells with improved stability, Nat. Energy 7 (2022) 352–359, https://doi.org/10.1038/s41560-022-00997-9.

[31] Tijana Tomašević-Ilić, Đorđe Jovanović, Igor Popov, Rajveer Fandan, Jorge Pedrós, Marko Spasenović, Radoš Gajić, Reducing sheet resistance of self-assembled transparent graphene films by defect patching and doping with UV/ozone treatment, Appl. Surf. Sci. 458 (2018) 446–453, https://doi.org/10.1016/j.apsusc.2018.07.111.

[32] A. Matković, I. Milošević, M. Milićević, T. Tomašević-Ilić, J. Pešić, M. Musić, M. Spasenović, Dj. Jovanović, B. Vasić, C. Deeks, R. Panajotović, M. Belić, R. Gajić, Enhanced sheet conductivity of Langmuir–Blodgett assembled graphene thin films by chemical doping, 2D Mater. 3 (2016), 015002, https://doi.org/10.1088/2053-1583/3/1/015002.

[33] T. Tomašević-Ilić, J. Pešić, I. Milošević, J. Vujin, A. Matković, M. Spasenović, R. Gajić, Transparent and conductive films from liquid phase exfoliated graphene, Opt. Quant. Electron. 48 (2016) 319, https://doi.org/10.1007/s11082-016-0591-1.

[34] Kangho Lee, Beata M. Szydłowska, Olive Hartwig, Synnatschke Kevin, Bartłomiej Tywoniuk, Tomas Hartman, Tijana Tomašević-Ilić, Cian P. Gabbett, Coleman N. Jonathan, Zdenek Sofer, Marko Spasenović, Claudia Backes, Georg S. Duesberg, Highly conductive and long-term stable films from liquid-phase exfoliated platinum diselenide, J. Mater. Chem. C 11 (2023) 593–599, https://doi.org/10.1039/D2TC03889G.

[35] https://www.pveducation.org/pvcdrom/materials/general-properties-of-silicon.

[36] Joachim Wagner, A. Jesús, del Alamo, Band-gap narrowing in heavily doped silicon: a comparison of optical and electrical data, J. Appl. Phys. 63 (1988) 425, https://doi.org/10.1063/1.340257.

[37] M.V. Khenkin, et al., Consensus statement for stability assessment and reporting for perovskite photovoltaics based on ISOS procedures, Nat. Energy 5 (2020) 35–49, https://doi.org/10.1038/s41560-019-0529-5.

[38] Tuan-Hoang Tran, Raul D. Rodriguez, Marco Salerno, Aleksandar Matković, Christian Teichert, Evgeniya Sheremet, Twisted graphene in graphite: impact on surface potential and chemical stability, Carbon 176 (2021) 431–439, https://doi.org/10.1016/j.carbon.2021.01.152.

[39] S.K. Cheung, N.W. Cheung, Extraction of Schottky diode parameters from forward current-voltage characteristics, Appl. Phys. Lett. 49 (1986) 85, https://doi.org/10.1063/1.97359.

[40] Christopher M. Proctor, Thuc-Quyen Nguyen, Effect of leakage current and shunt resistance on the light intensity dependence of organic solar cells, Appl. Phys. Lett. 106 (2015), 083301, https://doi.org/10.1063/1.4913589.

[41] N.H. Reich, W.G.J.H.M. Van Sark, E.A. Alsema, S.Y. Kan, S. Silvester, Ash Van der Heide, R.E.I. Rw Lof, Schropp, Proc. of the 20th EU PVSEC, 2005, p. 2120.

[42] Gabriela E. Bunea, Karen E. Wilson, Yevgeny Meydbray, Matthew P. Campbell, M. Denis, De Ceuster, IEEE 4th World Conference on Photovoltaic Energy Conference, 2006, p. 1312.

[43] P. Grunow, S. Lust, D. Sauter, V. Hoffmann, C. Beneking, B. Litzenburger, L. Podlowski, in: 19th European Photovoltaic Solar Energy Conference, 2004, p. 2190. Paris, France.

[44] Masafumi Yamaguchi, et al., Development of high-efficiency solar cell modules for photovoltaic-powered vehicles, Sol. RRL 6 (2021), 2100429, https://doi.org/10.1002/solr.202100429.

[45] Mario El-Tahchi, Antonio Khoury, Marc De Labardonnie, Pierre Mialhe, Frédéric Pelanchon, Degradation of the diode ideality factor of silicon n–p junctions, Sol. Energy Mater. Sol. Cell. 62 (2000) 393–398, https://doi.org/10.1016/S0927-0248(99)00171-3.

[46] Ronald A. Sinton, Richard M. Swanson, Recombination in highly injected Silicon, IEEE Trans. Electron. Dev. 34 (1987) 1380–1389, https://doi.org/10.1109/T-ED.1987.23095.

[47] John Bardeen, Surface states and rectification at a metal semi-conductor contact, Phys. Rev. 71 (1947) 717, https://doi.org/10.1103/PhysRev.71.717.

[48] S.M. Sze, Physics of Semiconductor Devices, second ed., John Wiley and Sons, New York, 1981.

[49] Serdar Yavuz, Graphene/Silicon Schottky Junction Based Solar Cells, University of California, San Diego, 2018.

[50] D. Tomer, S. Rajput, L.J. Hudy, C.H. Li, L. Li, Intrinsic inhomogeneity in barrier height at monolayer graphene/SiC Schottky junction, Appl. Phys. Lett. 105 (2014), 021607, https://doi.org/10.1063/1.4890405.

[51] M.V. Bracamonte, G.I. Lacconi, S.E. Urreta, L.E.F. Foa Torres, On the nature of defects in liquid-phase exfoliated graphene, J. Phys. Chem. C 118 (2014) 15455–15459, https://doi.org/10.1021/jp501930a.

[52] A. Eckmann, A. Felten, I. Verzhbitskiy, R. Davey, C. Casiraghi, Raman study on defective graphene: effect of the excitation energy, type, and amount of defects, Phys. Rev. B 88 (2013), 035426, https://doi.org/10.1103/PhysRevB.88.035426.

Check for updates

Highly conductive and long-term stable films from liquid-phase exfoliated platinum diselenide†

Kangho Lee, [ID] [a] Beata M. Szydłowska, [ID] [ab] Oliver Hartwig, [ID] [a] Kevin Synnatschke, [ID] [c] Bartlomiej Tywoniuk, [ID] [a] Tomáš Hartman, [d] Tijana Tomašević-Ilić, [e] Cian P. Gabbett, [c] Jonathan N. Coleman, [ID] [c] Zdeněk Sofer, [ID] [d] Marko Spasenović, [ID] [f] Claudia Backes [ID] [bg] and Georg S. Duesberg [ID] *[a]

Liquid-phase exfoliation (LPE) has been introduced as a versatile and scalable production method for two-dimensional (2D) materials. This method yields dispersions that allow for the fabrication of printable and flexible electronic devices. However, the fabrication of uniform and homogeneous films from LPE dispersions with a performance similar to that of bottom-up grown materials remains a challenge, as the film quality strongly influences the optical and electrical performance of devices. Furthermore, long-term stability remains a major challenge for all 2D material based applications. In this study, we report on highly conductive tiled network films made of platinum diselenide ($PtSe_2$) flakes derived using a scalable LPE method. We characterized the homogeneous films in terms of morphology and electrical behavior. As an example of applicability, we produce a chemiresistive sensor structure with the $PtSe_2$ films and show significant resistance changes upon periodic ammonia gas exposures, revealing a sub-0.1 part per million (ppm) detection limit (DL). More remarkably the devices are fully functional after 15 months, underlining the high stability of $PtSe_2$ based devices.

Introduction

The unique properties of two-dimensional (2D) materials that enable high potential for their employment in numerous applications have led to enormous scientific interest.[1–3] In particular, they have been proposed for chemical sensing due to their high surface-area-to-volume ratio. Graphene-based sensors have shown ultimate sensitivity, detecting even individual gas molecules[4] while 2D transition metal dichalcogenide (TMD) materials showed extreme sensitivities to trace gases.[5–13] In particular, $PtSe_2$ has been shown to have superior gas sensitivity,[11] and gas selectivity was predicted by density functional theory.[14] Moreover, the outstanding electrochemical properties of platinum chalcogen compounds show promise for further applications.[15,16]

Within the toolset for the production of these materials, liquid phase exfoliation (LPE) has been proposed as a means for achieving high volume and yield. LPE has been used to exfoliate a range of 2D materials including graphite,[17–22] boron nitride,[23,24] pnictogens,[25–30] TMDs,[24,31–37] III–V semiconductors,[38] metal oxides,[39–41] and many others.[42–47] LPE is used to produce 2D materials in liquid dispersions, which can be used as inks, making the method attractive for various printing technologies, which allow for the fabrication of flexible devices or back end of line (BEOL) integration with existing integrated chips.[24,48] Most recently we were able to report on LPE-$PtSe_2$.[49]

Methods for producing films from LPE materials include vacuum filtration,[17,19] Langmuir–Blodgett (LB) deposition,[50–54] spray-coating[55] and inkjet printing.[56] However, many of these methods suffer from flake reaggregation into clusters in solution and on the substrate, leading to inhomogeneous films. In order to compensate for this, extra layers of materials must be added resulting in thick films (>1 μm) which is detrimental

[a] *Institute of Physics, EIT 2, Faculty of Electrical Engineering and Information Technology, University of the Bundeswehr Munich & SENS Research Center, Werner-Heisenberg-Weg 39, 85577, Neubiberg, Germany. E-mail: duesberg@unibw.de*

[b] *Institute of Physical Chemistry, Heidelberg University, 69120, Heidelberg, Germany*

[c] *School of Physics, CRANN & AMBER Research Centres, Trinity College Dublin, Dublin 2, Ireland*

[d] *Department of Inorganic Chemistry, University of Chemistry and Technology Prague, Technicka 5, 166 28, Prague 6, Czech Republic*

[e] *Institute of Physics Belgrade, University of Belgrade, Pregrevica 118, 11080, Belgrade, Serbia*

[f] *Center for Microelectronic Technologies, Institute of Chemistry, Technology and Metallurgy, University of Belgrade, Njegoševa 12, 11000, Belgrade, Serbia*

[g] *Physical Chemistry of Nanomaterials, University of Kassel, Heinrich-Plett-Str. 40, 34132, Kassel, Germany*

† Electronic supplementary information (ESI) available: Additional comparison of LB-type nanosheet networks. See DOI: https://doi.org/10.1039/d2tc03889g

in numerous applications and significantly increases production costs. Therefore, the formation of very thin homogenous films from LPE materials is not only crucial to the electrical and optical performance of devices, but is also a determining factor in the applicability of production methods.

Here we report for the first time film formation from $PtSe_2$ dispersions using a modified LB method at a liquid–liquid interface. Homogeneous films with low roughness and controllable thickness could be produced. These films were characterized using Raman spectroscopy, atomic force microscopy (AFM), and scanning electron microscopy (SEM) and compared to the conventional spray-deposited films. We contacted the LB films with interdigitated electrodes for electrical characterization. In a simple chemiresistive sensor structure, we show high sensitivity and fast response upon exposure to ammonia (NH_3) gas. Notably, we demonstrate the long-term stability of our films over 15 months.

Experimental

Synthesis of bulk crystals

Platinum sponge (Pt 99.99%, Surepure Chemetals) and selenium (Se 99.9999%, granules 2–4 mm, Wuhan Xinrong New Materials Co.) were placed in a quartz ampoule and sealed by an oxygen–hydrogen welding torch at a pressure of 1 mPa. Selenium was used in 2 at% excess. The ampoule was heated at 1270 °C in a 5 °C per minute of ramping speed and cooled down to 1000 °C at a 1 °C per minute of cooling rate after 30 minutes of dwell time. Afterwards, it was completely cooled down to room temperature. The selenium excess condensed on the opposite side of the ampoule, and the formed crystalline block of $PtSe_2$ was removed from the ampoule.

Preparation of the dispersions

The $PtSe_2$ dispersions were prepared using our previously established methodology of tip sonication and size selection by centrifugation in aqueous sodium cholate solution[57] followed by transfer to N-methyl-2-pyrrolidone (NMP) to aid the deposition at the liquid–liquid interface. $PtSe_2$ crystals were ground and immersed in 35 mL of aqueous sodium cholate (SC) solution (concentrations: C_{PtSe_2} = 0.5 g L^{-1} and C_{SC} = 1.7 g L^{-1}) and ultrasonicated (Sonics VXC500, 500 W, equipped with a tapered microtip) for 7.5 hours at 30% amplitude with a pulse of 6 seconds on and 4 seconds off. The dispersion was kept in a 4 °C cooling cell during sonication to avoid heating. The polydispersity of the as-produced dispersion was reduced by two consecutive centrifugation runs. High mass nanosheets which are larger and simultaneously thicker were discarded as sediment after the first run at lower centrifugal acceleration, while smaller/thinner nanosheets were removed as the supernatant after the second step at higher centrifugal acceleration. Specifically, unless otherwise noted, centrifugation was performed in a Hettich Mikro 220R centrifuge for 2 hours at 13 °C. The first step at a relative centrifugal force of 3000g (where g denotes the earth's gravitational field) was carried out with a fixed-angle rotor 1016 in

50 mL centrifuge tubes filled with ∼17 mL each. The supernatant was decanted and subjected to a second centrifugation at 5000g (with a fixed-angle rotor 1995-A in 1.5 mL Eppendorf tubes) after which the sediment was collected in deionized (DI) water and the supernatant discarded.

Preparation of films

Films were deposited after pre-assembly of the nanosheets at the liquid–liquid interface. First, the aqueous dispersion was transferred to NMP. To this end, the dispersion was centrifuged at 6000g (2 hours) to force the nanosheets to sediment and the sediment was redispersed in isopropanol (IPA) by bath-sonication for 5 minutes. The aqueous supernatant containing mostly water/surfactant was discarded. The centrifugation was repeated, the supernatant containing residual water and IPA was discarded and the sediment redispersed in NMP by 5 minutes of bath sonication. As substrates, SiO_2/Si wafers were chosen with an oxide thickness of 300 nm. These were diced to a size of 15 by 7.5 mm^2, cleaned by bath sonication in acetone, IPA, ethanol, and water for 20 min in each solvent and subsequently dried under a stream of pressured nitrogen. Fig. 1 depicts a schematic of the controlled deposition of $PtSe_2$ nanosheets on a SiO_2/Si substrate. Overall, the procedure can be regarded as a LB type deposition using two immiscible solvents, in this case water and toluene. It has been demonstrated that nanoflakes can be trapped at the liquid–liquid interface when injecting the LPE dispersion at an angle close to 90° with respect to the interface.[58,59] To form the liquid–liquid interface, first, a 15 mL glass beaker was filled with 12 mL of DI water and 0.5 mL of toluene was layered on top. Next, 0.1 mL of the $PtSe_2$ dispersion in NMP were gently injected on top and allowed to rest for 3 minutes to allow diffusion of the nanosheets to the toluene/water interface. After a uniform layer was formed, the toluene was allowed to evaporate and subsequently the transfer to the substrate was performed. To this end, the substrate was vertically introduced into the water phase, then tilted to an angle near 90° relative to the interface and then lifted up manually with a tweezer at speeds as constant as possible.[60] Generally, a smaller angle between the substrate and film is more favorable for the film transfer. Finally, the film was left to dry in air for ∼15 min with a tilt angle of ∼30° before performing a washing step by rinsing the films gently with a 1 : 1 mixture of IPA and DI water. Excess of unnecessary film
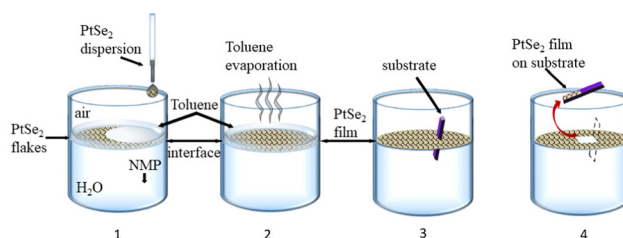

Fig. 1 Schematic of the modified Langmuir−Blodgett method to produce tiled nanosheet networks after pre-assembly at a liquid−liquid interface (1-film formation, 2-interface area reduction by evaporation, 3-substrate immersion, and 4-film deposition).

594 | J. Mater. Chem. C, 2023, **11**, 593–599

This journal is © The Royal Society of Chemistry 2023

area was removed by gently scraping with a cotton swab, leaving an area of approximately 5 by 5 mm^2 in the center of the substrate.

Characterization

Scanning electron microscopy (SEM) characterization was performed with a JEOL JSM-6700F field emission SEM at 1 kV of acceleration voltage. Raman characterization was performed by mapping a region of 50 by 50 μm^2 with 100 measurement spots with a Witec alpha300 R confocal Raman microscope at an excitation wavelength of 532 nm at 0.5 mW of LASER power. For atomic force microscopy (AFM) imaging, a Dimension ICON3 scanning probe microscope (Bruker AXS S.A.S.) was used in ScanAsyst mode (non-contact) in air under ambient conditions using aluminium coated silicon cantilevers (OLTESPA-R3). Typical image sizes were 3 by 3 μm^2 scanned with 1024 lines at scan rates of ~ 0.4 Hz.

Device fabrication and measurement

Electrical characterization was performed in a Suss probe-station using a SourceMeter$^{\circledR}$ Unit (Keithley model 2612A) at a scan rate of 10 mV s^{-1}. For gas sensor tests, interdigitated electrodes (Ni/Au = 40/45 nm) forming a 200 μm channel with a channel length-to-width ratio 1 : 277 were deposited on top of the films through a metal shadow mask. The PtSe$_2$ sensors were annealed for 2 hours at 150 °C in N$_2$ at ambient pressure to desorb attached gaseous molecules on the surface and then loaded into a custom-made sensing chamber. The annealing temperature was kept low in order to avoid changes in morphology that were cautioned against in work previously reported.[61] The sensing chamber pressure is kept at approximately 900 mbar by constantly flowing 100 standard cubic centimeters per minute (sccm) of gas through the chamber. The gas concentration is remotely controlled through a flow rate ratio modulation between dry N$_2$ and 10 part per million (ppm) of NH$_3$ gas. A SourceMeter$^{\circledR}$ Unit (Keithley model 2636B) monitors current changes upon periodic NH$_3$ gas exposure at a constant voltage bias.

Results and discussion

A liquid–liquid interface is created by layering toluene on top of water. The PtSe$_2$-NMP dispersion was added to the interface in a similar way as demonstrated earlier for LB graphene films at a water–air interface.[53,54,62] The interfacial tension at the toluene–water interface exerts surface pressure that compresses the interfacial nanosheets into a close-packed structure.[63] The substrate coverage can be controlled by adjusting the concentration of flakes in the solution and the interfacial area between the two phases. In this case, the optimum PtSe$_2$ concentration was found by trial and error.

After drying (see the Experimental section), SEM (Fig. 2a) and AFM (Fig. 2b) of the LB film reveal that it consists of a homogenous nanosheet network over large areas. The films appear continuous with feature sizes, typically <100 nm. The AFM measurement reveals a root-mean square (RMS) roughness of
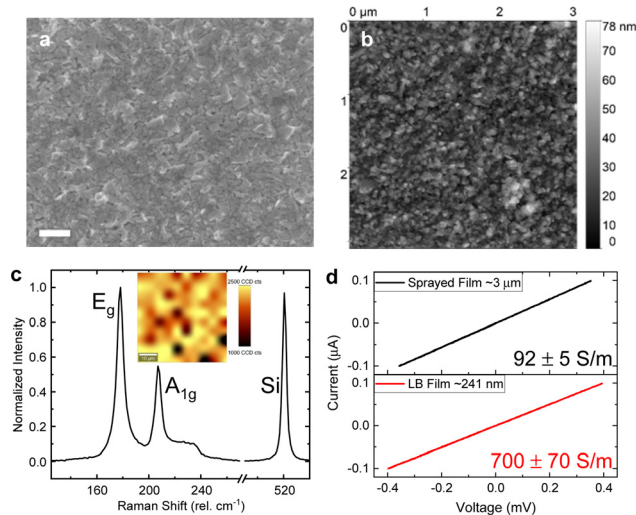

Fig. 2 (a) SEM image (scale bar: 200 nm) showing good nanosheet alignment and (b) AFM image of the LPE–PtSe$_2$ LB film. (c) Averaged Raman spectrum of the LPE–PtSe$_2$ LB film. Inset: scanning Raman map of the E$_g$ peak sum over a 50 by 50 μm^2 area. (d) Current–voltage characteristics of conventional spray-deposited and LPE–LB deposited films, resulting in film conductivities of 92 ± 5 and 700 ± 70 S m^{-1}, respectively. Note that the film thickness of the LB film (~ 240 nm) is more than 12-fold thinner compared to the sprayed network (~ 3 μm).

8.2 nm with only a few gaps between the sheets that are otherwise homogeneously deposited with maximum edge–edge contact. A scan at the edge of the film revealed a film thickness of ~ 30 nm (see the ESI†). Thus, one can conclude that thin films from platelets of PtSe$_2$ have been produced.

An averaged Raman spectrum from 100 positions on a sample is shown in Fig. 2c. Two prominent peaks can be identified at 178 and 207 cm^{-1}, which correspond to the in-plane E$_g$ and out-of-plane A$_{1g}$ vibrational Raman active modes, respectively. The inset depicts the spatial distribution of the E$_g$ mode at a location on the sample from which the averaged spectrum was measured. The Raman spectra contain well-defined, relatively narrow modes suggesting intact, crystalline nanosheets are deposited. Using our previously established quantitative metric for the estimation of PtSe$_2$ nanosheet thickness from Raman spectroscopy,[57] we estimate an average layer number of the nanosheets of 5.5. In previous work, we also established a correlation between the nanosheet layer number and lateral size,[57,64] which allows us to infer the average lateral dimensions of the nanosheets as ~ 60 nm (across the longest dimension) which is consistent with the microscopic characterization described above.

This modified LB film production method promises a higher conductive tiled network structure in comparison to randomly restacked porous nanosheet films produced by conventional spray deposition. To confirm this, another set of films were produced to allow for a direct comparison of LB-type and sprayed PtSe$_2$ networks, respectively. Due to the relatively high mass required for spray deposition, a more polydisperse PtSe$_2$ dispersion was used that was produced from centrifugation with a wider spread in the centrifugation boundaries (400g in the first step and 30 000g in the second step). Note that this resulted in a

more polydisperse size distribution and thicker, rougher films compared to the production method used for the remainder of the work (see the ESI†). Therefore, it was required to perform two subsequent deposition cycles in the case of this sample to yield a continuous network. While the more than 12 times thicker, ~ 3 μm thick sprayed PtSe$_2$ film (Fig. S2a, ESI†) showed a conductivity of 92 ± 5 S m^{-1}, the ~ 240 nm thick PtSe$_2$-LB film (Fig. S2c, ESI†) showed approximately 7.6 times higher conductivity, 700 ± 70 S m^{-1} in 4-point probe measurements as shown in Fig. 2d. This is a result tentatively assigned to the better alignment of PtSe$_2$ nanoflakes in the modified LB films. As a result, the modified LB film yields generally much thinner films with good conductivity. On the one hand, this reduces the material mass required for 2D material nanosheet network structures which is an important aspect for PtSe$_2$ containing a precious metal. On the other hand, this can be beneficial for sensing applications due to better accessibility of the active material.

Fig. 3a depicts the current–voltage (I_{ds}–V_{ds}) curves measured on a sensor device where the film shown in Fig. 2a–c was contacted with interdigitated electrodes (inset) directly after fabrication and after 15 months. The slope of the curve yields a resistance of 61.8 kΩ for this device which corresponds to a conductivity of ~ 1.95 S m^{-1} in this device structure. The lower conductivity of this 30 nm thin film compared to the 240 nm thick LB-type film (Fig. 2d) can be rationalized by a different nanosheet size distribution and hence different junction resistance, as well as a different device structure. The high

resistance indicates lower conductivity than PtSe$_2$ films grown by chemical vapour deposition[11,65–67] which may be attributed to flake-to-flake junctions hampering charge carrier transport.[52,68,69]

The contacted films were tested as ammonia sensors immediately after preparation and 15 months later to test the long-term stability of the device. Since many 2D materials, including group VI transition metal dichalcogenides,[70] are prone to degradation, for example by exposure to ambient conditions, we placed particular emphasis on the long-term stability of the sensor, as nanosheet degradation can cause inferior device performance. The device was tested as a gas sensor by exposing it to various concentrations of NH$_3$ in N$_2$ (0.1 to 0.8 ppm). The analyte was periodically introduced for 1 minute at a fixed concentration and at room temperature, followed by introduction of dry N$_2$ for 5 minutes for sensor recovery. No further treatments to enhance the recovery speed, *e.g.*, ultraviolet light illumination or annealing at higher temperatures, were applied. At 5 V of bias voltage, real-time current changes of the structured LPE-PtSe$_2$ LB film sensor can be calculated,

$$S = \frac{R_S - R_0}{R_0} \times 100\%$$

where R_0 and R_S are the resistances of the sensor before and after gas introduction. Fig. 3b shows a typical relative percentile resistance change as sensor responses. The resistance of the sensor increases upon NH$_3$ exposure because PtSe$_2$ is known as a p-type material and NH$_3$ donates an electron which results in reduction of the majority carrier in the semiconducting channel. To verify the sensor responses, simple signal processing was used.[7,11,71] The initial sensor resistance is calculated from the first 200 data points just before the first gas introduction. In the same regime, the root-mean-square (RMS) noise for a measured R_S is derived from the initial sensor resistance,

$$\text{Noise}_{RMS} = \sqrt{\sum \frac{(R_S - R_{Base})^2}{N}}$$

where R_{Base} is the baseline of the initial sensor resistance, and N is the number of data points. The signal-to-noise ratios (SNRs) derived from the resistance increments at various NH$_3$ concentrations are proportional to the gas concentration which is well-fitted to an exponential decay curve as shown in Fig. 3c. To be a true signal, the SNR must be at least three times larger or more according to the International Union of Pure and Applied Chemistry (IUPAC) definition.[72] In our measurements, an SNR of 3.4 was obtained for a concentration of 0.1 ppm of NH$_3$, setting a detection limit for this gas with LPE-PtSe$_2$ LB film sensors. In the SNR changes depicted at various concentrations (Fig. 3c), one can determine a theoretical detection limit (DL) by extrapolation to the point where the SNR drops below 3. This theoretical DL reaches a value of only 0.059 ppm, which is remarkable, as detection of low concentrations of NH$_3$ is challenging in chemiresistors because little charge is transferred compared to other analytes. This DL is one of the lowest values reported for LPE derived 2D material based gas sensors.[14,73,74]
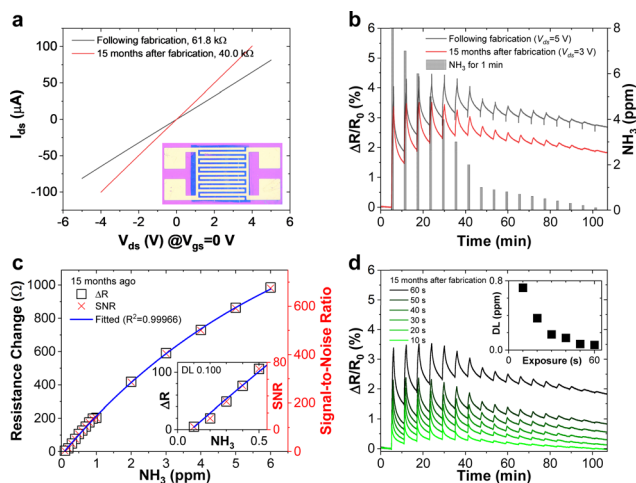

Fig. 3 (a) Current–voltage (I_{ds}–V_{ds}) characteristics of an LPE-PtSe$_2$ LB film sensor showing a noticeable conductance change after long-term exposure to the atmosphere. Inset: photograph of an LPE-PtSe$_2$ LB film (blue area) underneath interdigitated electrodes. (b) Sensor response curves of the LPE-PtSe$_2$ LB film sensor upon introduction of periodically decreasing concentrations of NH$_3$ from 8 down to 0.1 ppm (gray columns) at room temperature. A NH$_3$ sensor response is still observed 15 months later. (c) Resistance (open boxes) and SNR (red x-crosses) changes are proportional to the introduced gas concentration. Inset: zoomed-in plot in the lower NH$_3$ concentration range. (d) Sensor response curves for 10 to 60 seconds of NH$_3$ gas introduction (from light green to dark green). Inset: detectable NH$_3$ gas concentration inversely decreases as the gas exposure time increases.

596 | *J. Mater. Chem. C*, 2023, **11**, 593–599

This journal is © The Royal Society of Chemistry 2023

The long-term stability of 2D material based devices under ambient conditions has often been a point of debate. Grown $PtSe_2$ films are known to be stable under ambient conditions, however exfoliated films have never been investigated. Thus, we compare the performance of a sensor after it has been in N_2 flow storage for 15 months. The film conductance surprisingly increased slightly as shown in Fig. 3a. The improved conductivity after 15 months of storage could be due to the formation of better intersheet contacts or residual water in the film acting as a p-dopant increasing the concentration of majority charge carriers. During NH_3 gas sensing, interestingly, the peak-to-peak value of relative resistance changes slightly as the initial resistance decreased after 15 months, but the device exhibits higher SNR values because the RMS noise decreased. Fig. 3d presents the sensor response upon decreasing the NH_3 introduction time from 60 to 10 seconds in the same period, indicating that the estimated detection limit exponentially increases from 0.059 to 0.721 ppm (inset).

In conclusion, the devices still function as a very sensitive ammonia sensor after 15 months of storage. This is a remarkable finding as the long-term stability of LPE derived devices has always been a point of discussion while the high stability $PtSe_2$ has been so far only reported for thermally-assisted conversion (TAC) derived films.[11]

Conclusions

The formation of LB-type films into tiled networks from LPE-$PtSe_2$ dispersions was achieved for the first time. This combination resembles a cornerstone for a high yield, scalable, low cost production of sensors. This method is suitable for highly sought after flexible and wearable devices. We characterized the tiled network films structurally and revealed homogeneous films with little roughness indicating good alignment of the $PtSe_2$ flakes. We showed ~ 7.6 times higher conductivity in the tiled nanosheet network films through the modified LB production method in comparison to the conventional spray-deposited films. Thus, this method allows deposition to much thinner conducting networks forming 2D materials. The sensor performance of the LPE-$PtSe_2$ LB films showed high sensitivity toward NH_3 down to 0.100 ppm, which is remarkably low compared to those of most other 2D material based gas sensors. Furthermore, we demonstrated the long-term stability of the $PtSe_2$ based sensor over more than one year.

Author contributions

K. L.: data curation, formal analysis, investigation, validation, visualization, writing – original draft, and writing – review & editing; B. M. S.: conceptualization, data curation, investigation, methodology, and writing – original draft; O. H.: formal analysis, investigation, and visualization; K. S.: data curation, formal analysis, and investigation, B. T.: investigation; T. H.: investigation; T. T.: investigation, methodology, visualization, and writing – review & editing; C. P. G.: formal analysis and investigation;

J. N. C.: funding acquisition, and resources; Z. S.: funding acquisition and resources; M. S.: conceptualization, funding acquisition, methodology, supervision, and writing – review & editing; C. B.: conceptualization, funding acquisition, methodology, resources, visualization, supervision, and writing – review & editing; G. S. D.: funding acquisition, project administration, supervision, and writing – review & editing.

Conflicts of interest

There are no conflicts to declare.

Acknowledgements

Notes and references

1 A. K. Geim and K. S. S. Novoselov, *Nat. Mater.*, 2007, **6**, 183–191.

2 H. Schmidt, F. Giustiniano and G. Eda, *Chem. Soc. Rev.*, 2015, **44**, 7715–7736.

3 C. Backes, A. M. Abdelkader, C. Alonso, A. Andrieux-Ledier, R. Arenal, J. Azpeitia, N. Balakrishnan, L. Banszerus, J. Barjon, R. Bartali, S. Bellani, C. Berger, R. Berger, M. M. B. Ortega, C. Bernard, P. H. Beton, A. Beyer, A. Bianco, P. Bøggild, F. Bonaccorso, G. B. Barin, C. Botas, R. A. Bueno, D. Carriazo, A. Castellanos-Gomez, M. Christian, A. Ciesielski, T. Ciuk, M. T. Cole, J. Coleman, C. Coletti, L. Crema, H. Cun, D. Dasler, D. De Fazio, N. Díez, S. Drieschner, G. S. Duesberg, R. Fasel, X. Feng, A. Fina, S. Forti, C. Galiotis, G. Garberoglio, J. M. García, J. A. Garrido, M. Gibertini, A. Gölzhäuser, J. Gómez, T. Greber, F. Hauke, A. Hemmi, I. Hernandez-Rodriguez, A. Hirsch, S. A. Hodge, Y. Huttel, P. U. Jepsen, I. Jimenez, U. Kaiser, T. Kaplas, H. Kim, A. Kis, K. Papagelis, K. Kostarelos, A. Krajewska, K. Lee, C. Li, H. Lipsanen, A. Liscio, M. R. Lohe, A. Loiseau, L. Lombardi, M. Francisca López, O. Martin, C. Martín, L. Martínez, J. A. Martin-Gago, J. Ignacio Martínez, N. Marzari, Á. Mayoral, J. McManus, M. Melucci, J. Méndez, C. Merino, P. Merino, A. P. Meyer, E. Miniussi,

This journal is © The Royal Society of Chemistry 2023

J. Mater. Chem. C, 2023, **11**, 593–599 | **597**

V. Miseikis, N. Mishra, V. Morandi, C. Munuera, R. Muñoz, H. Nolan, L. Ortolani, A. K. Ott, I. Palacio, V. Palermo, J. Parthenios, I. Pasternak, A. Patane, M. Prato, H. Prevost, V. Prudkovskiy, N. Pugno, T. Rojo, A. Rossi, P. Ruffieux, P. Samorì, L. Schué, E. Setijadi, T. Seyller, G. Speranza, C. Stampfer, I. Stenger, W. Strupinski, Y. Svirko, S. Taioli, K. B. K. Teo, M. Testi, F. Tomarchio, M. Tortello, E. Treossi, A. Turchanin, E. Vazquez, E. Villaro, P. R. Whelan, Z. Xia, R. Yakimova, S. Yang, G. R. Yazdi, C. Yim, D. Yoon, X. Zhang, X. Zhuang, L. Colombo, A. C. Ferrari and M. Garcia-Hernandez, *2D Mater.*, 2020, **7**, 022001.

4 F. Schedin, A. K. Geim, S. V. Morozov, E. W. Hill, P. Blake, M. I. Katsnelson and K. S. Novoselov, *Nat. Mater.*, 2007, **6**, 652–655.

5 H. Li, Z. Yin, Q. He, H. Li, X. Huang, G. Lu, D. W. H. Fam, A. I. Y. Tok, Q. Zhang and H. Zhang, *Small*, 2012, **8**, 63–67.

6 D. J. Late, Y. K. Huang, B. Liu, J. Acharya, S. N. Shirodkar, J. Luo, A. Yan, D. Charles, U. V. Waghmare, V. P. David and C. N. R. Rao, *ACS Nano*, 2013, **7**, 4879–4891.

7 K. Lee, R. Gatensby, N. McEvoy, T. Hallam and G. S. Duesberg, *Adv. Mater.*, 2013, **25**, 6699–6702.

8 H. Fang, S. Chuang, T. C. Chang, K. Takei, T. Takahashi and A. Javey, *Nano Lett.*, 2012, **12**, 3788–3792.

9 M. O'Brien, K. Lee, R. Morrish, N. C. Berner, N. McEvoy, C. A. Wolden and G. S. Duesberg, *Chem. Phys. Lett.*, 2014, **615**, 6–10.

10 D. J. Late, T. Doneux and M. Bougouma, *Appl. Phys. Lett.*, 2014, **105**, 233103.

11 C. Yim, K. Lee, N. McEvoy, M. O'Brien, S. Riazimehr, N. C. Berner, C. P. Cullen, J. Kotakoski, J. C. Meyer, M. C. Lemme and G. S. Duesberg, *ACS Nano*, 2016, **10**, 9550–9558.

12 L. Pi, L. Li, K. Liu, Q. Zhang, H. Li and T. Zhai, *Adv. Funct. Mater.*, 2019, **1904932**, 1904932.

13 X. Chen, C. Liu and S. Mao, *Nano-Micro Lett.*, 2020, **12**, 95.

14 M. Sajjad, E. Montes, N. Singh and U. Schwingenschlögl, *Adv. Mater. Interfaces*, 2017, **4**, 1600911.

15 X. Chia, A. Adriano, P. Lazar, Z. Sofer, J. Luxa and M. Pumera, *Adv. Funct. Mater.*, 2016, **26**, 4306–4318.

16 N. Rohaizad, C. C. Mayorga-Martinez, Z. Sofer, R. D. Webster and M. Pumera, *Appl. Mater. Today*, 2020, **19**, 100606.

17 Y. Hernandez, V. Nicolosi, M. Lotya, F. M. Blighe, Z. Sun, S. De, I. T. McGovern, B. Holland, M. Byrne, Y. K. Gun'Ko, J. J. Boland, P. Niraj, G. Duesberg, S. Krishnamurthy, R. Goodhue, J. Hutchison, V. Scardaci, A. C. Ferrari and J. N. Coleman, *Nat. Nanotechnol.*, 2008, **3**, 563–568.

18 A. B. Bourlinos, V. Georgakilas, R. Zboril, T. A. Steriotis and A. K. Stubos, *Small*, 2009, **5**, 1841–1845.

19 M. Lotya, Y. Hernandez, P. J. King, R. J. Smith, V. Nicolosi, L. S. Karlsson, F. M. Blighe, S. De, Z. Wang, I. T. McGovern, G. S. Duesberg and J. N. Coleman, *J. Am. Chem. Soc.*, 2009, **131**, 3611–3620.

20 Y. T. Liang and M. C. Hersam, *J. Am. Chem. Soc.*, 2010, **132**, 17661–17663.

21 K. R. Paton, E. Varrla, C. Backes, R. J. Smith, U. Khan, A. O'Neill, C. Boland, M. Lotya, O. M. Istrate, P. King, T. Higgins, S. Barwich, P. May, P. Puczkarski, I. Ahmed, M. Moebius, H. Pettersson, E. Long, J. Coelho, S. E. O'Brien, E. K. McGuire, B. M. Sanchez, G. S. Duesberg, N. McEvoy, T. J. Pennycook, C. Downing, A. Crossley, V. Nicolosi and J. N. Coleman, *Nat. Mater.*, 2014, **13**, 624–630.

22 T. J. Nacken, C. Damm, J. Walter, A. Rüger and W. Peukert, *RSC Adv.*, 2015, **5**, 57328–57338.

23 C. Zhi, Y. Bando, C. Tang, H. Kuwahara and D. Golberg, *Adv. Mater.*, 2009, **21**, 2889–2893.

24 J. N. Coleman, M. Lotya, A. O'Neill, S. D. Bergin, P. J. King, U. Khan, K. Young, A. Gaucher, S. De, R. J. Smith, I. V. Shvets, S. K. Arora, G. Stanton, H.-Y. Kim, K. Lee, G. T. Kim, G. S. Duesberg, T. Hallam, J. J. Boland, J. J. Wang, J. F. Donegan, J. C. Grunlan, G. Moriarty, A. Shmeliov, R. J. Nicholls, J. M. Perkins, E. M. Grieveson, K. Theuwissen, D. W. McComb, P. D. Nellist and V. Nicolosi, *Science*, 2011, **331**, 568–571.

25 P. Yasaei, B. Kumar, T. Foroozan, C. Wang, M. Asadi, D. Tuschel, J. E. Indacochea, R. F. Klie and A. Salehi-Khojin, *Adv. Mater.*, 2015, **27**, 1887–1892.

26 V. Sresht, A. A. H. Pádua and D. Blankschtein, *ACS Nano*, 2015, **9**, 8255–8268.

27 J. Kang, J. D. Wood, S. A. Wells, J.-H. Lee, X. Liu, K.-S. Chen and M. C. Hersam, *ACS Nano*, 2015, **9**, 3596–3604.

28 J. R. Brent, N. Savjani, E. A. Lewis, S. J. Haigh, D. J. Lewis and P. O'Brien, *Chem. Commun.*, 2014, **50**, 13338–13341.

29 D. Hanlon, C. Backes, E. Doherty, C. S. Cucinotta, N. C. Berner, C. Boland, K. Lee, A. Harvey, P. Lynch, Z. Gholamvand, S. Zhang, K. Wang, G. Moynihan, A. Pokle, Q. M. Ramasse, N. McEvoy, W. J. Blau, J. Wang, G. Abellan, F. Hauke, A. Hirsch, S. Sanvito, D. D. O'Regan, G. S. Duesberg, V. Nicolosi and J. N. Coleman, *Nat. Commun.*, 2015, **6**, 8563.

30 C. Gibaja, D. Rodriguez-San-Miguel, P. Ares, J. Gómez-Herrero, M. Varela, R. Gillen, J. Maultzsch, F. Hauke, A. Hirsch, G. Abellán and F. Zamora, *Angew. Chem., Int. Ed.*, 2016, **55**, 14345–14349.

31 Y. Liu, R. Cheng, L. Liao, H. Zhou, J. Bai, G. Liu, L. Liu, Y. Huang and X. Duan, *Nat. Commun.*, 2011, **2**, 579.

32 R. J. Smith, P. J. King, M. Lotya, C. Wirtz, U. Khan, S. De, A. O'Neill, G. S. Duesberg, J. C. Grunlan, G. Moriarty, J. Chen, J. Wang, A. I. Minett, V. Nicolosi and J. N. Coleman, *Adv. Mater.*, 2011, **23**, 3944–3948.

33 G. S. Bang, K. W. Nam, J. Y. Kim, J. Shin, J. W. Choi and S.-Y. Choi, *ACS Appl. Mater. Interfaces*, 2014, **6**, 7084–7089.

34 E. Varrla, C. Backes, K. R. Paton, A. Harvey, Z. Gholamvand, J. McCauley and J. N. Coleman, *Chem. Mater.*, 2015, **27**, 1129–1139.

35 Y. Liu, X. Ji, J. Liu, W. W. L. Tong, D. Askhatova and J. Shi, *Adv. Funct. Mater.*, 2017, **27**, 1703261.

36 J. Kang, V. K. Sangwan, J. D. Wood, X. Liu, I. Balla, D. Lam and M. C. Hersam, *Nano Lett.*, 2016, **16**, 7216–7223.

37 P. Schiettecatte, A. Rousaki, P. Vandenabeele, P. Geiregat and Z. Hens, *Langmuir*, 2020, **36**, 15493–15500.

38 E. Petroni, E. Lago, S. Bellani, D. W. Boukhvalov, A. Politano, B. Gürbulak, S. Duman, M. Prato, S. Gentiluomo, R. Oropesa-Nuñez, J.-K. Panda, P. S. Toth, A. E. Del Rio Castillo, V. Pellegrini and F. Bonaccorso, *Small*, 2018, **14**, 1800749.

598 | *J. Mater. Chem. C*, 2023, **11**, 593–599

This journal is © The Royal Society of Chemistry 2023

39 M. M. Y. A. Alsaif, S. Balendhran, M. R. Field, K. Latham, W. Wlodarski, J. Z. Ou and K. Kalantar-zadeh, *Sens. Actuators, B*, 2014, **192**, 196–204.

40 D. Hanlon, C. Backes, T. M. Higgins, M. Hughes, A. O'Neill, P. King, N. McEvoy, G. S. Duesberg, B. Mendoza Sanchez, H. Pettersson, V. Nicolosi and J. N. Coleman, *Chem. Mater.*, 2014, **26**, 1751–1763.

41 Y. Wang, Y.-Z. Zhang, D. Dubbink and J. E. ten Elshof, *Nano Energy*, 2018, **49**, 481–488.

42 J. A. Carrasco, A. Harvey, D. Hanlon, V. Lloret, D. McAteer, R. Sanchis-Gual, A. Hirsch, F. Hauke, G. Abellán, J. N. Coleman and E. Coronado, *Chem. Commun.*, 2019, **55**, 3315–3318.

43 A. J. Molina-Mendoza, E. Giovanelli, W. S. Paz, M. A. Niño, J. O. Island, C. Evangeli, L. Aballe, M. Foerster, H. S. J. van der Zant, G. Rubio-Bollinger, N. Agraït, J. J. Palacios, E. M. Pérez and A. Castellanos-Gomez, *Nat. Commun.*, 2017, **8**, 14409.

44 Y. Niu, J. Villalva, R. Frisenda, G. Sanchez-Santolino, L. Ruiz-González, E. M. Pérez, M. García-Hernández, E. Burzurí and A. Castellanos-Gomez, *2D Mater.*, 2019, **6**, 035023.

45 M. Naguib, O. Mashtalir, J. Carle, V. Presser, J. Lu, L. Hultman, Y. Gogotsi and M. W. Barsoum, *ACS Nano*, 2012, **6**, 1322–1331.

46 R. Z. Lange, K. Synnatschke, H. Qi, N. Huber, G. Hofer, B. Liang, C. Huck, A. Pucci, U. Kaiser, C. Backes and A. D. Schlüter, *Angew. Chem., Int. Ed.*, 2020, **59**, 5683–5695.

47 A. Harvey, C. Backes, Z. Gholamvand, D. Hanlon, D. McAteer, H. C. Nerl, E. McGuire, A. Seral-Ascaso, Q. M. Ramasse, N. McEvoy, S. Winters, N. C. Berner, D. McCloskey, J. F. Donegan, G. S. Duesberg, V. Nicolosi and J. N. Coleman, *Chem. Mater.*, 2015, **27**, 3483–3493.

48 C. Backes, B. M. Szydłowska, A. Harvey, S. Yuan, V. Vega-Mayoral, B. R. Davies, P. L. Zhao, D. Hanlon, E. J. G. Santos, M. I. Katsnelson, W. J. Blau, C. Gadermaier and J. N. Coleman, *ACS Nano*, 2016, **10**, 1589–1601.

49 B. M. Szydłowska, O. Hartwig, B. Tywoniuk, T. Hartman, T. Stimpel-Lindner, Z. Sofer, N. McEvoy, G. S. Duesberg and C. Backes, *2D Mater.*, 2020, **7**, 045027.

50 X. Li, G. Zhang, X. Bai, X. Sun, E. Wang and H. Dai, *Nat. Nanotechnol.*, 2008, **3**, 538–542.

51 L. J. Cote, F. Kim and J. Huang, *J. Am. Chem. Soc.*, 2009, **131**, 1043–1049.

52 H. Kim, C. Mattevi, H. J. Kim, A. Mittal, K. A. Mkhoyan, R. E. Riman and M. Chhowalla, *Nanoscale*, 2013, **5**, 12365.

53 T. Tomašević-Ilić, J. Pešić, I. Milošević, J. Vujin, A. Matković, M. Spasenović and R. Gajić, *Opt. Quantum Electron.*, 2016, **48**, 319.

54 S. Andrić, M. Sarajlić, M. Frantlović, I. Jokić, D. Vasiljević-Radović and M. Spasenović, *Chemosensors*, 2021, **9**, 342.

55 P. Blake, P. D. Brimicombe, R. R. Nair, T. J. Booth, D. Jiang, F. Schedin, L. A. Ponomarenko, S. V. Morozov, H. F. Gleeson, E. W. Hill, A. K. Geim and K. S. Novoselov, *Nano Lett.*, 2008, **8**, 1704–1708.

56 F. Torrisi, T. Hasan, W. Wu, Z. Sun, A. Lombardo, T. S. Kulmala, G.-W. Hsieh, S. Jung, F. Bonaccorso, P. J. Paul, D. Chu and A. C. Ferrari, *ACS Nano*, 2012, **6**, 2992–3006.

57 T. Tomašević-Ilić, Đ. Jovanović, I. Popov, R. Fandan, J. Pedrós, M. Spasenović and R. Gajić, *Appl. Surf. Sci.*, 2018, **458**, 446–453.

58 F. Reincke, S. G. Hickey, W. K. Kegel and D. Vanmaekelbergh, *Angew. Chem., Int. Ed.*, 2004, **43**, 458–462.

59 H. Duan, D. Wang, D. G. Kurth and H. Möhwald, *Angew. Chem., Int. Ed.*, 2004, **43**, 5639–5642.

60 A. G. Kelly, D. O'Suilleabhain, C. Gabbett and J. N. Coleman, *Nat. Rev. Mater.*, 2021, **7(3)**, 217–234.

61 J. Wu, H. Li, Z. Yin, H. Li, J. Liu, X. Cao, Q. Zhang and H. Zhang, *Small*, 2013, **9**, 3314–3319.

62 A. Matković, I. Milošević, M. Milićević, T. Tomašević-Ilić, J. Pešić, M. Musić, M. Spasenović, D. Jovanović, B. Vasić, C. Deeks, R. Panajotović, M. R. Belić and R. Gajić, *2D Mater.*, 2016, **3**, 015002.

63 Y.-J. Li, W.-J. Huang and S.-G. Sun, *Angew. Chem., Int. Ed.*, 2006, **45**, 2537–2539.

64 C. Backes, D. Campi, B. M. Szydlowska, K. Synnatschke, E. Ojala, F. Rashvand, A. Harvey, A. Griffin, Z. Sofer, N. Marzari, J. N. Coleman and D. D. O'Regan, *ACS Nano*, 2019, **13**, 7050–7061.

65 Y. Zhao, J. Qiao, Z. Yu, P. Yu, K. Xu, S. P. Lau, W. Zhou, Z. Liu, X. Wang, W. Ji and Y. Chai, *Adv. Mater.*, 2017, **29**, 1604230.

66 C. Yim, V. Passi, M. C. Lemme, G. S. Duesberg, C. Ó. Coileáin, E. Pallecchi, D. Fadil and N. McEvoy, *npj 2D Mater. Appl.*, 2018, **2**, 5.

67 T. Das, E. Yang, J. E. Seo, J. H. Kim, E. Park, M. Kim, D. Seo, J. Y. Kwak and J. Chang, *ACS Appl. Mater. Interfaces*, 2021, **13(1)**, 1861–1871.

68 G. Eda and M. Chhowalla, *Nano Lett.*, 2009, **9**, 814–818.

69 Q. Zheng, W. H. Ip, X. Lin, N. Yousefi, K. K. Yeung, Z. Li and J. K. Kim, *ACS Nano*, 2011, **5**, 6039–6051.

70 Q. Li, Q. Zhou, L. Shi, Q. Chen and J. Wang, *J. Mater. Chem. A*, 2019, **7**, 4291–4312.

71 J. Li, Y. Lu, Q. Ye, M. Cinke, J. Han and M. Meyyappan, *Nano Lett.*, 2003, **3**, 929–933.

72 L. A. Currie, *Pure Appl. Chem.*, 1995, **67**, 1699–1723.

73 O. Leenaerts, B. Partoens and F. Peeters, *Phys. Rev. B: Condens. Matter Mater. Phys.*, 2008, **77**, 125416.

74 S. Zhao, J. Xue and W. Kang, *Chem. Phys. Lett.*, 2014, **595–596**, 35–42.

This journal is © The Royal Society of Chemistry 2023

J. Mater. Chem. C, 2023, **11**, 593–599 | **599**

Electronic Supplementray Information

Highly Conductive and Long-term Stable Films from Liquid-Phase Exfoliated Platinum Diselenide

Kangho Lee,[a] Beata M. Szydłowska,[ab] Oliver Hartwig,[a] Kevin Synnatschke,[c] Bartlomiej Tywoniuk,[a] Tomáš Hartman,[d] Tijana Tomašević-Ilić,[e] Cian P. Gabbet,[c] Jonathan N. Coleman,[c] Zdeněk Sofer,[d] Marko Spasenović,[f] Claudia Backes [bg] and Georg S. Duesberg *[a]

a. *Institute of Physics, EIT 2, Faculty of Electrical Engineering and Information Technology, University of the Bundeswehr Munich & SENS Research Center, Werner-Heisenberg-Weg 39, 85577 Neubiberg, Germany*
b. *Institute of Physical Chemistry, Heidelberg University, 69120 Heidelberg, Germany*
c. *School of Physics, CRANN & AMBER Research Centres, Trinity College Dublin, Dublin 2, Ireland*
d. *Department of Inorganic Chemistry, University of Chemistry and Technology Prague, Technicka 5, 166 28 Prague 6, Czech Republic*
e. *Institute of Physics Belgrade, University of Belgrade, Pregrevica 118, 11080 Belgrade, Serbia*
f. *Center for Microelectronic Technologies, Institute of Chemistry, Technology and Metallurgy, University of Belgrade, Njegoševa 12, 11000 Belgrade, Serbia*
g. *Physical Chemistry of Nanomaterials, University of Kassel, Heinrich-Plett-Str. 40, 34132 Kassel, Germany*

We would like to note that during the course of this work, dozens of devices were fabricated and tested. While all of the devices with relatively pinhole free networks showed good sensor performance, we found that film homogeneity was key for a stable and reproducible performance. We realised that the reproducibility of the film production (and thus device performance) is greatly improved when dispersions with narrowed nanosheet size distributions are used. Therefore, for the main part of the work in the main manuscript, a $PtSe_2$ dispersion was used where larger/thicker nanosheets were removed as sediment after centrifugation at 3000 g and small/thin nanosheets were removed as supernatant after centrifugation at 5000 g (see methods). For details on the characterisation of the nanosheets produced this way (including size/thickness distributions), the reader is referred to our previous report.[1] The disadvantage of this approach is that only a fraction of the nanosheets produced by sonication is selected which means that the mass is relatively low. While we attempted spraying such as size-selected dispersion, the mass was not sufficient to produce a film with close coverage. Therefore, to compare LB-tiled and sprayed networks with respect to conductivity and film thickness, a different set of dispersion had to be used with a much broader size/thickness distribution. Specifically, the centrifugation boundaries were set to 400 g and 30,000 g. This greatly affects the film morphology (homogeneity and thickness) in the tiled network as shown by the visual comparison in Fig. S1. The films produced from dispersions with narrower nanosheet size distribution (Fig. S1a-c) show greater homogeneity, lower roughness, better edge to edge contact of the nanosheets and a reduced overall thickness compared to the dispersion with the broader distribution (Fig. S1d-f).

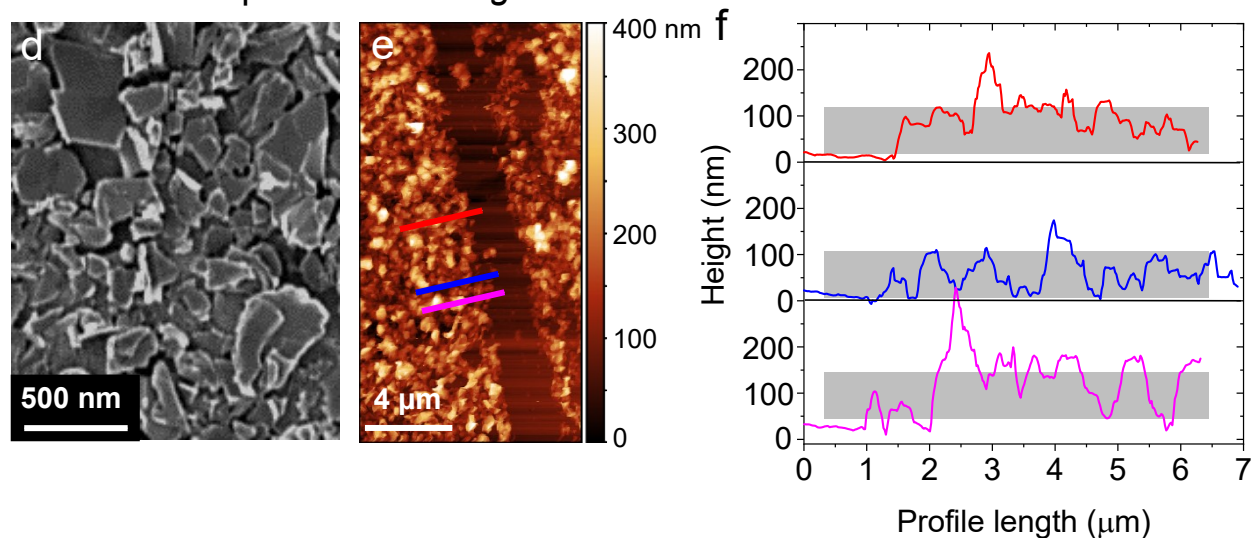# LB Film- Sample 3000-5000 g
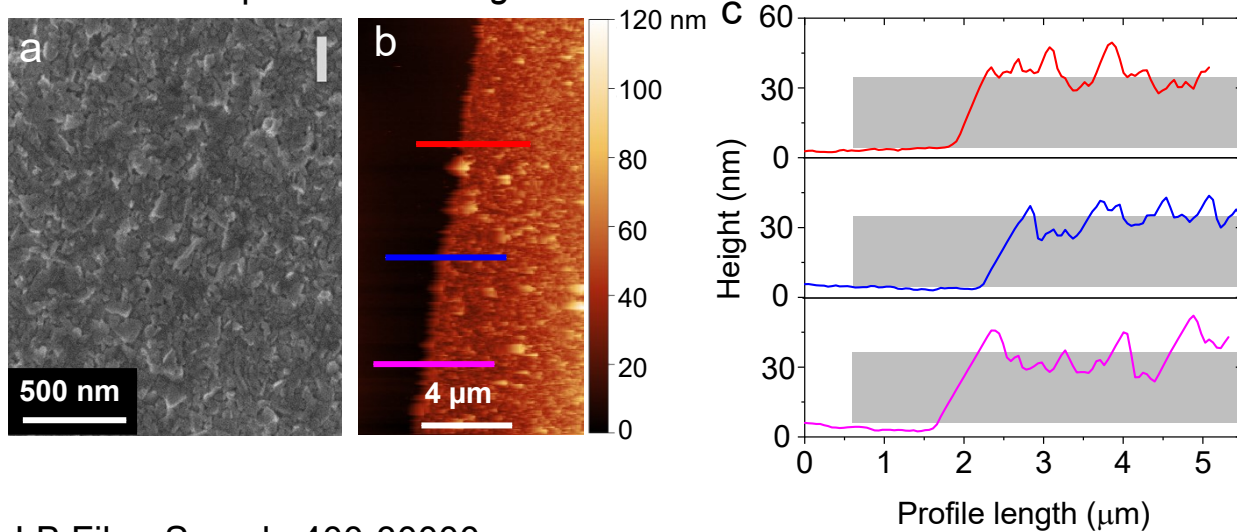
LB Film- Sample 400-30000 g

Fig. S1 Comparison of LB-type nanosheet networks produced from LPE-PtSe$_2$ using different size/thickness distributions through modification of the centrifugation conditions. (a-c) Data from the dispersion with narrower size distribution used for the gas sensing experiments. (a) SEM image, (b) AFM image of a scratched film. (c) Profiles of the lines indicated in (b). The gray box has a height of 30 nm and serves as guide for the eye to indicate the film thickness. (d-f) Same data from a dispersion with broader size distribution used to compare the conductivity of LB type and sprayed networks. (d) SEM image, (e) AFM image of a scratched film. (f) Profiles of the lines indicated in (e). The gray box in (f) has a height of 100 nm.
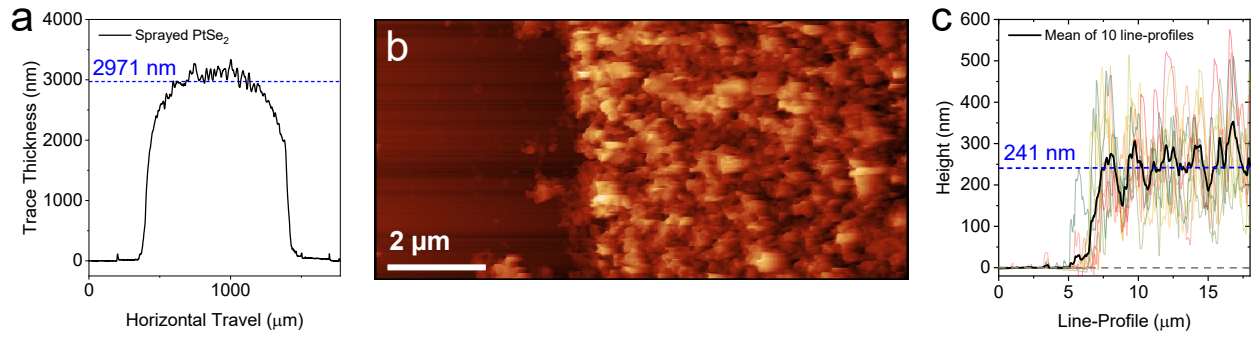
Fig. S2 (a) Profilometry curve indicates ~3 μm of film thickness produced by conventional spray deposition. (b) AFM image of an LPE-PtSe$_2$ film produced by the modified LB method using two subsequent deposition cycles of the 400-30000 g sample and (c) ~240 nm film thickness is estimated from the mean of 10 height profiles.

References

1   B. M. Szydłowska, O. Hartwig, B. Tywoniuk, T. Hartman, T. Stimpel-Lindner, Z. Sofer, N. McEvoy, G. S. Duesberg and C. Backes, *2D Mater.*, 2020, **7**, 045027.

Ultrafast humidity sensor based on liquid phase exfoliated graphene

Stevan Andrić[1]**, Tijana Tomašević-Ilić**[2] **, Marko V Bošković**[1]**, Milija Sarajlić**[1] **, Dana Vasiljević-Radović**[1]**, Milče M Smiljanić**[1] **and Marko Spasenović**[1,3]

[1] Center for Microelectronic Technologies, Institute of Chemistry, Technology and Metallurgy, University of Belgrade, Njegoševa 12, 11000, Belgrade, Serbia
[2] Institute of Physics Belgrade, University of Belgrade, Pregrevica 118, 11080, Belgrade, Serbia

E-mail: spasenovic@nanosys.ihtm.bg.ac.rs

CrossMark

Abstract

Humidity sensing is important to a variety of technologies and industries, ranging from environmental and industrial monitoring to medical applications. Although humidity sensors abound, few available solutions are thin, transparent, compatible with large-area sensor production and flexible, and almost none are fast enough to perform human respiration monitoring through breath detection or real-time finger proximity monitoring via skin humidity sensing. This work describes chemiresistive graphene-based humidity sensors produced in few steps with facile liquid phase exfoliation followed by Langmuir–Blodgett assembly that enables active areas of practically any size. The graphene sensors provide a unique mix of performance parameters, exhibiting resistance changes up to 10% with varying humidity, linear performance over relative humidity (RH) levels between 8% and 95%, weak response to other constituents of air, flexibility, transparency of nearly 80%, and response times of 30 ms. The fast response to humidity is shown to be useful for respiration monitoring and real-time finger proximity detection, with potential applications in flexible touchless interactive panels.

Supplementary material for this article is available online

Keywords: graphene, liquid phase exfoliation, humidity sensing, respiration monitoring

(Some figures may appear in colour only in the online journal)

1. Introduction

Humidity monitoring is essential for numerous applications across industries, such as environmental and industrial monitoring, and healthcare [1, 2]. Aside from traditional uses in monitoring atmospheric and room conditions, technological progress keeps enabling new uses for humidity sensors. In healthcare, humidity sensing could be used for human respiration monitoring [3, 4] due to the high level of water vapor in breath. In electronics and robotics industries, humidity clouds near human skin could be used to detect finger position for touchless control interfaces [5, 6]. However, humidity sensors made of established materials such as metal/polymer composites have temporal response rates that are far too slow for these applications, in the range 5–50 s [2]. Emerging composite and nanomaterials such as ZnO and Pd–SnO$_2$ also suffer from the same debilitating disadvantage [7, 8]. More recently, graphene and graphene oxide have emerged as a promising material for fast humidity sensing, with response times ranging from 10's of milliseconds to a few seconds, depending on the method of production [9–15].

Compared to many other materials, graphene has the added benefits of being thin, flexible, and transparent, enabling applications in wearable and flexible electronics. Nevertheless, graphene humidity sensors to date have been made from graphene that is either industrially irrelevant (mechanically exfoliated), expensive (chemical vapor deposited, CVD) or

---

[3] Author to whom any correspondence should be addressed.

made with several complex chemistry steps, such as with reduction of graphene oxide.

Here, we demonstrate fast humidity sensors made with an inexpensive and facile production method that is compatible with large-area sensor production. The active sensing area is made from liquid-phase exfoliated graphene [16] that requires only a single ultrasonic processing step. The humidity response times of our sensors are as low as ~30 ms, which allows us to show real-time breath monitoring and finger proximity detection as exemplary applications of ultrafast humidity sensing. Breath monitoring and proximity detection are only two examples of potentially numerous applications of these novel ultrafast humidity sensors, enabled by the fast response. We demonstrate sensing capability on three different substrates, including flexible transparent ones. The sensors fare very well against standard gas sensor performance metrics, such as insensitivity to other components of air and response time [17].

2. Material and methods

2.1. Fabrication of graphene films and humidity sensors

The graphene dispersion was produced by dissolving graphite powder (Sigma Aldrich, product no. 332 461) at a concentration of 18 mg ml^{-1} in N-Methly-2-pyrrolidone (NMP) (Sigma Aldrich, product no. 328 634). The dispersion was sonicated in a low energy ultrasonic bath for 14 h. After sonication the dispersion was centrifuged at 3000 rpm for 60 min in order to separate non-exfoliated graphite flakes, which remain in the precipitate, and the exfoliated graphene flakes which are dispersed in the supernatant. A small volume of the supernatant is added to deionized water (18 MΩ cm^{-1}) resulting in self-assembly of graphene nanoplatelets into a thin film on the water/air interface. The thin film is deposited on a pre-immersed substrate of choice following the Langmuir–Blodgett method [16, 18–20].

Our film, made of graphene that is exfoliated in the liquid phase and assembled with the Langmuir–Blodgett method, consists of graphene nanoplatelets in contact with each other, as shown in the atomic force micrograph in supporting information (figure S1) (available online at http://stacks.iop.org/NANO/31/025505/mmedia).

Although nanoplatelets conform to a distribution of thicknesses, the average thickness of the film is ~10 layers of graphene (3.4 nm), as measured with UV–VIS absorption spectroscopy and shown in supporting information (figure S2). For well-defined channel geometry and accurate sheet resistance measurements, we use a SiO$_2$/Si substrate with four microfabricated metal contacts (figure 1(a)). The substrate is a 380 μm thick n-doped Si wafer with a thermally grown 800 nm thick SiO$_2$ insulating layer. We deposit a layer of chromium (20 nm) and a layer of gold (100 nm) with radio-frequency cathode sputtering. Subsequently the layers of chromium and gold are coated with 0.5 μm of photoresist (AZ-1505) that is subjected to direct laser writing (LW405, MicroTech, Italy)
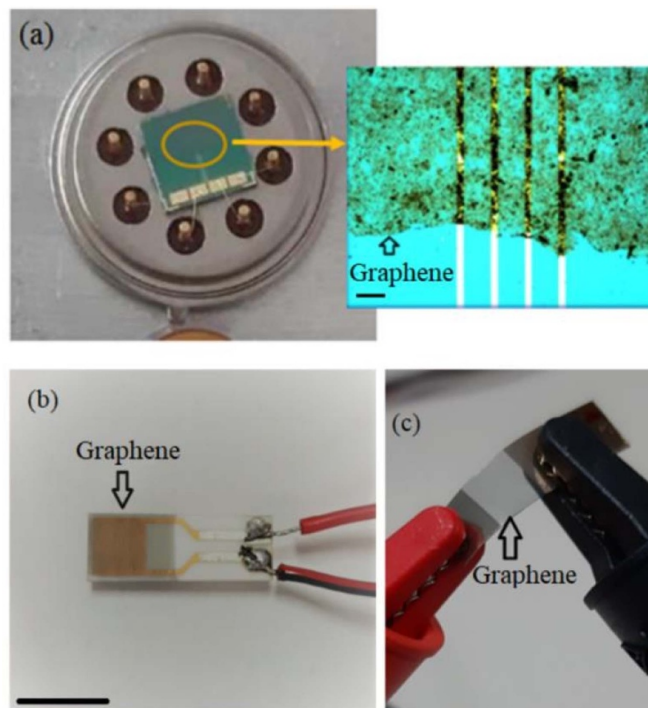

Figure 1. (a) Graphene humidity sensors on different substrates. (a) Optical image of a sensor with four contacts and the graphene sensor active area. Inset: optical micrograph of graphene film on contacts. The scale bar is 50 μm. (b) Optical image of the graphene film on the ceramic commercial substrate with interdigitated electrodes. The scale bar is 1 cm. (c) Optical image of graphene film on PET with macroscopic gold contacts.

[21] to pattern the contacts. The gold is removed with a solution of potassium iodide and the chromium is removed with a solution of ammonium cerium (IV) sulfate. The wafer is diced into 3 × 3 mm chips, each chip containing a set of four metal contacts. After film deposition, the chips are mounted to TO-8 housing. Sensor fabrication is reproducible, with AFM and UV–VIS measurements yielding the same average thickness for every device made.

The inset of figure 1(a) depicts an optical micrograph of the graphene film deposited on the contacts. Darker spots indicate remaining unexfoliated or thick graphite material. The film area between contacts has dimensions of ~1500 μm × 190 μm. Taking into account film geometry yields sheet resistance of 3–7 kΩ sq^{-1} for our films consistently, the smallest values reported for post-processing-free single-deposition Langmuir–Blodgett graphene films to date [16, 18, 20, 22]. Such small sheet resistance is a result of fabrication process streamlining and careful four-terminal resistance measurements. For obtaining the largest sensing area and highest signal-to-noise ratio, we employ a commercial ceramic substrate with pre-made interdigitated electrodes (DropSens IDEAU200), figure 1(b). This substrate is easy to handle, versatile, low-cost, and easily connected to macroscopic wires by soldering, and the active sensing area is ~15 mm^2. Finally, for flexible transparent humidity sensors we employ a polyethylene terephthalate (PET) substrate with macroscopic gold contacts thermally evaporated over a shadow mask, as in
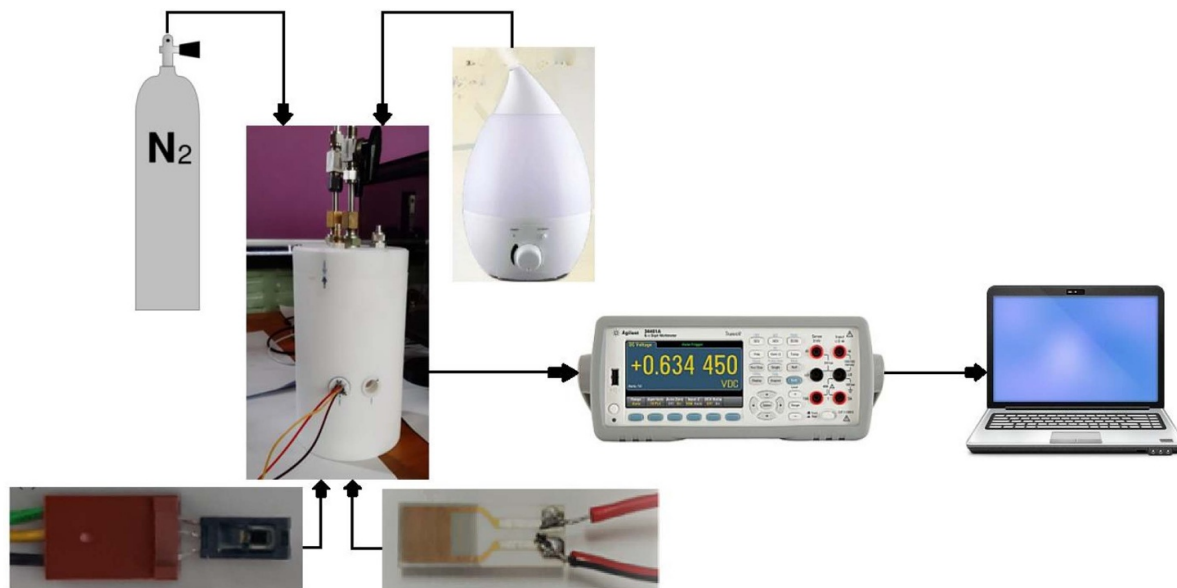
Figure 2. Experimental setup for measuring humidity response. A homebuilt humidity chamber is designed with slots for the graphene sensor and a reference sensor. It has inlets for water vapor from a room humidifier and for purging with nitrogen N_2 gas. The sensors are connected to measurement electronics.

figure 1(c). The size of the active area on this substrate is 5×5 mm. The optical transmittance at a wavelength of 660 nm is 78%, as shown in figure S2 of supporting information.

2.2. Humidity sensing

We perform humidity sensing in a homebuilt humidity chamber made of polytetrafluoroethylene (PTFE), as depicted in figure 2. The chamber is equipped with separate valves for injection of water vapor and another gas, a gas outlet valve, and auxiliary connectors. Our sensor in its TO-8 housing is integrated into a custom-made PTFE plug that we insert into a matching slot in the chamber, next to a reference humidity sensor (Honeywell HIH-4000-001). A thermocouple is placed near the sensors to measure the local temperature. All measurements were performed at room temperature (21 °C–23 °C). We apply a current of 10 μA between the outer electrode pair and measure the induced voltage across the inner electrode pair to obtain the resistance. The voltage was measured with a Keysight 34 461 a DMM. In the cases of the commercial ceramic substrate and the PET substrate we monitored two-terminal resistance with the same DMM operated in ohmmeter mode. Relative humidity (RH) was decreased to 8% by purging the sealed chamber with nitrogen (N_2) gas. Water vapor is produced with a commercial room humidifier and injected into the chamber at a constant flow rate. Once a desired humidity level is reached the water vapor inlet valve is manually closed.

To measure sensor speed below the limit imposed by humidity chamber filling time, we placed the sensors on a table in free space at RH $\sim$40%. A nitrogen gun was used to induce nitrogen flow across the sensor surface, quickly drying the active area while we monitored the sensor response and recovery times [11].

2.3. Respiration monitoring and touchless sensing

Respiration monitoring and touchless sensing were performed at atmospheric conditions, at a temperature of $\sim$25 °C and RH $\sim$40%. The graphene sensors were placed on a table and connected to measurement electronics as described above, and a volunteer proceeded to breathe onto the sensor surface or bring a finger nearby the sensor. All three types of substrates were tested under the same conditions.

3. Results and discussion

3.1. Humidity sensing

The humidity sensing performance of our devices was tested by monitoring device resistance while controlling relative humidity in the humidity chamber. Figure 3(a) depicts three cycles of a humidity ramp in the test chamber and corresponding measurements with our graphene sensor on the ceramic substrate with interdigitated electrodes (black) and the reference sensor (purple). During each cycle the humidity in the chamber is increased from $\sim$8% to 95% and then decreased to $\sim$8%. The resistance of our sensor rises with humidity, as was shown earlier for other films that consist of conducting NbS_2 nanoplatelets [23]. The increase in resistance is attributed to water adsorption at nanoplatelet edges and between the platelets, both of which disrupt electrical conduction paths of the film. In the case of graphene, other mechanisms could also play a role, such as electron donation from graphene to water and disruption of molecular symmetries of graphene by the water molecules [24]. For a clear perception of the sensitivity of our sensor, we plot a second vertical axis next to the resistance axis that depicts the percent change of resistance, described by $S = 100 \cdot \frac{\Delta R}{R_0}$, where R_0 is the initial resistance value and ΔR is the difference between the given and the
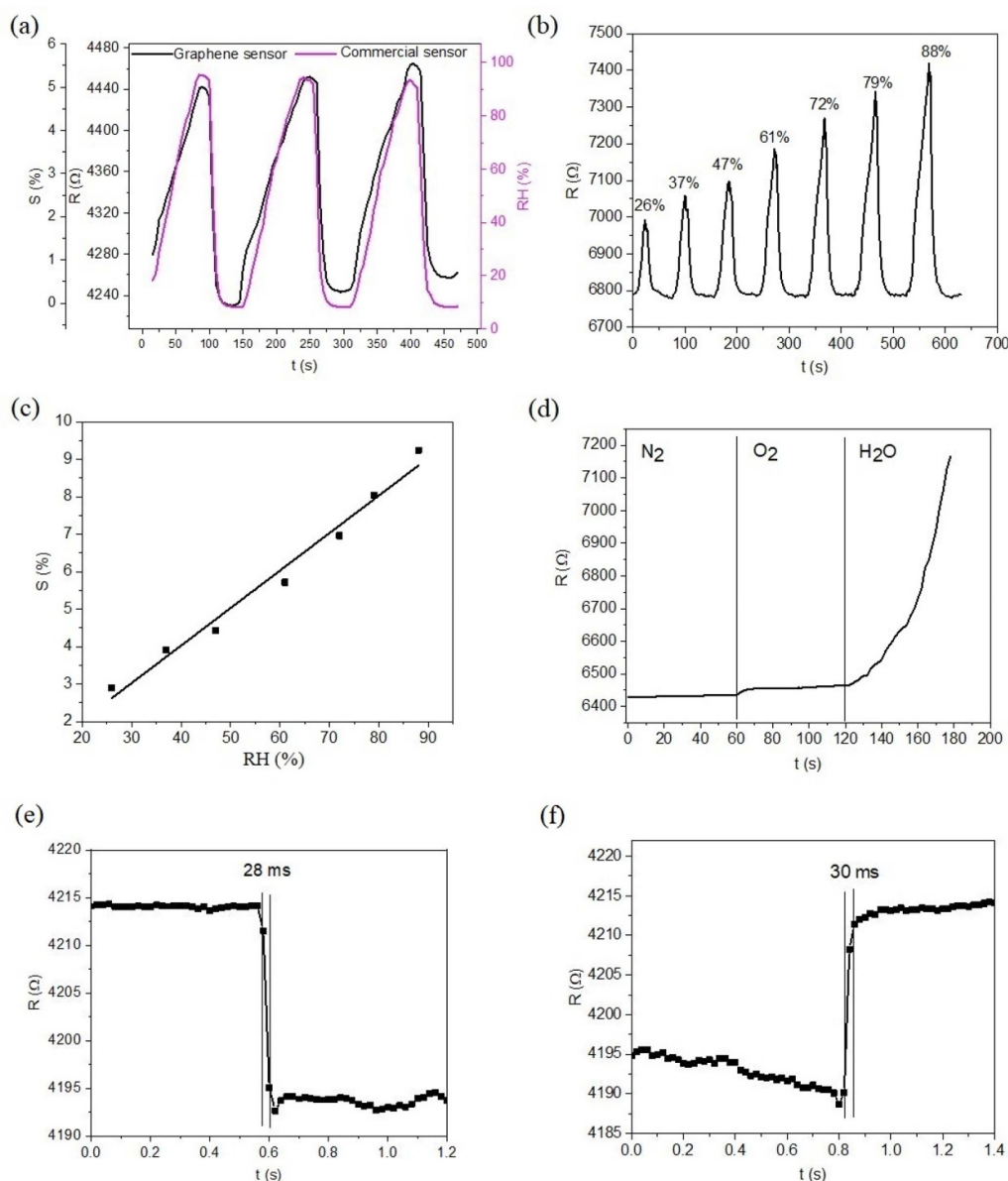
Figure 3. Response to humidity and other constituents of air. Measurements are conducted on the ceramic substrate with interdigitated electrodes. (a) Graphene sensor response measured in conjunction with the reference sensor response over three cycles of ramping RH from ∼8% to 95%. (b) Graphene sensor response to repeat stepwise increase of relative humidity, from 26% to 88%, in time. (c) Peak sensor response as function of maximum RH. (d) Sensor response to nitrogen, oxygen and water vapor over 60 s each. (e) Response time of graphene sensor when a nitrogen N_2 gun is used to flush the device. (f) Recovery time of graphene sensor after flushing with nitrogen N_2 gun.

initial resistance value. The resistance of the graphene sensor changes by 5% when changing humidity from 8% to 95%. The sensitivity is thus higher than reported for CVD graphene [10, 11], which is more costly than liquid phase exfoliation as per word graphene, and higher than for industrially irrelevant mechanically exfoliated graphene [25]. Sensor repeatability indicates that the likely dominant mechanism is physisorption of water molecules, with little chemisorption. There is a small baseline drift that occurs when the sensor rests in air which is visible on figure 3(a). A similar drift was observed in mechanically exfoliated bilayer graphene [11]. Although such a drift could potentially be detrimental to the practical

use of graphene-based gas sensors, we found that the drift is fully reversible with heating to temperatures around 150 °C that could easily be achieved with an on-chip integrated heater [26].

Figure 3(b) depicts the response of the graphene sensor over several cycles with different maximum RH. In this image the baseline drift has been corrected for by linear subtraction. The raw data that includes the drift is provided in supporting information (figure S3). The relative change in resistance, S, as a function of maximum humidity is shown in figure 3(c). The sensor response is clearly linear with humidity (r = 0.981), which indicates potential for applications in
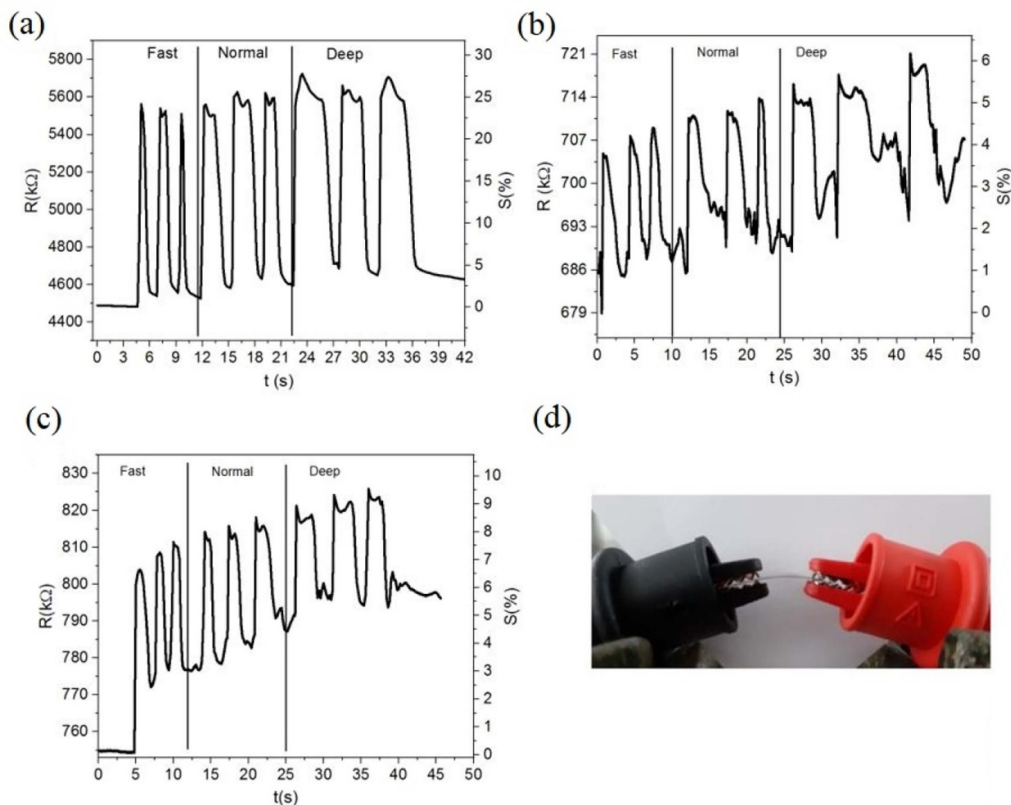
Figure 4. Respiration monitoring. (a) Monitoring fast, normal and deep breathing with graphene sensor on ceramic substrate. (b) Monitoring breathing rate on flat PET substrate, and (c) on PET that is bent at an angle of 10 degrees, as seen in (d).

diverse conditions. In the case of our graphene sensors on Si/SiO$_2$ substrates, the linearity is similar to that reported here, while the sensitivity is ~10 times smaller (see supporting information, figure S4). The sensing response on the two substrates should not be directly compared, because of the vastly different active sensing areas and contact spacing. The ceramic substrate is optimized for high sensing performance, whereas the contact design on the Si/SiO$_2$ substrate is optimized for sheet resistance measurements.

To confirm that our sensor reacts to water vapor and not to other constituent gases of air, we tested the response to nitrogen and oxygen. Figure 3(d) depicts the sensor response to nitrogen gas (injected into the chamber at t = 0 s), to oxygen gas replacing nitrogen (at t = 60 s), and finally to water vapor injected instead of oxygen (at t = 120 s). The sensor does not respond to nitrogen N$_2$, reacts very little to O$_2$ and has a strong response to H$_2$O gas, an effect that could be used to implement selectivity. Humidity was reduced to ~0% before starting the experiment.

Sensor response and recovery times cannot be measured in the humidity chamber due to the limited chamber-filling and chamber-flushing times, hence we proceed to measure the sensor response time by rapidly drying the sensor surface in ambient with a nitrogen gun and observing sensor dynamics. In figure 3(e) we show nitrogen gun drying of the sample, with observed rapid recovery shown in figure 3(f). We set a 10% and a 90% change threshold for measuring rise and fall times. The sensor responds in 28 ms and recovers in

30 ms. Similar dynamics are observed in other samples on the same substrate. The obtained response is significantly faster than that reported earlier for single-layer and double-layer CVD graphene (~700 ms) [10, 11] and is two orders of magnitude faster than the commercial reference sensor (Honeywell HIH6100 Series Datasheet). The response time in the case of our graphene sensors on Si/SiO$_2$ substrates is longer, in the range of 240 ms (see supporting information figure S5). The fast response of our sensors is likely due to additional carrier scattering introduced by edge defects [27, 28].

3.2. Respiration monitoring

High-speed humidity sensors enable the monitoring of human respiration by breath detection. To test the usefulness of our sensors for respiration monitoring, we placed the sensors on a table and had a volunteer breathe near the sensor surface. Figure 4(a) depicts the response of a sensor on a ceramic substrate to breathing cycles in a fast, regular, and slow pattern. A recording of respiration detection is shown in Supporting Video 1. It is evident that the sensor responds to human respiration and can be used as a biometric detector of respiration rate. In real-life conditions outside the humidity chamber, the resistance changes by up to 20% during breathing, which offers an excellent on/off ratio that is useful for applications. The sensitivity to breath is larger than can be found in literature that describes other graphene-based sensors, which are also generally produced with more complex chemistry steps
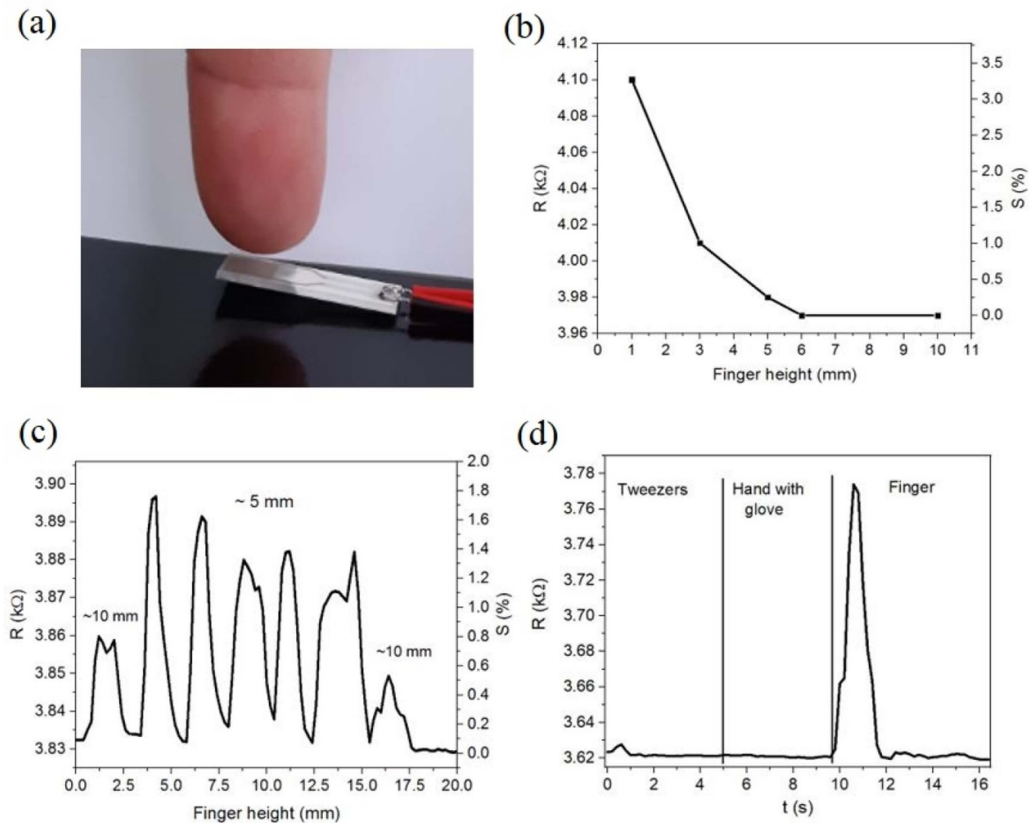
Figure 5. Finger proximity detection. (a) Optical image of the touchless proximity sensing experiment. (b) Resistance as a function of fingertip distance to device. (c) Demonstration of ultrafast proximity detection as a finger is swept across the device at different distances. (d) Response of touchless sensor to metallic tweezers and hand with glove.

[29]. The high sensitivity of our sensor is likely due to the abundancy of reactive edge sites in the film consisting of interconnected nanoplatelets. The sensor on the SiO$_2$/Si substrate also responds to breath, although with a smaller sensitivity (see supporting information figure S6). A resistance change of ∼24% is measured for respiration monitoring on the ceramic substrate (figure 4(a)), while changes of ∼6%–8% are measured on the PET substrate (figures 4(b) and (c)).

3.3. Transparent flexible sensors

For certain applications, such as for monitoring the respiration rate of first responders or medical patients via sensors attached to transparent masks, or for transparent touchless control panels, it would be advantageous to have the sensor on a transparent substrate. Results of respiration monitoring of our large-area sensors on PET are shown in figure 4(b). Qualitatively, the performance is similar as on the rigid substrate. Quantitatively, the response is an order of magnitude weaker on PET, with a more pronounced background drift. We emphasize again that the sensing performance on the different substrates should not be directly compared, as the contact and sensor geometry is differently optimized on the various substrates for different purposes. The speed of sensor response on a PET substrate is ∼20 ms, as shown in supporting information (figure S7). We purposely made the sensor on a flexible substrate to

demonstrate compatibility with flexible electronics and wearable technology. Flexing the substrate is not detrimental to the humidity sensing performance of the sensor, and results in similar response to breath, as seen in figure 4(c). The data shown in figure 4(c) was taken for a sensor bent with a curvature of 10 degrees, as in figure 4(d). The method of measuring curvature is presented in supporting information (figure S8). To demonstrate operational performance of our sensors under different conditions, we present sensor response at different temperatures (figure S9) and in a flexed state (figure S10). Sensitivity decreases with temperature, as is common for chemiresistive humidity sensors [30].

3.4. Finger proximity detection

Our devices have an interesting application in proximity sensing, as part of positioning interfaces for touchless screens and applications in robotics [5]. It is well known that human skin emits a cloud of moisture that decays over a distance of ∼1 cm, an effect that has been proposed as a working mechanism for positioning interfaces that detect the presence of a human finger [6]. However, practical realization of such interfaces has been elusive, primarily due to the low speed of the materials considered thus far. Devices based on VS$_2$ [6] and graphene oxide [31–33] have response and recovery times ranging from 1 s to more than 20 s, which causes a delay in finger position detection that is impractical. Figure 5(a) depicts an

optical image of the proximity detection experiment. A finger is held at a specific distance from the device as the resistance is measured. Figure 5(b) depicts the distance-dependent device response to the presence of a fingertip. The sensor responds at a finger distance of 10 mm and resistance significantly increases for smaller distances. To demonstrate ultrafast performance of our proximity sensor, the volunteer swipes his finger above the device at different distances (figure 5(c)). It is clear that the device responds to finger motion in real time, enabling practical development of novel man-machine interactive systems. Real-time finger proximity detection is demonstrated in Supporting Video 2. We show that the response to human finger proximity is due to humidity and not a capacitive effect by testing the sensor response to the presence of metal tweezers and a finger covered with a rubber glove (figure 5(d)). The maximum measured resistance change for an approaching finger is ∼1,6%.

4. Conclusions

We have demonstrated humidity sensors based on graphene that are sensitive, thin, flexible, nearly 80% transparent, only weakly reactive to other constituents of air, and fast enough to be used for advanced applications such as respiration rate monitoring and finger proximity detection. The principles of operation shown here, combined with the ease of manufacture of the sensors, indicate strong technological potential for wearable health monitoring and touchless control panels. The demonstrated behavior is unparalleled in literature, surpassing other state of the art solutions in terms of sensor response and recovery times, ease of manufacture, substrate compatibility, transparency and scale-up potential.

Acknowledgments

ORCID iDs

Tijana Tomašević-Ilić ⬤ https://orcid.org/0000-0003-2870-0765
Milija Sarajlić ⬤ https://orcid.org/0000-0002-1267-1827
Milče M Smiljanić ⬤ https://orcid.org/0000-0002-3420-0823
Marko Spasenović ⬤ https://orcid.org/0000-0002-2173-0972

References

[1] Liu X, Cheng S, Liu H, Hu S, Zhang D and Ning H 2012 A survey on gas sensing technology *Sensors* **12** 9635–65

[2] Blank T A, Eksperiandova L P and Belikov K N 2016 Recent trends of ceramic humidity sensors development: A review *Sensors Actuators* B **228** 416–42

[3] Manolis A 1983 The diagnostic potential of breath analysis *Clin. Chem.* **29** 5–15

[4] Earthrowl-Gould T, Jones B and Miller M R 2001 Chest and abdominal surface motion measurement for continuous monitoring of respiratory function *Proc. Inst. Mech. Eng.* H **215** 515–20

[5] Zirkl M *et al* 2011 An all-printed ferroelectric active matrix sensor network based on only five functional materials forming a touchless control interface *Adv. Mater.* **23** 2069–74

[6] Feng J, Peng L, Wu C, Sun X, Hu S, Lin C, Dai J, Yang J and Xie Y 2012 Giant moisture responsiveness of vs $_2$ ultrathin nanosheets for novel touchless positioning interface *Adv. Mater.* **24** 1969–74

[7] Nguyen K, Hung C M, Ngoc T M, Le D T T, Nguyen D H, Van D N and Van H N 2017 Low-temperature prototype hydrogen sensors using Pd-decorated SnO_2 nanowires for exhaled breath applications *Sensors Actuators* B **253** 156–63

[8] Yoo R, Park Y, Jung H, Rim H J, Cho S, Lee H S and Lee W 2019 Acetone-sensing properties of doped ZnO nanoparticles for breath-analyzer applications *J. Alloys Compd.* **803** 135–44

[9] Papamatthaiou S, Argyropoulos D P, Farmakis F, Masurkar A, Alexandrou K, Kymissis I and Georgoulas N 2016 The effect of thermal reduction and film thickness on fast response transparent graphene oxide humidity sensors *Procedia Eng.* **168** 301–4

[10] Smith A D *et al* 2015 Resistive graphene humidity sensors with rapid and direct electrical readout *Nanoscale* **7** 19099–109

[11] Fan X, Elgammal K, Smith A D, Östling M, Delin A, Lemme M C and Niklaus F 2018 Humidity and CO2 gas sensing properties of double-layer graphene *Carbon* **127** 576–87

[12] Taylor A P and Velásquez-García L F 2015 Electrospray-printed nanostructured graphene oxide gas sensors *Nanotechnology* **26** 505301

[13] Xiao S, Nie J, Tan R, Duan X, Ma J, Li Q and Wang T 2019 Fast-response ionogel humidity sensor for real-time monitoring of breathing rate *Mater. Chem. Front.* **3** 484–91

[14] Borini S, White R, Wei D, Astley M, Haque S, Spigone E, Harris N, Kivioja J and Ryhänen T 2013 Ultrafast graphene oxide humidity sensors *ACS Nano* **7** 11166–73

[15] Jiang B, Bi Z, Hao Z, Yuan Q, Feng D, Zhou K, Zhang L, Gan X and Zhao J 2019 Graphene oxide-deposited tilted fiber grating for ultrafast humidity sensing and human breath monitoring *Sensors Actuators* B **293** 336–41

[16] Tomašević-Ilić T, Jovanović Đ, Popov I, Fandan R, Pedrós J, Spasenović M and Gajić R 2018 Reducing sheet resistance of self-assembled transparent graphene films by defect patching and doping with UV/ozone treatment *Appl. Surf. Sci.* **458** 446–53

[17] Mackin C, Fasoli A, Xue M, Lin Y, Adebiyi A, Bozano L and Palacios T 2020 Chemical sensor systems based on 2D and thin film materials *2D Mater.* **7** 022002

[18] Matković A *et al* 2016 Enhanced sheet conductivity of Langmuir-Blodgett assembled graphene thin films by chemical doping *2D Mater.* **3** 015002

[19] Tomašević-Ilić T, Pešić J, Milošević I, Vujin J, Matković A, Spasenović M and Gajić R 2016 Transparent and conductive films from liquid phase exfoliated graphene *Opt. Quantum Electron.* **48** 1–7

[20] Kim H, Mattevi C, Kim H J, Mittal A, Mkhoyan K A, Riman R E and Chhowalla M 2013 Optoelectronic properties of graphene thin films deposited by a Langmuir-Blodgett assembly *Nanoscale* **5** 12365–74

[21] Sarajlić M, Frantlović M, Smiljanić M M, Rašljić M, Cvetanović-Zobenica K, Lazić Ž and Vasiljević-Radović D 2019 Thin-film four-resistor temperature sensor for measurements in air *Meas. Sci. Technol.* **30** 115102

[22] Li X, Zhang G, Bai X, Sun X, Wang X, Wang E and Dai H 2008 Highly conducting graphene sheets and Langmuir-Blodgett films *Nat. Nanotechnol.* **3** 538–42

[23] Divigalpitiya W M R, Frindt R F and Morrison S R 1990 Effect of humidity on spread NbS2 films *J. Phys. D: Appl. Phys.* **23** 966–70

[24] Yavari F, Kritzinger C, Gaire C, Song L, Gulapalli H, Borca-Tasciuc T, Ajayan P M and Koratkar N 2010 Tunable bandgap in graphene by the controlled adsorption of water molecules *Small* **6** 2535–8

[25] Massera E, La Ferrara V, Miglietta M, Polichetti T, Nasti I and Di Francia G 2012 Gas sensors based on graphene. comparison of two different fabrication approaches *Chim. Oggi/Chem. Today* **30** 29–31

[26] Sarajlić M, Đurić Z, Jović V, Petrović S and Đorđević D 2013 Detection limit for an adsorption-based mercury sensor *Microelectron. Eng.* **103** 118–22

[27] Dan Y, Lu Y, Kybert N J, Luo Z and Johnson A T C 2009 Intrinsic response of graphene vapor sensors *Nano Lett.* **9** 1472–5

[28] Zhang Y H, Chen B Y, Zhou K G, Liu C H, Zeng J, Zhang H L and Peng Y 2009 Improving gas sensing properties of graphene by introducing dopants and defects: A first-principles study *Nanotechnology* **20** 185504

[29] Pang Y *et al* 2018 Wearable humidity sensor based on porous graphene network for respiration monitoring *Biosens. Bioelectron.* **116** 123–9

[30] Björkqvist M, Paski J, Salonen J and Lehto V-P 2005 Temperature dependence of thermally-carbonized porous silicon humidity sensor *Phys. Status Solidi* **202** 1653–7

[31] Cheng H, Huang Y, Qu L, Cheng Q, Shi G and Jiang L 2018 Flexible in-plane graphene oxide moisture-electric converter for touchless interactive panel *Nano Energy* **45** 37–43

[32] An J, Le T S D, Huang Y, Zhan Z, Li Y, Zheng L, Huang W, Sun G and Kim Y J 2017 All-graphene-based highly flexible noncontact electronic skin *ACS Appl. Mater. Interfaces* **9** 44593–601

[33] Wee B H, Khoh W H, Sarker A K, Lee C H and Hong J D 2015 A high-performance moisture sensor based on ultralarge graphene oxide *Nanoscale* **7** 17805–11

Three Types of Films from Liquid-phase-exfoliated Graphene for Use as Humidity Sensors and Respiration Monitors

Stevan Andrić,[1*] Tijana Tomašević-Ilić,[2] Lazar Rakočević,[3]
Dana Vasiljević-Radović,[1] and Marko Spasenović[1**]

[1]Center for Microelectronic Technologies, Institute of Chemistry, Technology and Metallurgy,
National Institute of the Republic of Serbia, University of Belgrade, Njegoševa 12, Belgrade 11000, Serbia
[2]Institute of Physics Belgrade, University of Belgrade, Pregrevica 118, Belgrade 11080, Serbia
[3]INS Vinca, Department of Atomic Physics, University of Belgrade,
Mike Petrovića Alasa 12–14, Belgrade 11351, Serbia

Measuring relative humidity is important for a myriad of industries, including production, agriculture, environmental monitoring, and medicine. Thin-film, fast-response sensors are particularly interesting for wearable applications, such as monitoring breathing. We report on humidity sensors made from graphene deposited as a thin film by the Langmuir–Blodgett (LB) method from three types of graphene in solution. We demonstrate humidity sensing and respiration monitoring from graphene made by bath sonication, probe sonication, and electrochemical exfoliation. We characterize the morphology and chemical composition of the three film types and compare their performance as sensors. We conclude that although all three types can be used for sensing, they each have their particular advantages and drawbacks.

1. Introduction

Knowledge of relative humidity (RH) is of crucial importance for various industries such as production, agriculture, environmental monitoring, and medicine.[1,2] Standard materials used for humidity sensing are based on metal and polymers;[2] however, insufficient transparency, thermal stability, flexibility, and response speed (in tens of seconds) have motivated research on other active materials for humidity sensing, especially in wearable applications.

Graphene has excellent mechanical and thermal stabilities, high transparency, and high flexibility, making it suitable for implementation in sensors such as humidity sensors.[3,4] Graphene obtained by chemical vapor deposition (CVD) and liquid-phase exfoliation (LPE) has been reported to have applications in humidity sensing and respiration monitoring, because water vapor is present in human breath.[5–9] The goal of graphene sensor research in general is to synthesize graphene films at a low cost while retaining the material's basic characteristics and achieving high reactivity to the sensed gas. One of the methods of synthesis is the formation of

graphene dispersions, which are obtained by LPE using several techniques, such as ultrasonic exfoliation, electrochemical exfoliation, ball milling, and high-shear mixing.[10] After obtaining a dispersion, one needs to deposit graphene from the solution onto a substrate to obtain solid-state graphene. For this purpose, Langmuir–Blodgett (LB) deposition, spin coating, or drop casting is used.[11] Both the LPE and LB methods are economical and efficient for synthesizing graphene films.[12]

In this paper we demonstrate three types of graphene humidity sensors, where graphene films were obtained from three types of LPE, with the LB method used to deposit graphene from a dispersion onto a solid substrate. The graphene films were tested as active humidity sensors as well as real-time respiration monitors. Their morphology and chemical composition were also characterized. We demonstrate that although there are differences in the chemical composition of the obtained graphene dispersions and in the morphology of the deposited films that contribute to different sensitivities to humidity, all three types of graphene exhibit humidity-sensing behavior, showing that LPE followed by the LB method is a robust approach for fabricating graphene-based humidity sensors.

In our previous work, we demonstrated ultrafast humidity sensing with bath-exfoliated graphene films.[13] The novelty of the current paper is a direct comparison of the sensor used in our previous work with other types of LPE graphene sensors. This is also, to the best of our knowledge, the first report of humidity sensing with commercially obtained electrochemically exfoliated graphene. First reports on in-lab electrochemically exfoliated graphene as a humidity sensor have appeared recently.[14]

2. Materials and Methods

2.1 Synthesis of graphene film

The first graphene dispersion was prepared by dispersing graphite powder (Sigma Aldrich, product no. 332461), with a concentration of 18 mg/ml in *N*-methyl-2-pyrrolidone (NMP) (Sigma Aldrich, product no. 328634). Such a dispersion was sonicated for 14 h in a low-power ultrasonic bath. After sonication, the obtained dispersion was centrifuged for 60 min at 3000 rpm to separate non-exfoliated graphite flakes, leaving only graphene flakes in the supernatant.[15] The second graphene dispersion was prepared using the same graphite powder with the same initial graphite concentration in aqueous sodium dodecylbenzenesulfonate (SDBS) (Sigma Aldrich, product no. 289957). This dispersion was sonicated for 6 h with an ultrasonic probe of 200 W power. Sonication was performed for 1 h, after which the solution was centrifuged for 90 min at 5000 rpm, then the sonication was continued for 5 h. The obtained dispersion was centrifuged for 90 min at 1500 rpm, whereby the non-exfoliated graphite flakes remained in the sediment and the supernatant contained exfoliated graphene flakes. The water-based graphene dispersion was transferred to NMP owing to its compatibility with LB deposition at an air/water interface. [10,12,16] For the transfer process, a mixture of 1 ml graphene dispersion in 11 ml isopropyl alcohol (IPA) was used. The mixture was centrifuged at 10000 rpm for 90 min to separate

graphene flakes of all sizes in the sediment. The supernatant was removed, and 2 ml cuvettes containing the sediment were refilled to the lines. The centrifugation step was repeated with the same parameters. After centrifugation, the described process was repeated one more time, for a total of three centrifugations. Instead of IPA, ~120 μm of NMP was poured into the final sediment, and all the dispersions were collected in one bottle. The third graphene dispersion was commercially obtained from Sixonia Tech GmbH (G-DISP-NMP-CSO-2+, Dresden, Germany). This dispersion was obtained by electrochemical exfoliation in NMP.

The three types of exfoliation have distinct advantages and disadvantages over each other. An ultrasonic bath with low-power ultrasound (around 30 W) is compatible with any solvent that is suitable for exfoliation, without the need to consider thermal stability. For instance, *N*-methyl-2-pyrrolidone (NMP) can be used as a solvent in exfoliation, from which homogeneous films can be directly deposited onto a liquid surface.[17] Exfoliation with an ultrasonic probe, on the other hand, is quick, powerful, and compatible with upscaling. Nevertheless, owing to the high power of exfoliation of up to 400 W, only thermally stable solvents can be used in exfoliation. After exfoliation, the graphene flakes must be transferred from the thermally stable solvent to one that can be used for LB deposition. The third dispersion is a commercially obtained graphene dispersion formed by electrochemical exfoliation. The advantage of using a commercial solution is that it removes the need for exfoliating in the laboratory where film formation and subsequent experiments are performed. However, the disadvantage is the lack of control over the exfoliation process and the final chemical composition of the material.

The LB method was used to produce the films from the above-described dispersions, in which a small amount, between 0.1 and 1 ml depending on the dispersion, of a graphene dispersion was carefully dripped in deionized water (18 MΩ/cm). The self-assembly of graphene flakes at the surface of the water resulted in the formation of a graphene film. This film was deposited on a suitable substrate.[12] Figure 1 shows photographs of all three graphene films deposited on a ceramic substrate with interdigitated gold electrodes (DropSens IDEAU200).

2.2   Characterization

To obtain the thickness of each graphene film without damaging the surface, UV–VIS (Thermo Scientific, Evolution 60) measurement in transmittance mode was used. Graphene was first assembled on transparent slides and the spectrum was recorded in the range from 300 to 700 nm with an emphasis on 660 nm, where the thickness was calculated from the optical transmittance. To measure the size of the graphene flakes and more closely examine the topography of the films, atomic force microscopy (AFM) was used with a scan area of 5×5 μm^2. For AFM, the films were deposited on a Si/SiO_2 substrate. Gwyddion software was used for the analysis of AFM images. For a clear understanding of the sensor mechanism during the interaction with humidity, namely, with water molecules, the chemical structure of graphene must be well known; therefore, X-ray photoelectron spectroscopy (XPS) was used. The analysis was performed with SPECS systems with an XP50M X-ray source for a Focus 500 X-ray monochromator and a PHOIBOS 100/150 analyzer. An AlKα source of 1486.74 eV at 12.5 kV
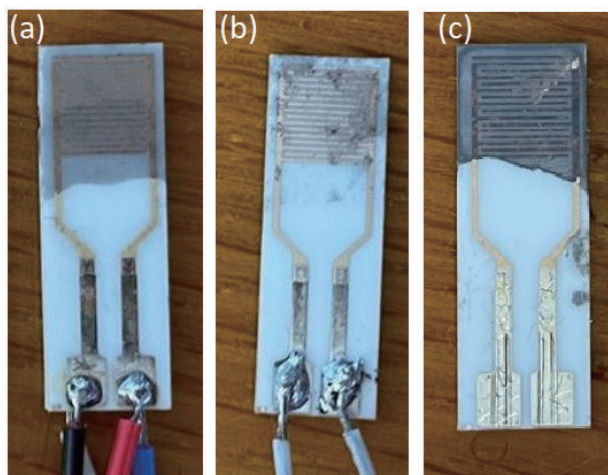
Fig. 1. (Color online) Photographs of films deposited from all three types of graphene dispersions on interdigitated ceramic substrates with gold electrodes: (a) graphene from ultrasonic bath, (b) graphene from ultrasonic probe, and (c) commercially available electrochemical graphene. The width and length of the graphene films are ~1 cm.

and 32 mA was used for this study. Survey spectra from binding energies of 0 to 1000 eV were recorded with a constant pass energy of 40 eV, a step size of 0.5 eV, and a dwell time of 0.2 s in the FAT mode. Detailed spectra for the C 1s peak were recorded with a pass energy of 20 eV, a step size of 0.1 eV, and a dwell time of 2 s in the FAT mode. Spectra were collected with the SpecsLab data analysis software and studied with the CasaXPS software package.

2.3   Humidity sensing

For humidity sensing and respiration monitoring, each of the three graphene films was assembled on a commercially available ceramic substrate with interdigitated gold contacts (Fig. 1). Such sensors were individually inserted in a custom-made chamber made of polytetrafluoroethylene (PTFE). A reference sensor (Honeywell HIH-4000-001) was placed next to the graphene sensor at a distance of ~2 cm. The humidity chamber was equipped with several valves by which gases could be injected and vented. The sensor response to humidity was monitored with a Keysight 34461a digital multimeter (DMM) in the two-terminal resistance mode (Fig. 2). Before the start of the measurement, the chamber was dried with nitrogen (N_2) gas through one of the valves. The lowest RH was ~10%, after which water vapor was injected through a second valve until RH reached a maximum of ~90%, upon which the injection of water vapor was stopped and the chamber was again dried out with N_2. Three cycles of such measurement were repeated. To establish the linearity of the sensor, a repeated stepwise increase in RH was performed.
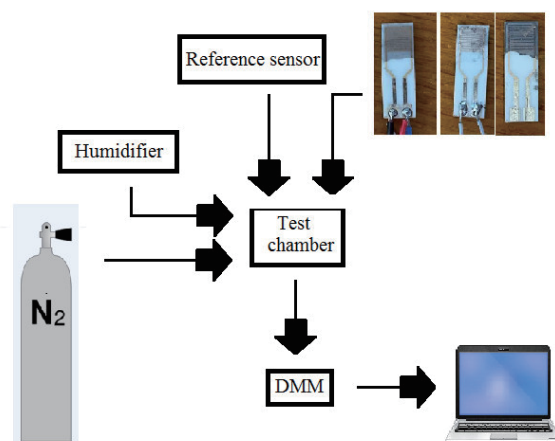
Fig. 2.   (Color online) Experimental setup used in this study.

2.4   Respiration monitoring

Respiration monitoring was conducted in a basic experiment under laboratory conditions (temperature ~25 ℃, room humidity ~50% RH). A graphene sensor was placed on a table while a volunteer breathed on the sensor. The sensor responded with a change in resistance. The volunteer breathed at three different paces: fast, normal, and slow.

3.   Results and Discussion

3.1   Characterization

Figure 3 depicts the UV–VIS spectrum used to calculate the thickness of each graphene film. The thickness was calculated from the optical transmittance of the film at a wavelength of 660 nm.[4] The graphene film obtained from the dispersion formed with the ultrasonic bath has a transmittance of 77%. Given that one layer of graphene absorbs 2.3% of light at this wavelength, this type of graphene has a thickness of ~3.45 nm (10 graphene layers).[18] The transmittance of the film made from commercial electrochemical graphene is 33%, which indicates a thickness of ~10 nm (29 graphene layers). These two graphene sensors were easily characterized owing to the uniformity of the films [Figs. 1(a) and 1(c)]. The films made from graphene obtained by probe sonication are heterogeneous with different thicknesses in different regions of the film [Fig. 1(b) and inset of Fig. 3]. The transmittance of such a film is 83%, which corresponds to a thickness of 2.55 nm (7.5 graphene layers). Although this thickness was obtained across a large portion of the film, there are also smaller thicker parts, which are visually comparable to the other two graphene films.

Figure 4 shows AFM images from which the average lateral sizes of graphene flakes were determined. Figures 4(a)–4(c) depict the surfaces of graphene obtained by bath sonication, probe
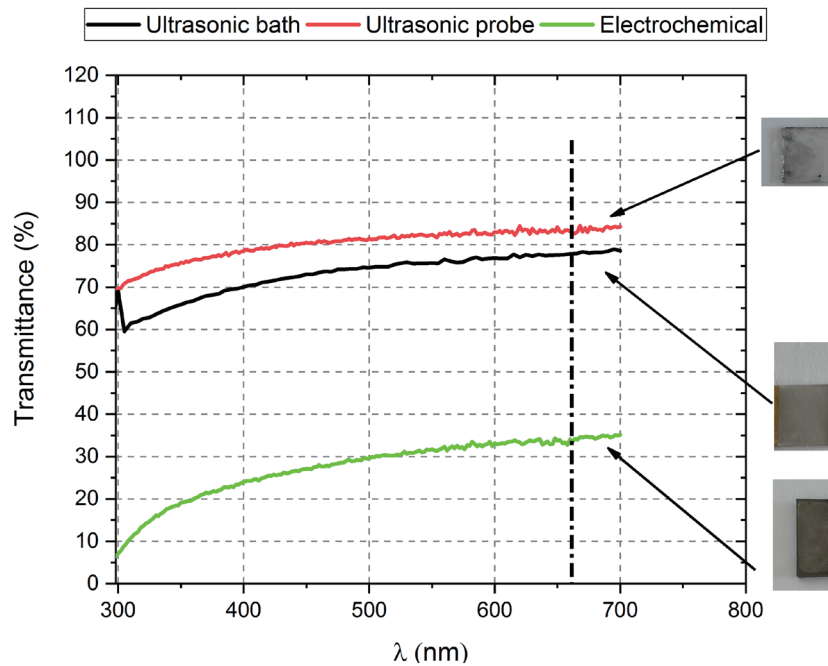
Fig. 3.   (Color online) UV–VIS characterization in transmittance mode, by which the thicknesses of the graphene films measured. Insets: photographs of the characterized graphene films. The green, black, and red curves represent the electrochemically exfoliated graphene, bath-sonicated, and probe-sonicated films, respectively.
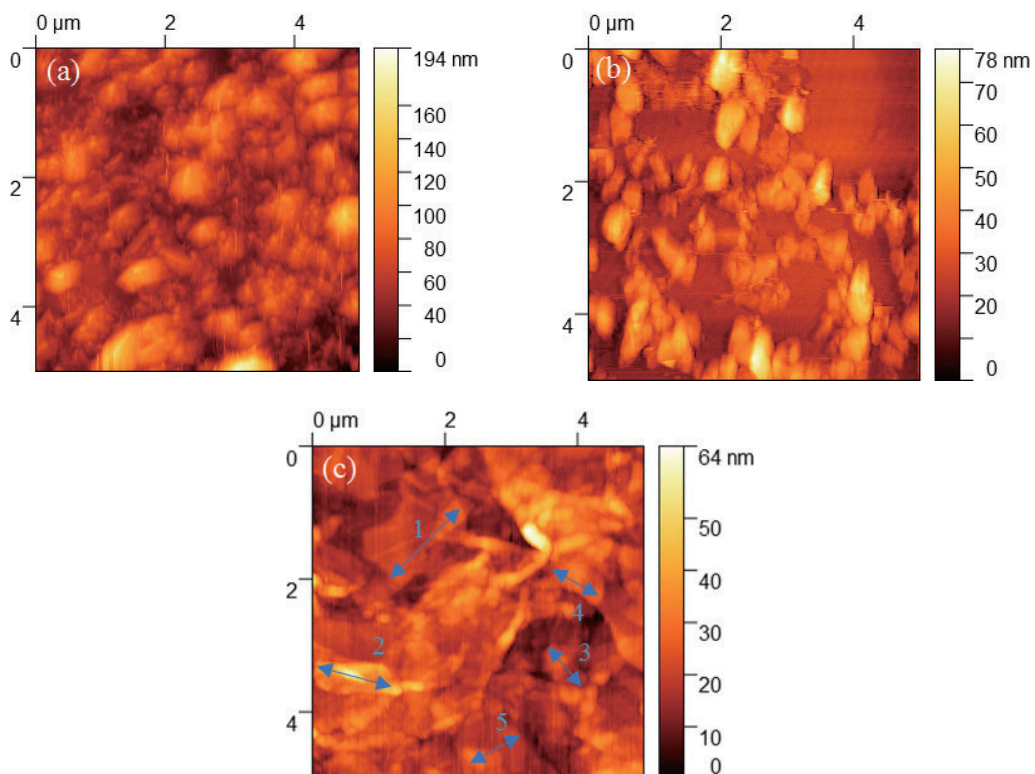

Fig. 4.   (Color online) Sample characterization with AFM. Different nanoplatelet sizes are visible in the images: (a) graphene from ultrasonic bath, (b) graphene from ultrasonic probe, and (c) commercially available electrochemical graphene.

sonication, and electrochemical exfoliation, respectively. Lateral sizes were determined by manually measuring the sizes of five random flakes on each image and taking the average. AFM images for graphene obtained by bath and probe sonications [Figs. 4(a) and 4(b)] are easy to interpret, because the flakes are small and have little overlap. Electrochemically exfoliated graphene yields flakes that are larger and have significant overlap; thus, in Fig. 4(c), we show the flakes that we measured, with numbered arrows that correlate with the flake sizes indicated in Table 1. In Table 1, we also provide the average flake sizes for the three exfoliation conditions. Bath sonication yielded an average size of 147 nm, in agreement with the values reported earlier.[15] For comparison, probe sonication yielded flakes that are on average larger (444 nm) but also have a wider size distribution. Electrochemical exfoliation produced the largest flakes, with lateral sizes above 600 nm and reaching ~1500 nm.

Figure 5 illustrates the chemical properties of each graphene film obtained via surveys of XPS spectra. Roughly, all three spectra have similar characteristics but with slight differences.

Table 1
Summary of randomly selected results measured by AFM, extracted from Fig. 4.

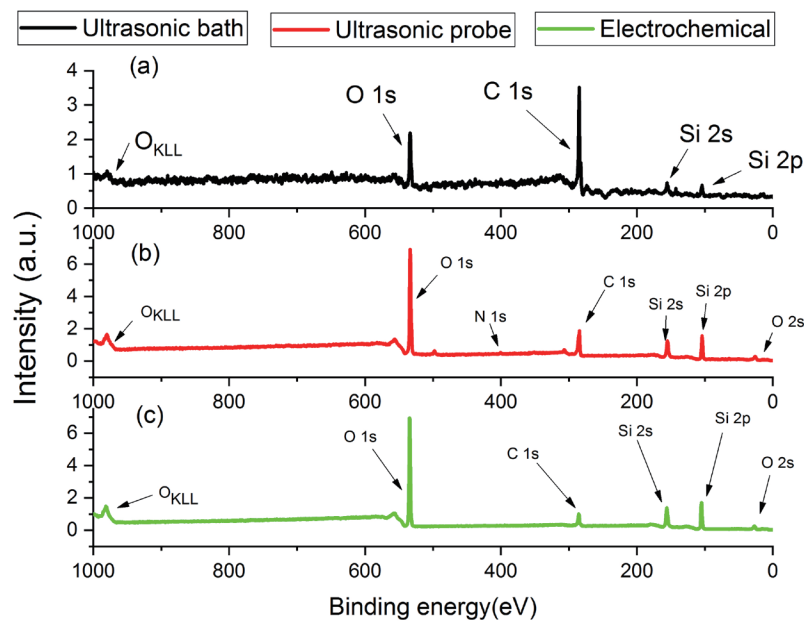|	R_1 (nm)	R_2 (nm)	R_3 (nm)	R_4 (nm)	R_5 (nm)	Average size (nm)
Ultrasonic bath	165	117	87	238	126	147
Ultrasonic probe	736	185	287	412	600	444
Commercial electrochemical	1513	1229	847	652	1020	1052

Fig. 5.　(Color online) Survey XPS spectra of each graphene: (a) graphene from ultrasonic bath, (b) graphene from ultrasonic probe, and (c) commercially available electrochemical graphene.

All of them show the presence of C, O, and Si (from the substrate) as expected, while in Fig. 5(b), a small peak, which originates from nitrogen appears at approximately 400 eV. The deconvoluted XPS spectrum for C 1s, corresponding to graphene obtained from the ultrasonic bath, has two peaks at 284.9 and 285.2 eV, which correspond to sp^3 and sp^2 hybridizations, respectively, and another peak at 286.4 eV, which corresponds to the C−O bond [Fig. 6(a)].[19] Graphene obtained from the ultrasonic probe has slight shifts of 0.6 and 0.3 eV for the peaks for sp^3 and sp^2 hybridizations, respectively, relative to graphene from the ultrasonic bath, where the C−C bond is located at 284.3 eV and the C=C bond is at 285.5 eV with a O−C=O functional group at 288.8 eV [Fig. 6(b)].[20] This shift can be attributed to different levels of oxidation between the two films. Figure 6(c) represents C 1s peaks for the electrochemically exfoliated graphene. The C−C bond is at 284.5 eV and the C=C bond is at 285.2 eV, while the peak corresponding to the C−O bond is located at 287.1 eV. Figure 6 indicates that the film obtained from graphene exfoliated in an ultrasonic bath has the lowest oxidation. Both the graphene from the ultrasonic probe and the electrochemically exfoliated graphene have higher intensity peaks related to the oxygen bond than graphene from the ultrasonic bath. Their peaks are of similar intensity but with different bond types, as indicated by the 1.7 eV shift in peak position between them. Graphene obtained
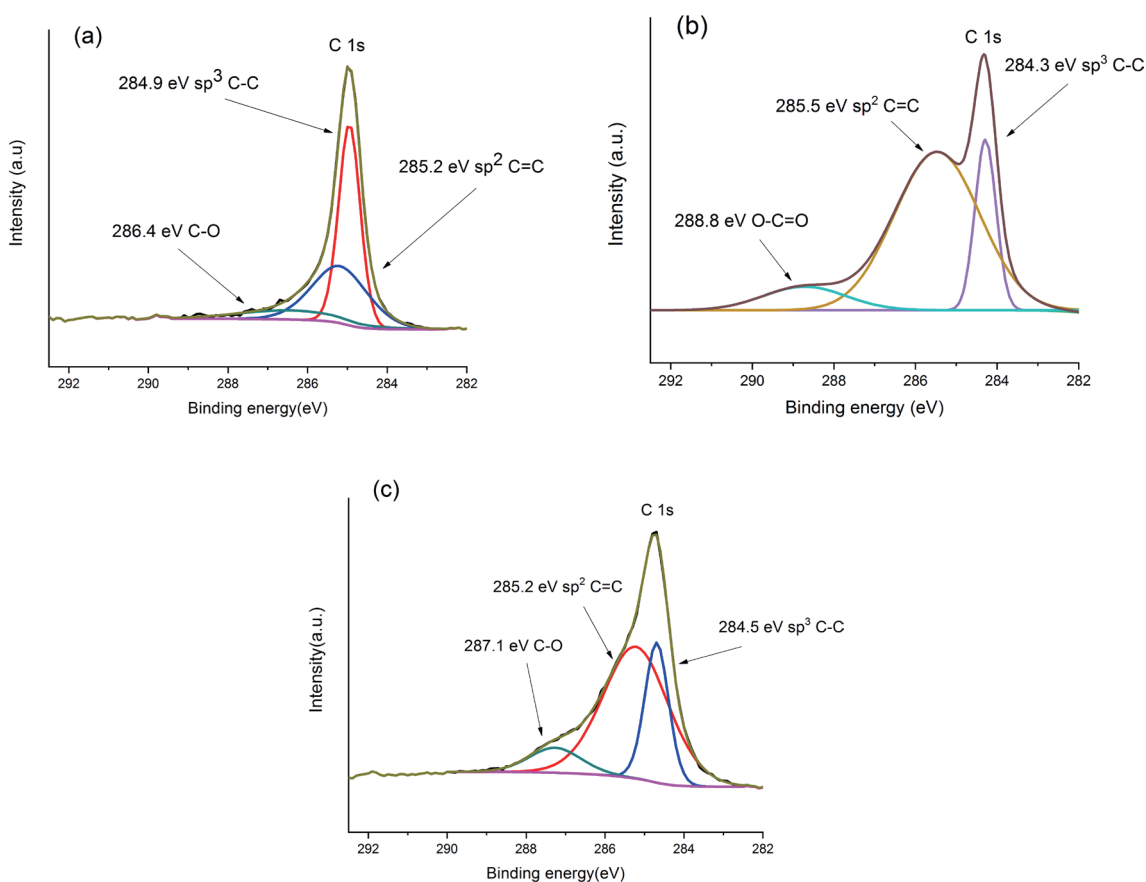

Fig. 6.   (Color online) Deconvoluted XPS peaks for C1s for (a) graphene from ultrasonic bath, (b) graphene from ultrasonic probe, and (c) commercially available electrochemical graphene.

from the ultrasonic probe shows a stronger oxidation than graphene from the ultrasonic bath and electrochemically exfoliated graphene, which is distinguished by having an O−C=O group instead of a simple C−O bond, as a result of a complex synthesis process in which several solvents are exchanged.

3.2   Humidity sensing

Figure 7 shows the response of the graphene-based sensors to changes in humidity. The output of the graphene-based sensors was measured in parallel to the output of a reference sensor, which provides the exact RH in the chamber (pink line in Fig. 7). For the starting point, a minimum of ~10% RH was established, and then the humidity was increased to a maximum of ~90% RH in the chamber. The maximum RH was chosen on the basis of the saturation point of the particular graphene sensor, beyond which the resistance did not change significantly. The saturation point for all three sensors occurred at around 90% RH. After reaching the maximum RH, the chamber was cleared out with a blast of nitrogen, which produced a rapid decrease in RH. These steps were repeated in three cycles. All three types of liquid-phase-exfoliated graphene were distinguished by a stable baseline and repeatability. Graphene obtained by bath sonication yielded sensors with the largest baseline drift due to chemisorption [Fig. 7 (a)]. Graphene obtained by probe sonication had the highest inhomogeneity, yielding sensors with the largest noise, as seen in Fig. 7(b). However, the assembled film was ~2.2 nm thick, making it the
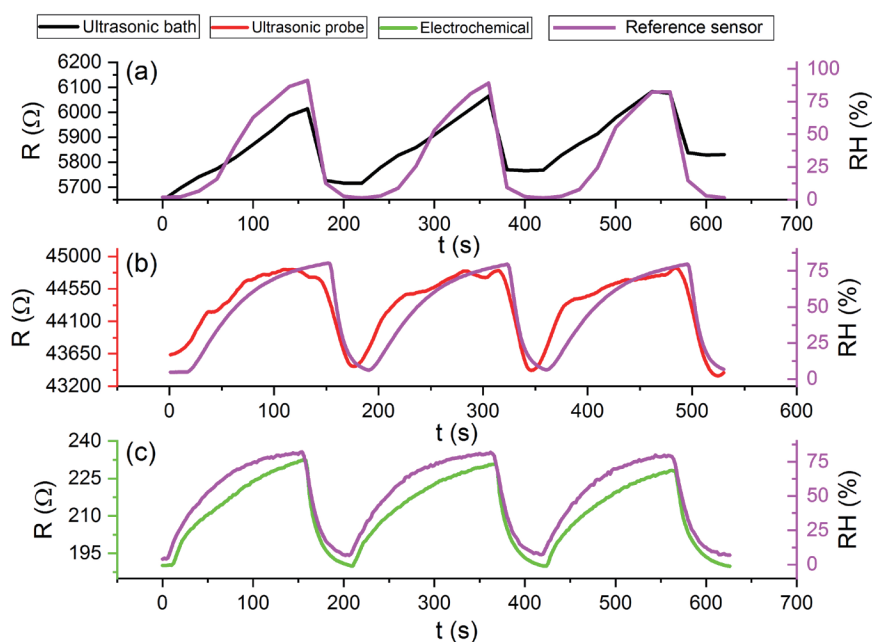

Fig. 7.   (Color online) Response over time of graphene sensors to humidity with reference to commercial humidity sensor (Honeywell HIH-4000-001), measured in three cycles from ~10% to ~90% RH: (a) graphene sensor obtained with the ultrasonic bath, (b) graphene sensor obtained with an ultrasonic probe, and (c) sensor fabricated from electrochemically synthesized graphene. In (b), the data has been smoothed for clarity.

thinnest among the three films. Figure 7(c) shows the results obtained from commercially available electrochemically exfoliated graphene. This film had the lowest resistance among the three films, starting at a value below 200 Ω, which is a result of a thickness of ~10 nm. A comparison of the sensitivities of the three different sensors is given in Table 2.

The sensitivity (*S*) of a chemiresistive gas sensor is given as

$$S = 100 \cdot \frac{\Delta R}{R_0} , \qquad (1)$$

where R_0 is the initial resistance and ΔR is the difference between the given resistance and the initial resistance. The most interesting RH range is between 30 and 80%, corresponding to the naturally occurring range of values. Table 2 shows the average sensitivity of each type of graphene sensor in this target range. The average sensitivities are 1% for graphene obtained with an ultrasonic probe, 2.4% for graphene obtained with an ultrasonic bath, and 13.4% for the commercially available electrochemical graphene. The obtained average sensitivity across the RH range is correlated with the graphene thickness, where the thinnest graphene film has the lowest sensitivity and the thickest film has the highest sensitivity. For a clearer view of the graphene sensor performance, a comparison was pursued with the data obtained with different graphene sensor types. Single- and double-layer CVD graphene films show sensitivities of 0.31 and 0.2% respectively, while the thinnest graphene film that comes from an ultrasonic probe has a sensitivity of 1%.[6,21] Electrospray-printed graphene shows a sensitivity up to ~20%, which is higher than that shown in this paper; however, the resistance for such graphene is near 200 kΩ, which is higher than that shown in this paper.[7]

Figure 8 shows the response of each graphene sensor over several cycles of increasing RH in a stepwise manner. The original baseline drift was corrected by linear subtraction to observe the results better. The apparent response and recovery times that could be inferred from these graphs are actually a measure of the chamber filling and purging times, and hence do not represent the response times of the graphene sensor, which are orders of magnitude smaller than the chamber response times. Figure 8(d) depicts the linearity of the relative change in resistance (*S*) as a function of RH at the maximum value. For a clear view of the linearity, the Pearson correlation coefficient (*r*) was calculated. The correlation coefficients of the graphene sensors from the ultrasonic bath, ultrasonic probe, and electrochemically exfoliated graphene are *r* = 0.97653, 0.99129, and 0.99289, respectively. All three sensors have linear behavior with high Pearson correlation coefficient.

Table 2
Percentage change of resistance for each graphene sensor in the range 30–80% for each cycle (ascending path) and average sensitivity. Results taken from Fig. 7.

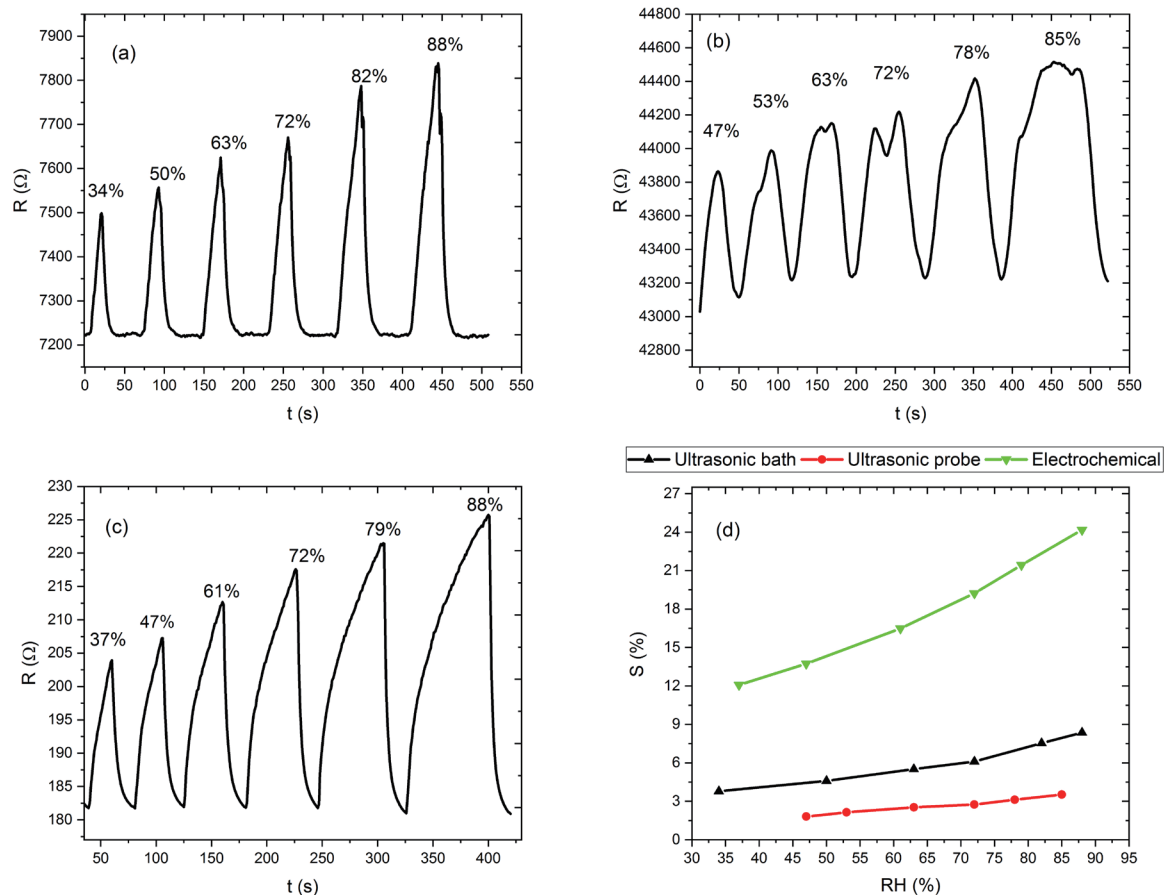|	Cycle 1 (%)	Cycle 2 (%)	Cycle 3 (%)	Average (%)
Ultrasonic bath	2.6	2.2	2.5	2.4
Ultrasonic probe	1	1	0.9	1
Commercial electrochemical	14	14	12.3	13.4

Fig. 8.   (Color online) Graphene senor response over time to rapid stepwise increase in RH: (a) sensor output from graphene obtained from an ultrasonic bath, (b) sensor output from graphene obtained with an ultrasonic probe, (c) sensor output from electrochemically synthesized graphene, and (d) peak response as a function of RH for all three graphene sensors. In (b), the data has been smoothed for clarity.

3.3   Respiration monitoring

Ultrafast graphene-based humidity sensors, in addition to determining the static RH, can be used to monitor human inhalation and exhalation, namely, respiration. Figure 9 depicts the results of breathing on each type of graphene sensor at fast, normal, and slow paces. Graphene sensors were placed on a table, and a volunteer exhaled and inhaled directly on each sensor in three cycles at each of the breathing paces. For fast breathing, it can be seen that there is a sharp peak, after which the output returns to the baseline. The signal output for normal breathing is distinguished by plateaus of ~2, ~8, and ~8 s for graphene from the ultrasonic bath, graphene from the ultrasonic probe, and electrochemically exfoliated graphene, respectively. The distinguished plateaus for slow breathing are ~4, ~14, and ~22 s for the three types of graphene, respectively (Fig. 9). All three graphene sensor types show similar trends at different respiration rates, with different time intervals for the plateaus, which are related to the thickness and topography of the individual graphene materials. The usefulness of such sensors for respiration monitoring lies in their practicality of use in a basic experiment, i.e., the sensor is placed on a
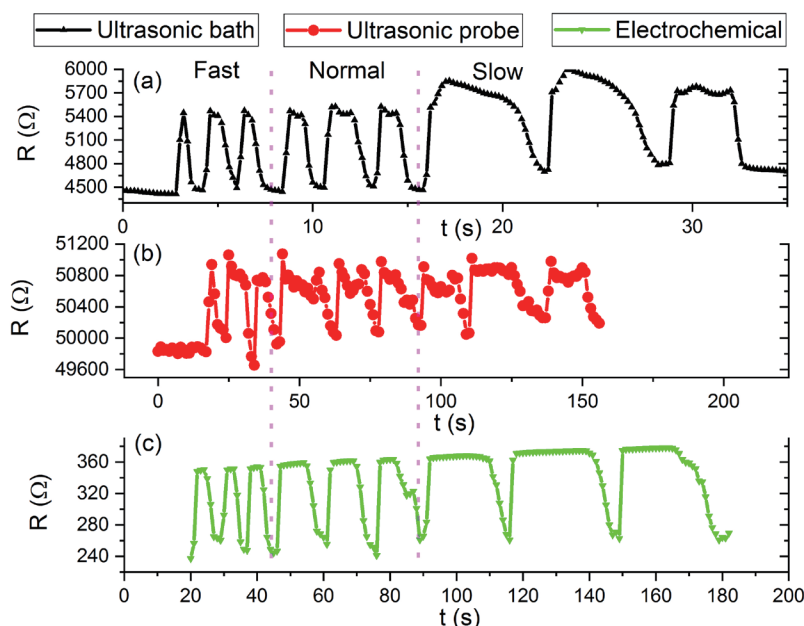
Fig. 9.   (Color online) Sensor response over time while monitoring fast, normal, and slow respirations for each graphene sensor: (a) graphene from ultrasonic bath, (b) graphene from ultrasonic probe, and (c) commercially obtained electrochemical graphene.

desk and the volunteer simply takes breaths, directly breathing on the sensor without wearing a mask, showing potential for further applications. The sensitivity is high at values up to ~40% for the commercially obtained graphene.

4.   Discussion

The process of obtaining graphene significantly affects the sensor performance owing to differences in film homogeneity, thickness, and functional group, all of which may affect the interaction of the film with water molecules in humid air. There is an evident inverse correlation between the measured film resistance and sensitivity to changes in humidity. The sensor with the lowest resistance has the highest sensitivity, and the sensor with the highest resistance has the lowest sensitivity. Higher resistance stems from the inhomogeneity of some of the films, which consist of islands of materials that do not cover the full sensor area, particularly our films made from probe-sonicated graphene. Since for such films the area covered by graphene is smaller than in the other two cases, the total volume reactive to gas is also smaller, resulting in lower sensitivity. The film made from bath-sonicated graphene is continuous and thinner than that made from electrochemically exfoliated graphene (EEG), but it also consists of smaller flakes (Fig. 3). Although it would be reasonable to expect that a film consisting of smaller flakes is more reactive to gases than that consisting of larger flakes because the former contains a higher density of reactive edge sites,[16,22–24] that made from EEG is more reactive than that made from bath-sonicated graphene. The likely reason for the higher sensitivity is the larger film thickness, which translates to a larger total reaction volume. Thus, in future work on thin-film

gas sensors made from liquid-phase-exfoliated graphene, care should be taken about the trade-off between flake size (edge density) and film thickness (total reactive volume).

5.   Conclusion

In this paper, we presented a comparison of three types of graphene humidity sensors, with appropriate characterization that aids in understanding the obtained results. All graphene films were obtained by LPE but exfoliated with different methods, which implies that the obtained graphene films have different characteristics, with different films utilized depending on the application. In contrast to traditional humidity sensors, which have slow response times, graphene-based sensors are fast enough for dynamic applications such as respiration monitoring. We have demonstrated that, regardless of the exfoliation method used, films made from liquid-phase-exfoliated graphene and deposited by LB assembly are robust and useful for sensor applications.

References

1 T. A. Blank, L. P. Eksperiandova, and K. N. Belikov: Sens. Actuators, B **228** (2016) 416. https://doi.org/10.1016/j.snb.2016.01.015
2 X. Liu, S. Cheng, H. Liu, S. Hu, D. Zhang, and H. Ning: Sensors **12** (2012) 9635. https://doi.org/10.3390/s120709635
3 A. E. Galashev and O. R. Rakhmanova: Phys-Usp+. **57** (2014) 970. https://doi.org/10.3367/ufne.0184.201410c.1045
4 F. Bonaccorso, Z. Sun, T. Hasan, and A. C. Ferrari: Nat. Photonics **4** (2010) 611. https://doi.org/10.1038/nphoton.2010.186
5 S. Papamatthaiou, D. P. Argyropoulos, F. Farmakis, A. Masurkar, K. Alexandrou, I. Kymissis, and N. Georgoulas: Procedia Eng. **168** (2016) 301. https://doi.org/10.1016/j.proeng.2016.11.201
6 A. D. Smith, K. Elgammal, F. Niklaus, A. Delin, A. C. Fischer, S. Vaziri, F. Forsberg, M. Råsander, H. Hugosson, L. Bergqvist, S. Schröder, S. Kataria, M. Östling, and M. C. Lemme: Nanoscale **7** (2015) 19099. https://doi.org/10.1039/c5nr06038a
7 A. P. Taylor and L. F. Velásquez-García: Nanotechnology **26** (2015) 505301. https://doi.org/10.1088/0957-4484/26/50/505301
8 S. Borini, R. White, D. Wei, M. Astley, S. Haque, E. Spigone, N. Harris, J. Kivioja, and T. Ryhänen: ACS Nano **7** (2013) 11166. https://doi.org/10.1021/nn404889b
9 B. Jiang, Z. Bi, Z. Hao, Q. Yuan, D. Feng, K. Zhou, L. Zhang, X. Gan, and J. Zhao: Sens. Actuators, B **293** (2019) 336. https://doi.org/10.1016/j.snb.2019.05.024
10 C. Backes, T. M. Higgins, A. Kelly, C. Boland, A. Harvey, D. Hanlon, and J. N. Coleman: Chem. Mater. **29** (2017) 243. https://doi.org/10.1021/acs.chemmater.6b03335

11 S. Witomska, T. Leydecker, A. Ciesielski, and P. Samorì: Adv. Funct. Mater. **29** (2019) 1901126. https://doi.org/10.1002/adfm.201901126

12 H. Kim, C. Mattevi, H. J. Kim, A. Mittal, K. A. Mkhoyan, R. E. Riman, and M. Chhowalla: Nanoscale **5** (2013) 12365. https://doi.org/10.1039/c3nr02907g

13 S. Andrić, T. Tomasevic-Ilic, M. Bošković, M. Sarajlić, D. Vasiljević-Radović, M. M. Smiljanic, and M. Spasenović: Nanotechnology **32** (2020) 025505. https://doi.org/10.1088/1361-6528/abb973

14 F. Vasileva, V. Popov, I. Antonova, and S. Smagulova: Materials **15** (2022) 1256. https://doi.org/10.3390/ma15031256

15 A. Matković, I. Milošević, M. Milićević, T. Tomašević-Ilić, J. Pešić, M. Musić, M. Spasenović, D. Jovanović, B. Vasić, C. Deeks, R. Panajotović, M. R. Belić, and R. Gajić: 2D Mater. **3** (2016) 015002. https://doi.org/10.1088/2053-1583/3/1/015002

16 T. Tomašević-Ilić, Đ. Jovanović, I. Popov, R. Fandan, J. Pedrós, M. Spasenović, and R. Gajić: Appl. Surf. Sci. **458** (2018) 446. https://doi.org/10.1016/j.apsusc.2018.07.111

17 T. Tomašević-Ilić, J. Pešić, I. Milošević, J. Vujin, A. Matković, M. Spasenović, and R. Gajić: Opt. Quant. Electron. **48** (2016) 319. https://doi.org/10.1007/s11082-016-0591-1

18 R. R. Nair, P. Blake, A. N. Grigorenko, K. S. Novoselov, T. J. Booth, T. Stauber, N. M. R. Peres, and A. K. Geim: Science **320** (2008) 1308. https://doi.org/10.1126/science.1156965

19 L. Rakočević, I. Srejić, A. Maksić, J. Golubović, and S. Štrbac: Catalysts **11** (2021) 481. https://doi.org/10.3390/catal11040481

20 L. Rakočević, I. S. Simatović, A. Maksić, V. Rajić, S. Štrbac, and I. Srejić: Catalysts **12** (2022) 43. https://doi.org/10.3390/catal12010043

21 X. Fan, K. Elgammal, A. D. Smith, M. Östling, A. Delin, M. C. Lemme, and F. Niklaus: Carbon **127** (2018) 576. https://doi.org/10.1016/j.carbon.2017.11.038

22 Y. Yang and R. Murali: Phys. Lett. **98** (2011) 2011. https://doi.org/10.1063/1.3562317

23 G. C. Mastrapa and F. L. Freire: J. Sens. **2019** (2019). https://doi.org/10.1155/2019/5492583

24 M. Spasenovic, S. Andric, and T. Tomasevic-Ilic: Proc.2021 IEEE 32nd Int.l Conf. Microelectronics (IEEE, 2021) 25–28. https://doi.org/10.1109/MIEL52794.2021.9569192

About the Authors

Stevan Andrić received his B.S. degree at the Faculty of Physical Chemistry, University of Belgrade, Serbia in 2017 and his M.S. degree in 2018 also at the Faculty of Physical Chemistry, University of Belgrade. He is currently working at the Department of Microelectronic Technologies, Institute of Chemistry, Technology and Metallurgy, University of Belgrade, where he is pursuing his Ph.D. degree at the Faculty of Physical Chemistry. His research fields are in 2D materials, their exfoliation and application, gas sensors, motion detection sensors, and the electrochemical characterization of materials. (stevan@nanosys.ihtm.bg.ac.rs)

Tijana Tomašević-Ilić is a research associate at the Institute of Physics Belgrade, University of Belgrade. She obtained her Ph.D. in physical chemistry from the Faculty of Physical Chemistry, University of Belgrade in September 2019. Her work in the Laboratory for 2D Materials is focused on the liquid-phase exfoliation of layered, 2D nanomaterials, the controlled deposition of nanomaterials into thin films, the functionalization/surface modification of 2D materials by various covalent and noncovalent strategies, and the investigation of 2D material-based thin-film applications (e.g., FETs, sensors, and protective coatings). (ttijana@ipb.ac.rs)

Lazar Rakočević received his B.S. and M.S. degrees from the Faculty of Physical Chemistry, University of Belgrade, Serbia, in 2018 and 2019, respectively. He is currently pursuing his Ph.D. degree at the Faculty of Physical Chemistry, University of Belgrade. His research interests are in electrochemistry, catalysis, materials, and X-ray photoelectron spectroscopy. (lazar.rakocevic@vin.bg.ac.rs)

Dana Vasiljević Radović received her B.S. degree in electrical engineering from the School of Electrical Engineering, University of Belgrade in 1991 and her M.S. and Ph.D. degrees in material science from the University of Belgrade in 1995 and 1997, repetively. Currently, she is a full research professor and the head of the Department of Microelectronic Technologies, Institute of Chemistry, Technology and Metallurgy, University of Belgrade. Her main areas of expertise are the research and development of micro/nanosystem (MEMS and NEMS)-based sensors, detectors, and actuators, and also the AFM characterization of materials and MEMS/NEMS components. (dana@nanosys.ihtm.bg.ac.rs)

Marko Spasenović received his B.Eng. (engineering physics) from Carleton University in Ottawa, Canada, in 2005 and his M.S. in physics from the University of Toronto, Canada, in 2006. He received his Ph.D. degree in applied physics from the University of Twente and AMOLF in the Netherlands in 2011. From 2011 to 2014, he was a postdoctoral researcher at the Institute for Photonic Sciences (ICFO) near Barcelona, Spain. From 2014 to 2018, he was at the Institute of Physics in Belgrade, Serbia, where he held the positions of assistant research professor and associate research professor. Since 2018, he has been with the Institute of Chemistry, Technology and Metallurgy in Belgrade, Serbia, where he is an associate research professor. His research interests include the use of graphene and other 2D materials for sensing, particularly as gas sensors, physiological parameter sensors, and acoustic transducers. (spasenovic@nanosys.ihtm.bg.ac.rs)

Graphene-based Chemiresistive Gas Sensors

M. Spasenović, S. Andrić, and T. Tomašević-Ilić

Abstract - Gas sensors are an indispensable ingredient of the modern society, finding their use across a range of industries that include manufacturing, environmental protection and control, automotive and others. Novel applications have been arising, requiring new materials. Here we outline the principles of gas sensing with a focus on chemiresistive-type devices. We follow up with a summary of the advantages and use of graphene as a gas sensing material, discussing the properties of different graphene production methods. Finally, we showcase some recent results that point to novel applications of graphene-based gas sensors, including respiration monitoring and finger proximity detection.

I. INTRODUCTION

Gas sensors are devices that are ubiquitous in many industries, including manufacturing, automotive, building safety and others. Emerging applications such as widely available air quality sensors and wearable devices are exerting a pull on the development of devices from novel materials, that are often thin and flexible. Nanomaterials play an important role in fabricating thin, flexible sensors, due to their ease of manufacturing, scaling and application to a substrate, versatility, and favorable electronic properties such as efficient charge transport.
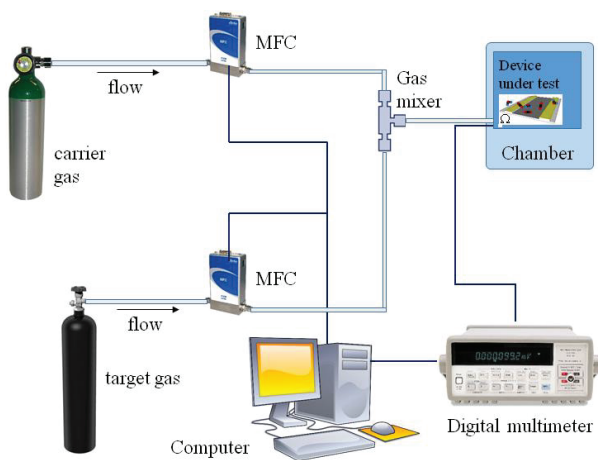

Fig. 1. Experimental setup for measuring response of gas sensors.

To characterize and calibrate the operation of a gas sensor, the sensor must be placed in a controlled environment

M. Spasenović and S. Andrić are with the Center for Microelectronic Technologies, Institute of Chemistry, Technology and Metallurgy, University of Belgrade, Njegoševa 12, 11000 Beograd, Serbia, e-mail: spasenovic@nanosys.ihtm.bg.ac.rs.

T. Tomašević-Ilić is with the Institute of Physics Belgrade, University of Belgrade, Pregrevica 118, 11080 Beograd, Serbia.

where key parameters are regulated. An example of an experimental setup for testing gas sensors is depicted in Fig. 1. The gas sensor (device under test, DUT) is placed in an environmental chamber. Often, such chambers are custom made by the sensor developer to satisfy requirements of the particular geometry and measurement parameter space. For example, if the sensor is cross-sensitive to temperature or humidity, these parameters must be controlled or at least monitored in the chamber [1].
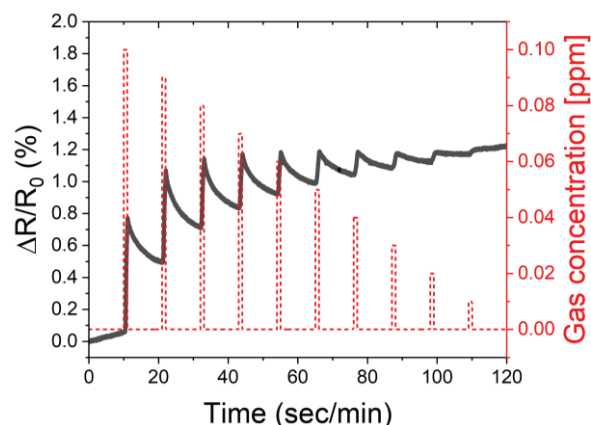

Fig. 2. Typical response of gas sensor to injection of known concentration of analyte. The red dashed line indicates injected gas concentration. The solid black line indicates resistance measured across two sensor terminals.

The DUT is contacted with wires that feed through the walls of the chamber and are connected to a measurement instrument, such as a digital programmable multimeter (DMM). The electrical characteristics of the DUT are measured as the environment is varied in a controlled manner. A constant flow of gas is introduced to the chamber via a gas inlet that is connected to mass flow controllers (MFC) or other gas flow control devices. For sensors boasting high sensitivity and accuracy of detection in the ppm or ppb range, the flow will consist mostly of an inert carrier gas, and a small percentage of the target analyte gas. The two gases are most often mixed in a simple T-shaped mixer prior to entering the detection chamber. MFC and DMM operation can be controlled and synchronized from a computer.

Fig. 2. depicts a common measurement protocol and sensor response of a chemiresistive gas sensor. The change in resistance, compared to measured resistance of the unexposed sensor, is monitored in time as the analyte gas flow is tuned to achieve different target concentrations. In the example shown, a short burst of analyte is introduced every 11s at varying concentrations, starting from the

highest. The sensor responds with an increase in resistance at burst onset, followed by a slow decrease when analyte flow is switched off and only carrier gas is flown over the sample. In the case of 2D material-based sensors, there is often a residue background drift of the measured response, which can be filtered out by signal differentiation [2].
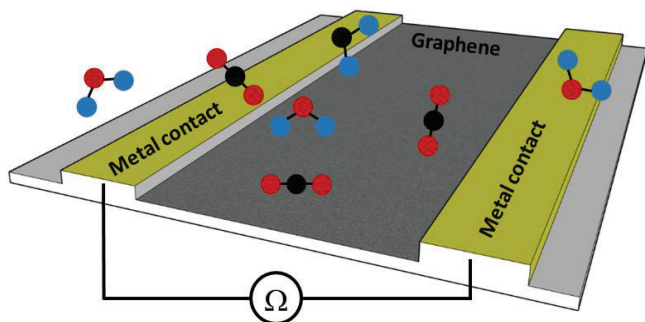

Fig. 3. Graphene-based chemiresistive gas sensing device. Graphene is laid on a substrate with metal contacts and exposed to a gas atmosphere.

Graphene is increasingly being investigated as an active material for gas sensing. Several physicochemical principles are commonly utilized to make gas sensors, including calorimetric sensors, optical sensors, electrochemical sensors, and chemiresistive sensors. Of these types, chemiresistive are the most versatile, and are easily integrated in a planar configuration. Chemiresistive sensors consist of a minimum of two electrical terminals connected to the active sensing layer. Fig. 3. depicts a graphene-based chemiresistive gas sensor. The graphene sits atop a substrate and is contacted with two planar metal contacts. Gas molecules in the vicinity of graphene can interact with the sensor, which is reflected in a changing electrical resistance between the two contacts with changing gas concentration or type.

In the following sections, we discuss the properties of several graphene fabrication techniques as they relate to use in gas sensing. We sketch the role that defects play in the interaction of graphene with gases. Finally, we demonstrate the application of chemiresistive graphene gas sensors to novel sensing technologies.

II. GRAPHENE-BASED GAS SENSORS

The chief properties required from a gas sensing material are efficient charge transport to a substrate or high carrier mobility, a large surface area, and an abundancy of active reaction sites. Various forms of graphene fulfill these requirements to different extents. In Fig. 4. we show the most common forms of graphene available in research laboratories and on the market. Micromechanical exfoliation is the oldest method of making graphene, which was utilized by Geim and Novoselov in their seminal paper [3] that sparked the graphene revolution. The method is based on mechanical cleavage of graphite flakes and separation of layers with adhesive tape. Thinned down graphite layers remain on the tape. The process is repeated several times, until visual inspection indicates the presence of very thin graphite layers on the tape. The tape is subsequently applied to a rigid substrate, such as Si/SiO2. After tape removal from the substrate, careful optical microscopy may reveal flakes of few-layer graphene, including single layers. One such flake is depicted in the optical micrograph of Fig. 4a. Typical lateral flake sizes are on the order of several tens of micrometers, whereas flakes are few and far apart on the substrate. This method yields graphene of the highest quality, with very few defects in the basal plane.

The main principle of interaction of micromechanically exfoliated graphene with gas species is through gas adsorption and desorption processes on the basal plane, i.e. physisorption. The adsorbed molecules change the local carrier concentration in graphene, which exerts changes in resistance. With extreme fabrication and noise control, mechanically exfoliated graphene has been used to achieve single-molecule sensitivity [4].
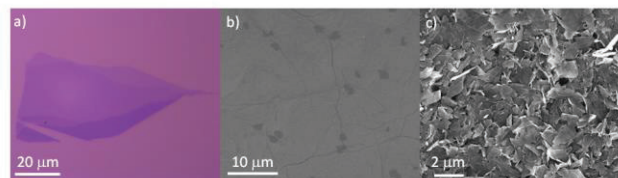

Fig. 4. Different types of graphene. a) depicts an optical micrograph of micromechanically exfoliated graphene; b) depicts a scanning electron micrograph (SEM) of CVD graphene (image courtesy of Graphenea); c) depicts a SEM of liquid phase exfoliated graphene.

The structure of micromechanically exfoliated graphene is similar to that of graphene grown by chemical vapor deposition (CVD). A scanning electron micrograph of CVD graphene is depicted in Fig. 4b. CVD graphene is grown on a catalyst substrate, such as a smooth copper foil, by placing the substrate in a chamber where temperature and growth precursors are controlled. Growth starts from seeds on the substrate and continues until the process is stopped or a continuous film is formed across the substrate. Growth from multiple seeds results in numerous grain boundaries. Because the growth takes place at highly elevated temperatures (>1,000ºC), the substrate and the graphene undergo a shrinking and expanding process, respectively, during cooling of the chamber. Due to a mismatch of thermal expansion coefficients of graphene and the substrate, wrinkles inevitably form on the graphene surface [5]. Hence, CVD growth results in graphene that is continuous over a large area, with some structural defects such as wrinkles and grain boundaries. Compared to micromechanically exfoliated graphene, CVD graphene may contain additional binding sites at these defects, which provide a channel for chemisorption in addition to physisorption that takes place on the surface of the basal

plane. It was found that polymer residue on graphene that remains after lithographic processes enhances the response of graphene gas sensors, with a surprisingly weak intrinsic response [6].

Graphene that is obtained from reduction of graphene oxide or from liquid phase exfoliation has the morphology of nanoplatelets – thin flakes of graphite or graphene. These flakes can have thicknesses ranging from a single layer of graphene up to tens of layers, and lateral sizes between several tens of nanometers and tens of micrometers. Such graphene is usually obtained in solution, which contains a range of nanoplatelet sizes. There exist several different methods for drawing nanoplatelets from solution into a film, such as spray coating, drop casting, spin coating, inkjet printing, and Langmuir-Blodgett assembly [7]. A film assembled from such nanoplatelets may look like that depicted in Fig. 4c.
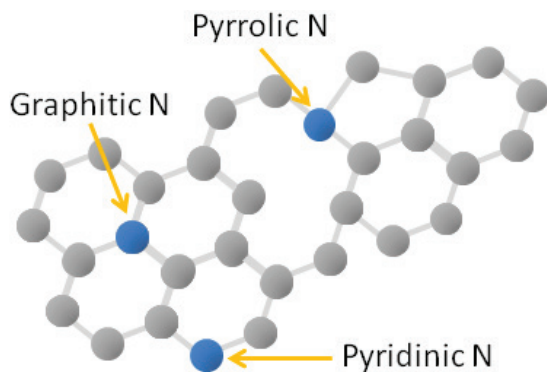

Fig. 5. A sketch of graphene structure and some commonly found defects.

Although films that are made from nanoplatelets typically show poor electrical conductivity compared to films made of CVD graphene, their response to gas exposure is different and may be stronger than the response of CVD graphene. A strong change of electrical properties upon exposure to an analyte in these materials can be attributed to the presence of reactive defect sites. As an example, nitrogen atoms can bind to graphene at various positions in the crystal lattice, as shown in Fig. 5. When a nitrogen atom simply substitutes a carbon atom in the basal plane, the substitution is termed graphitic nitrogen. When the nitrogen replaces carbon at a crystal defect site, one obtains pyrrolic nitrogen. Finally, when nitrogen replaces carbon at the edge of graphene, it is termed pyridinic nitrogen. Each of these species results in different electronic behavior, also affecting chemical reactivity of the graphene. It was observed that certain species such as water vapor will predominantly bind to edges, with a more pronounced effect in thicker platelets, whereas dry oxygen preferably reacts with the basal plane. Even in the case of micromechanically exfoliated graphene that is relatively free of edges, the reaction to water vapor is much stronger than to dry oxygen, which indicates high edge reactivity [8]. Similarly, it was observed that edges are the dominant

defect type in liquid-phase exfoliated films and that oxygen predominantly binds to these edges upon exposure to an oxygen plasma [9]. Researchers have also created edges by damaging graphene on purpose, to increase its reactivity to gases [10].

As a result of an abundancy of edges, films that are formed as a continuous sheet of interconnected nanoplatelets tend to react more strongly to the presence of gases than films that are constituted of continuous sheets with very few edge defects. At least one work has shown that films made from liquid-phase exfoliated graphene experience a significant drop in sheet resistance upon short exposure to an oxygen environment [9], as in Fig. 6. The value after 5 minutes of exposure can be less than 50% of the starting value, which is not the case for CVD graphene. The hypothesis presented in the referenced work is that oxygen binding to the edges of nanoplatelets dopes the graphene, causing a decrease in measured resistance. In contrast, CVD graphene reacts to treatment by a slight increase in sheet resistance, which is due to graphene lattice damage caused by oxygen ejecting carbon atoms. After 10 minutes of treatment, the damage becomes visually perceptible, whereas in the case of LPE graphene no damage will occur until all edges are saturated.
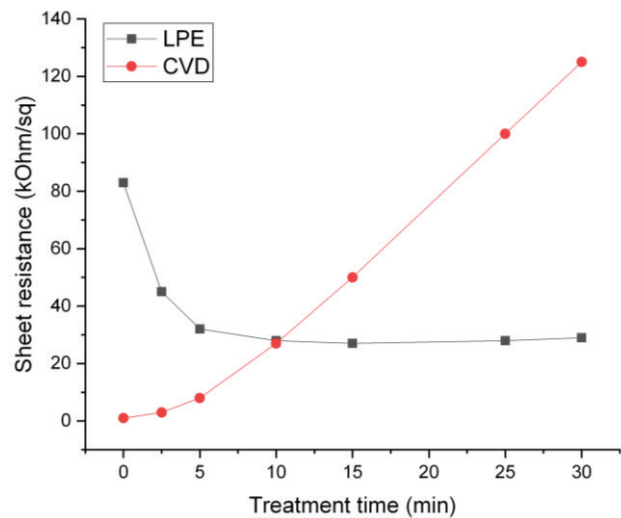

Fig. 6. Typical response of two types of graphene to a chemical treatment. The line with the red circles indicates response of CVD graphene. The line with the black squares indicates response of LPE graphene.

The strong sensitivity of LPE graphene to environmental gases can be exploited to produce gas sensors. In particular, such graphene has been used to detect NO_2 [11], [12] with ppm sensitivity, while theory predicts that graphene containing an abundancy of defect sites would react strongly to CO, NO, and NO_2[13].

Recently, it was found that LPE graphene is highly sensitive to changes in relative humidity of the ambient [14]. Changes in relative humidity can exert a change in measured resistance of chemiresistive graphene gas sensors

by up to 10%. It was also found that the response to humidity is much stronger than the response to other constituents of air, which makes this sensor ideal for open-air use as a humidity detector. Surprisingly, and in contrast to what has been observed in the case of NO_2 detection with LPE graphene [12], the response to humidity changes is extremely fast, on the order of 30 ms. Such extremely fast response opens avenues towards the use of these sensors in situations in which humidity changes more rapidly than can be detected with conventional humidity sensors, that are often based on the principle of humidity-induced swelling of a material and measuring a corresponding capacitance change. Indeed, it has been demonstrated that the ultrafast LPE graphene-based sensor can be used to monitor human respiration in real time (Fig. 7). The sensor was made by depositing LPE graphene, using Langmuir-Blodgett self-assembly, onto a pair of interdigitated metal contacts premade on a ceramic substrate. Breathing on the sensor resulted in real-time variation of the measured two-terminal resistance. Another novel application demonstrated in the same publication is real-time sensing of finger proximity detection. The application relies on the principle of detecting the cloud of moisture that exists in the vicinity of human skin. Real-time detection of finger proximity could be used to make novel devices, such as touchless control panels.
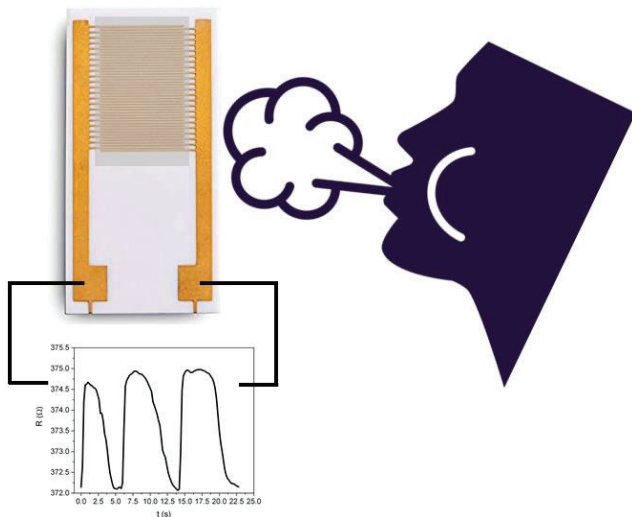

Fig. 7. The use of a chemiresistive graphene-based sensor as a respiration monitor. Resistance between two terminals changes in response to a person breathing on the sensor.

III. Conclusion

To conclude, liquid-phase exfoliated graphene presents an excellent opportunity to create practical gas sensors. Although theory predicts strong sensitivity to CO, NO, and NO_2, experiments have also shown a very strong response to changes in relative humidity, pointing to the potential for detection of other gases. Furthermore, the utlrafast response to humidity can be utilized to create novel devices, which may prove useful in particular for wearable biometric sensing.

References

[1] A. D. Smith et al., "Graphene-based CO_2 sensing and its cross-sensitivity with humidity", RSC Adv., 2017, vol. 7, no. 36, pp. 22329–22339.

[2] F. Ricciardella et al., "Calibration of Nonstationary Gas Sensors Based on Two-Dimensional Materials", ACS Omega, 2020, vol. 5, no. 11, pp. 5959–5963.

[3] K. S. Novoselov et al., "Electric field effect in atomically thin carbon films", Science (80-.)., 2004, vol. 306, no. 5696, pp. 666–9.

[4] F. Schedin et al., "Detection of individual gas molecules adsorbed on graphene", Nat. Mater., 2007, vol. 6, no. 9, pp. 652–5.

[5] W. Wang, S. Yang, and A. Wang, "Observation of the unexpected morphology of graphene wrinkle on copper substrate," Sci. Rep., 2017, vol. 7, no. 1, p. 8244.

[6] Y. Dan, Y. Lu, N. J. Kybert, Z. Luo, and T. C. Johnson, "Intrinsic Response of Graphene Vapor Sensors," Nano Lett., 2009, vol. 9, no. 4, pp. 1472–5.

[7] S. Witomska, T. Leydecker, A. Ciesielski, and P. Samorì, "Production and Patterning of Liquid Phase–Exfoliated 2D Sheets for Applications in Optoelectronics", Adv. Funct. Mater., 2019, vol. 29, no. 22, p. 1901126.

[8] Y. Yang and R. Murali, "Binding mechanisms of molecular oxygen and moisture to graphene", Appl. Phys. Lett., 2011, vol. 98, no. 9, p. 093116.

[9] T. Tomašević-Ilić et al., "Reducing sheet resistance of self-assembled transparent graphene films by defect patching and doping with UV/ozone treatment", 2018, Appl. Surf. Sci., vol. 458, pp. 446–453.

[10] G. Capote Mastrapa and F. L. Freire, "Plasma-Treated CVD Graphene Gas Sensor Performance in Environmental Condition: The Role of Defects on Sensitivity", J. Sensors, 2019, vol. 2019, pp. 1–7.

[11] F. Villani et al., "Study of the correlation between sensing performance and surface morphology of inkjet-printed aqueous graphene-based chemiresistors for NO_2 detection", Beilstein J. Nanotechnol., 2017, vol. 8, no. 1, pp. 1023–1031.

[12] F. Ricciardella et al., "Effects of graphene defects on gas sensing properties towards NO2 detection", Nanoscale, 2017, vol. 9, no. 18, pp. 6085–6093.

[13] Y. H. Zhang et al., "Improving gas sensing properties of graphene by introducing dopants and defects: A first-principles study", Nanotechnology, 2009, vol. 20, no. 18, p. 8.

[14] S. Andrić et al., "Ultrafast humidity sensor based on liquid phase exfoliated graphene", Nanotechnology, 2020, vol. 32, no. 2, p. 025505.

Langmuir-Blodgett films from liquid phase exfoliated 2D materials: surface modification and optoelectronic properties

T. Tomasević-Ilić[1], M. Spasenović[2]

[1]*Institute of Physics Belgrade, University of Belgrade, Pregrevica 118, 11080 Belgrade, Serbia*
[2]*Center for Microelectronic Technologies, Institute of Chemistry, Technology and Metallurgy, University of Belgrade, Njegoševa 12, 11000 Belgrade, Serbia*
e-mail:ttijana@ipb.ac.rs

Liquid phase exfoliation is an important production technique to obtaining a high yield of two-dimensional nanosheets in solution. It can be applied to numerous layered materials and satisfies practical applications. Langmuir-Blodgett deposition is a simple and versatile method based on self-organization of nanostructures that brings large surfaces of thin films on the substrate of choice. Although, Langmuir-Blodgett self-assembly (LBSA) of 2D materials in solution allows facile fabrication of highly transparent graphene films, the high density of defects that causes high sheet resistance of these films is unavoidable. Identifying the type of defect of these films and understanding how they can be manipulated is crucial for development of new strategies to adapt their electrical properties to the requirements of the optoelectronic industry. In this talk, the structure and optoelectronic properties of LBSA graphene films, the change and subsequent enhancement of their sheet conductivity with surface modification/functionalization by chemical doping, annealing, photochemical oxidation, and plasma exposure will be summarized [1-3]. Surface modification of these films results in a multifold reduction in sheet resistance of the films without changing their high transmittance. Edges are the dominant type of defect of these films and play a crucial role in defect patching and enhancing of electrical properties of modified LBSA graphene films. For materials beyond graphene, the properties and the encapsulation capability of LBSA films of h-BN for high-quality CVD graphene, ideal for transparent electronics but highly degradable in extreme environments such as photochemical oxidation, will be discussed.

[1] A. Matković, et al., 2D Mater. 3, 015002 (2016)
[2] T. Tomašević-Ilić, J. Pešić, I. Milošević, J. Vujin, A. Matković, M. Spasenović, R. Gajić, Opt. Quant. Electron. 48, 319 (2016)
[3] T. Tomašević-Ilić, Đ. Jovanović, I. Popov, R. Fandan, J. Pedrós, M. Spasenović, R. Gajić, Appl. Surf. Sci. 458, 446–453 (2018)

Plasma-assisted nitrogen doping of Langmuir-Blodgett self-assembled graphene films

T. Tomasević-Ilić[1], N. Škoro[1], N. Puač[1], M. Spasenović[2]

[1]*Institute of Physics Belgrade, University of Belgrade, Pregrevica 118, 11080 Belgrade, Serbia*
[2]*Center for Microelectronic Technologies, Institute of Chemistry, Technology and Metallurgy, University of Belgrade, Njegoševa 12, 11000 Belgrade, Serbia*
e-mail:ttijana@ipb.ac.rs

Application of highly transparent films obtained by self-organization of graphene flakes in optoelectronic devices seeks for appropriate surface modification/functionalization, which will adapt their electrical properties to the requirements of the electronic industry. Doping with nitrogen is one of the most promising methods to tailor the electronic properties of graphene [1]. Graphene films prepared from solution and deposited by Langmuir-Blodgett self-assembly (LBSA) [2, 3], were treated with radio-frequency (13.56 MHz) nitrogen plasma in order to investigate the influence of the time of nitrogen plasma exposure on the work function, sheet resistance and surface morphology of LBSA graphene films. Plasma treatments were performed in a chamber with plane-parallel electrode geometry with 5cm electrode gap and at 500 mTorr of N_2. Tuning parameter in this work was treatment duration. Kelvin probe force microscopy (KPFM) and sheet resistance measurements confirm nitrogen functionalization of our films, with the Fermi level shifting in the direction that indicates binding to a pyridinic and/or pyrrolic site [4], as would be expected for LBSA graphene, where edges are the dominant defect type [5]. We show that by tuning exposure time, we can decrease sheet resistance by a factor of two, without affecting surface morphology. Upon 1 min of nitrogen plasma exposure, the sheet resistance decreases and there is no obvious difference in film morphology. However, plasma exposure longer than 5 min leads to removal of graphene flakes and degradation of graphene films, in turn affecting the flake connectivityand increasing film resistance. Controllability of the plasma technique has an advantage for graphene functionalization over conventional doping techniques such as chemical drop-casting. It allows to controllably tune the work function, surface morphology and sheet resistance of LBSA films, which is substantial for applications in various optoelectronic and electronic devices.

REFERENCES
[1] A. Dey, A. Chroneos, N. St. J. Braithwaite, R. P. Gandhiraman, S. Krishnamurthy, Appl. Phys. Rev. 3, 021301 (2016)
[2] A. Matković, et al., 2D Mater. 3, 015002 (2016)
[3] T. Tomašević-Ilić, J. Pešić, I. Milošević, J. Vujin, A. Matković, M. Spasenović, R. Gajić, Opt. Quant. Electron. 48, 319 (2016)
[4] K. Akada, T. Terasawa, G. Imamura, S. Obata, K. Saiki, Appl. Phys. Lett. 104, 131602 (2014)
[5] T. Tomašević-Ilić, Đ. Jovanović, I. Popov, R.Fandan, J. Pedrós, M. Spasenović, R. Gajić, Appl. Surf. Sci. 458, 446–453(2018)

OGD-21, 17:00-17:15, Erzherzog Johann Auditorium

MAGNETIC GRAPHENE QUANTUM DOTS

Rajarshi Roy (1,2), (2) Lukáš Michal, (3) David Holec, (4) I. Jénnifer Gómez, (5) Nadězda Pizúrová, (6) David Nečas, (2) Anna Dolečková, (2) Jiřina Medalová, (6) Petr Lepcio (4,6) Lenka Zajíčková
(1) J. Heyrovsky Institute of Physical Chemistry, (2) CEITEC MU, (3) University of Leoben, (4) Masaryk University, (5) Institute of Physics and Materials, CZ, (6) CEITEC VUT

Over the last decade, graphene quantum dots have been one of the most important carbon nanomaterials owing to its quantum effects, excitation dependent luminescence, biocompatibility, nanosecond life-time, low toxicity, and highly water solubility. As a result, GQDs have incredible potential serving as a great platform for optical applications, sensors, and for bimodal or dual imaging nanoprobes such as magnetic resonance imaging (MRI) applications. However, synthesizing and characterization of such doped magnetic graphene quantum dots pose many challenges that must be overcome. Here, we discuss the prospect of chemically synthesizing a certain transition metal doped magnetic GQD with the sole aim to shed light on its magnetic property. Our results show under certain doping conditions long range magnetic ordering is possible which have been adequately validated with the help of robust complementary ab-initio simulations.

OGD-22, 17:15-17:30, Erzherzog Johann Auditorium

LANGMUIR-BLODGETT FILMS FROM LIQUID PHASE EXFOLIATED 2D MATERIALS

Tijana Tomasevic-Ilic

Institute of Physics Belgrade, University of Belgrade, Pregrevica 118, 11080 Belgrade, Serbia

Liquid phase exfoliation followed by Langmuir-Blodgett self-assembly (LBSA) deposition method is an important production technique for obtaining large surfaces of thin films on substrates of choice. It can be applied to numerous layered materials and satisfies practical applications. However, forming usable LBSA films remains a challenge, as the high density of defects of LBSA films strongly influences the electrical performance of devices. Identifying the type of defect of these films and understanding how they can be manipulated is crucial. In this talk, the structure and optoelectronic properties of LBSA graphene films, and the change of their conductivity with surface modification by chemical doping, photochemical oxidation, and plasma exposure will be summarized. A multifold reduction in sheet resistance of the graphene films upon surface modification can be attributed to the presence of edges as the dominant type of defect. The strong sensitivity of LBSA films to an analyte can be further exploited to produce sensors from graphene and other 2D materials. For materials beyond graphene, the properties and the encapsulation capability of LBSA films of h-BN for high-quality CVD graphene, optimal for various devices but degradable in aggressive environments such as photochemical oxidation, will be discussed.

Fe-nanoparticle-modified Langmuir-Blodgett Graphene Films for Pb(II) Water Purification

Ivana R. Milošević[a], Jasna Vujin[a], Muhammad Zubair Khan[b], Thomas Griesser[c], Christian Teichert[b] and Tijana Tomašević-Ilić[a]

[a]Institute of Physics Belgrade, University of Belgrade, 11080 Belgrade, Serbia
[b]Chair of Physics, Montanuniversität Leoben, Leoben, Austria
[c]Chair of Chemistry of Polymeric Materials, Montanuniversität Leoben, 8700 Leoben, Austria

Abstract. The surface of nonmagnetic Langmuir-Blodgett self-assembled (LBSA) graphene films is modified through structure engineering by chemical functionalization with Fe nanoparticles in order to induce local magnetic domains and investigate the application of such films for heavy metal water purification. We prepared and modified our films by single-step Langmuir-Blodgett procedure [1]. The influence of Fe-based magnetic nanoparticles on the structure and magnetic properties of LBSA films was examined by Raman spectroscopy, X-ray photoelectron spectroscopy (XPS), and Magnetic Force Microscopy (MFM). Raman and XPS confirmed the surface modification of the graphene films. Compared to an unmodified graphene film, which has no detectable magnetic response, MFM phase images show a strong phase shift difference compared to the substrate (~0.2°), indicating the presence of a local magnetic moment. In addition, we examined the use of magnetized LBSA graphene films for the adsorption of Pb(II) ions by immersing the films into Pb(II) solution. Results from XPS measurements depict the ability of modified films to detect and adsorb Pb(II) ions from water-based solutions. The development of a new generation of magnetic self-assembled 2D material films for heavy metal sensing and water purification that can overcome the deficiencies such as low purification efficiency, short-term stability, and high cost is of great interest for various applications in green technology.
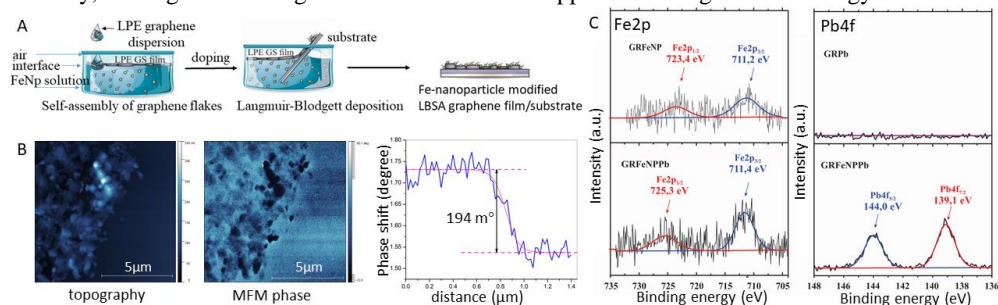
FIGURE 1. A) Fabrication of Fe-modified LBSA graphene films, B) AFM topography, MFM phase image, and representative MFM phase shift profile of Fe-modified LBSA films, C) XPS Fe2p spectra of modified films before and after interaction with Pb(II) ions, and Pb4f spectra of unmodified and modified films after interaction with Pb(II) ions.

REFERENCES

1. Milošević I. R. et al., *Sci. Rep.* **10**, 8476 (2020).

Фонд за науку Републике Србије
Бр. 5007/2023
08.11. 2023. год.
БЕОГРАД, Немањина бр. 22-26

ИНСТИТУТ ЗА ФИЗИКУ | БЕОГРАД
ИНСТИТУТ ОД НАЦИОНАЛНОГ
ЗНАЧАЈА ЗА РЕПУБЛИКУ СРБИЈУ
www.ipb.ac.rs

0301-187111
24. 11. 2023
Датум

РЕПУБЛИКА СРБИЈА
УНИВЕРЗИТЕТ УМЕТНОСТИ У БЕОГРАДУ
ФАКУЛТЕТ ПРИМЕЊЕНИХ УМЕТНОСТИ У БЕОГРАДУ
БЕОГРАД
Број 03-10/315
Датум 2 2 -11- 2023

Фонд за науку Републике Србије
Програм ПРИЗМА
Уговор о финансирању реализације Пројекта

УГОВОР О ФИНАНСИРАЊУ
РЕАЛИЗАЦИЈЕ НАУЧНОИСТРАЖИВАЧКОГ ПРОЈЕКТА

Назив Пројекта : 2D Material-based Tiled Network Films for Heritage Protection
Акроним Пројекта : 2DHeriPro
Регистрациони број Пројекта : 7456
У оквиру програма: ПРИЗМА Фонда за науку Републике Србије
Извор финансирања: Средства Пројекта акцелерације иновација и подстицања раста предузетништва у Републици Србији - SAIGE, уговор о гранту бр. TF C1389-YF и Буџет Републике Србије.

УГОВОРНЕ СТРАНЕ:

1. ФОНД ЗА НАУКУ РЕПУБЛИКЕ СРБИЈЕ, са регистрованим седиштем у Београду, ул. Немањина 22-26, Београд, матични број 17921410, ПИБ 111343775, број рачуна КЈС 840-670723-30, кога заступа др Милица Ђурић-Јовичић, в.д. директора (у даљем тексту: **Фонд за науку**),
са једне стране,

и

2. Реализатор истраживања/корисник средстава одобрених за финансирање Пројекта (у даљем тексту сваки од наведених појединачно означен као **Корисник средстава**, а сви заједнички означени као **Корисници средстава**):
    2.1. Акредитована научноистраживачка организација – НИО Институт за физику Београд, Универзитет у Београду, са седиштем на адреси Прегревица 118, Београд-Земун, ПИБ: 100105980, матични број: 07018029, коју заступа Александар Богојевић, директор, која је носилац реализације Пројекта (у даљем тексту: **Носилац пројекта**);
    2.2. Акредитоване научноистраживачке организације – НИО (у даљем тексту: **Учесници пројекта**):
    1) Факултет примењених уметности, Универзитет уметности у Београду, са седиштем на адреси Краља Петра 4, Београд, ПИБ: 100066998, матични број: 07007787, коју заступа Горан Чпајак, декан, (у даљем тексту: **Учесник пројекта**);

3. Тијана Томашевић-Илић, запослен/а у НИО Носиоцу пројекта, Институт за физику Београд, Универзитет у Београду (у даљем тексту: **Руководилац пројекта**),
са друге стране.

ОПШТИ ДЕО УГОВОРА

I ПРЕДМЕТ УГОВОРА

Члан 1.

Уговором о финансирању реализације научноистраживачког Пројекта (у даљем тексту: Уговор) уређују се међусобна права и обавезе уговорних страна у реализацији и финансирању Пројекта у оквиру програма ПРИЗМА (у даљем тексту: Програм).

Реализација Пројекта траје 36 месеци.

Фонд за науку је сагласан да финансира реализацију Пројекта у максималном износу од 33.628.752,76 динара.

Република Србија
МИНИСТАРСТВО ПРОСВЕТЕ,
НАУКЕ И ТЕХНОЛОШКОГ РАЗВОЈА
Број: 337-00-577/2021-09/50
Датум:. 30.06.2022.
Београд
Немањина 22-26

Институт за физику Београд, Универзитет у Београду
- Др Тијана Томашевић-Илић -

Прегревица 118
11 000 Београд

Поштована госпођо Томашевић-Илић,

Обавештавамо Вас да је на Трећем заседању Заједничке српско-аустријске Мешовите комисије, које је одржано је у Бечу, 24. јуна, Ваш предлог пројекта: **"Модулација магнетних особина самоорганизованих филмова графена за детекцију загађења и пречишћавање отпадних вода"** одобрен за финансирање, са почетком реализације од 1. јула 2022.године.

Финансирање мобилности истраживача на одобреним пројектима, реализоваће се у одређеним износима и на следећи начин: Српска страна ће средства намењена реализацији пројекта у износу од највише 2.000 евра по пројекту и по пројектној години, исплаћивати у динарској противвредности и то за трошкове превоза српских истраживача у Аустрију и трошкове боравка аустријских истраживача у Србији. Трошкови боравка аустријских истраживача по дану боравка у Републици Србији могу износити до 75 Евра у динарској противвредности (максимално до 14 дана) или укупно 1000 Евра у динарској противвредности за боравак аустријских истраживача за период од 15 дана до максимално 3 месеца. У случају да истраживач/и путују сопственим превозом, надокнада трошкова ће се извршити на основу Закона о коришћењу службеног возила.

Аустријска страна у износу од највише 4.000 евра по пројекту и по пројектној години, финансира трошкове превоза аустријских истраживача економском, до 100 евра по дану боравка српских истраживача који долазе у посету до 14 дана и 1.400 евра у укупном износу, за боравак српских истраживача у Аустрији у периоду од 15 дана до максимално 3 месеца..

Буџетска средства за финансирање активности биће уплаћена по појединачном захтеву који се доставља министарству у форми која је објављена на сајту министарства. Руководиоци пројеката су у обавези да поднесу годишњи извештај о реализацији активности на билатералном пројекту, на формулару који је такође објављен на званичном сајту.

Пројекти се реализују на основу Споразума између Владе Републике Србије и Владе Републике Аустрије о научној и технолошкој сарадњи, који је закључен 13. јула 2010. године у Бечу, Радног програма за 2021-2024. годину и Протокола Трећег заседања Заједничке српско-аустријске Мешовите комисије, који су потписани 24. јуна 2022. године.

Истовремено бих желео да Вам честитам на одобреном пројекту и пожелим успешну реализацију планираних активности.

С поштовањем,

ПРВИ ПОТПРЕДСЕДНИК ВЛАДЕ
И МИНИСТАР

Бранко Ружић

Conference Chairs

Vladimir Dobrosavljević, *Florida State University, USA*

Zorica Konstantinović, *Institute of Physics Belgrade*

Željko Šljivančanin, *Vinča Institute of Nuclear Sciences*

Organizing Committee

Jelena Pešić, *Institute of Physics Belgrade*- chair

Andrijana Šolajić, *Institute of Physics Belgrade*

Ivana Milošević, *Institute of Physics Belgrade*

Tijana Tomašević-Ilić, *Institute of Physics Belgrade*

Jelena Mitrić, *Institute of Physics Belgrade*

Bojana Višić, *Institute of Physics Belgrade*

Jovan Blagojević, *Institute of Physics Belgrade*

Marko Orozović, *Vinča Institute of Nuclear Sciences*

Mitra Stepić, *Vinča Institute of Nuclear Sciences*

Igor Popov, *Institute for Multidisciplinary Research, Belgrade*

Program Committee

Ivan Božović, *Brookhaven National Laboratory, USA*

Vladimir Dobrosavljević, *Florida State University, USA*

Milan Damnjanović, *Faculty of Physics, University of Belgrade, Serbia*

Vladimir Djoković, *Vinča Institute, University of Belgrade, Serbia*

Gyula Eres, *Oak Ridge National Laboratory, USA*

Laszló Forró, *University of Notre Dame, USA*